Supporting Information

Tuning the Circumference of Six-Porphyrin Nanorings

Renée Haver,[†#] Lara Tejerina,[†#] Hua-Wei Jiang,[†#] Michel Rickhaus,[†#] Michael Jirasek,[#] Isabell Grübner,[#] Hannah J. Eggimann,[§] Laura M. Herz,[§] and Harry L. Anderson*[#]

([†]These authors made equal contributions)

[#]Department of Chemistry, Chemistry University of Oxford, Research Laboratory, Oxford OX1 3TA, UK

[§]Department of Physics, University of Oxford, Clarendon Laboratory, Parks Road, Oxford OX1 3PU, UK

email: harry.anderson@chem.ox.ac.uk

Table of Contents

1 General Methods

Dry toluene, $CHCl_3$, CH_2Cl_2, THF, NEt_3 and pyridine were obtained from the solvent drying system MBraun MB-SPS-5-BenchTop under nitrogen atmosphere (H_2O content < 20 ppm as determined by Karl-Fischer titration). *N,N*-Diisopropylamine (*i*-Pr_2NH) was distilled from CaH_2 and kept over activated molecular sieves (3 Å, 8–12 mesh). Unless specified otherwise, all other solvents were used as commercially supplied. Flash chromatography was carried out using SiO_2 (60 Å, 230–400 mesh) under positive pressure. Analytical thin-layer chromatography was carried out on aluminum-backed silica gel 60 F254 plates. Petroleum ether (PE) 40−60°C was used unless specified otherwise.

All UV-vis-NIR spectra were recorded in solution using a Perkin-Lambda 20 spectrometer (1 cm path length quartz cell). Chloroform (containing *ca.* 0.5% ethanol as stabilizer) or toluene was used for all titrations without any further purification (HPLC grade). Fluorescence lifetimes were obtained from time correlated single-photon counting (TCSPC) using a single-photon avalanche diode detector with a time-resolution of 40 ps.[1]

Unless stated otherwise, ^1H and ^{13}C NMR spectra were recorded at 298 K using a Bruker AVIII HD 400, a Bruker AVII 500 or a Bruker AVIII 700 instrument. ^1H and ^{13}C NMR spectra are reported in ppm; coupling constants are given in Hertz, to the nearest 0.1 Hz. The solvent used was $CDCl_3$ which was calibrated to residual $CHCl_3$ at 7.26 ppm. Diffusion coefficients were measured at 298 K in $CDCl_3$ using a double stimulated echo sequence for convection compensation. The hydrodynamic radius was estimated from the diffusion coefficient using the Stoke-Einstein equation with a viscosity for $CDCl_3$ at 298 K of 5.28×10^{-4} Kg m^{-1} s^{-1}.

MALDI-ToF spectra were measured at the EPSRC UK National Mass Spectrometry Facility (NMSF, Swansea) using the Applied Biosystems Voyager DE-STR or at the University of Oxford using a Waters Micro MX spectrometer utilizing dithranol or *trans*-2-[3-(4-*tert*-butylphenyl)-2-methyl-2-propenylidene]malononitrile (DCTB) as a matrix.

Size exclusion chromatography (SEC) was carried out using Bio-Rad Bio-Beads S-X1 (40–80 µm bead size). Analytical GPC was carried out using JAIGEL-3H-A (8φ×500) and JAIGEL-4H-A (8φ×500) columns in THF + 1% pyridine as eluent with a flow rate of 1.0 mL/min. Semi-preparative GPC was carried out on a Shimadzu Recycling GPC system equipped with a LC-20 AD pump, SPD-20A UV detector and a set of JAIGEL 3H (20 × 600 mm) and JAIGEL 4H (20 × 600 mm) columns in toluene + 1% pyridine as the eluent at a flow rate of 3.5 mL/min. Where indicated NEt_3-deactivated silica was used, which was prepared by stirring a slurry of silica in $PE_{40\text{-}60}$/3% NEt_3 at 20 °C overnight before removing the solvents under reduced pressure.

2 Compound Naming System

The compounds discussed in this manuscript are systematically labeled according to the following naming system:

Porphyrin monomers: **R-P1-R**

Linear Porphyrin oligomers: **R-*l*-P*N*[b$_x$e$_y$]-R** in which
l : denotes linear.
N : number of porphyrin units in the linear oligomer.
b$_x$: *x* is the number of butadiyne [b] links between the porphyrin units in the linear oligomer.
e$_y$: *y* is the number of ethyne [e] links between the porphyrin units in the linear oligomer.
R = H, Br, TMS (denoting Me_3Si-acetylene), CPDMS (denoting $CN(CH_2)_3Me_2Si$-acetylene), CPDIPS (denoting $CN(CH_2)_3(i\text{-}Pr)_2Si$-acetylene), HC_2 (denoting unprotected acetylene).

Cyclic porphyrin hexamers: ***c*-P6[b$_x$e$_y$]** in which
c : denotes cyclic.
b$_x$: *x* is the number of butadiyne [b] links between the porphyrin units in the cyclic oligomer.
e$_y$: *y* is the number of ethyne [e] links between the porphyrin units in the cyclic oligomer.

The schematic representation of the nanorings (Figure S1), shows the porphyrin units as black spheres interconnected by either butadiyne (in black) or ethynyl linkages (in red).

Templates are labeled **T6** and **T6*** having phenyl or acetylene links between the hexasubstituted central benzene moiety and the pyridine arms, respectively:

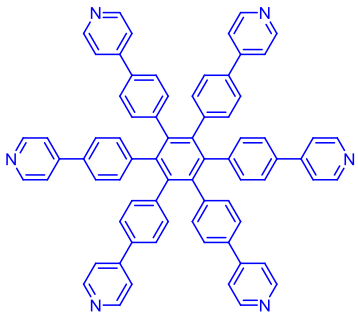

T6

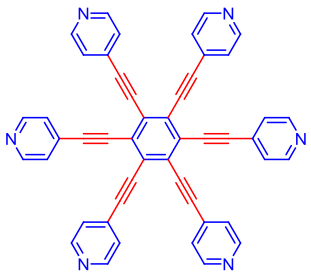

T6*

Peak assignments in ^{1}H are labeled according to the following conventions:
a1$^{(\#)}$/a2$^{(\#)}$ (belongs to EITHER **a1$^{(\#)}$** or **a2$^{(\#)}$**)
a1$^{(\#)}$,2$^{(\#)}$ (belongs to BOTH **a1$^{(\#)}$** and **a2$^{(\#)}$**)
a1–3 (belongs to **a1**, **a2**, **a3**, with and without #)

Correlations in 2D ^{1}H NMR are labeled according to the following conventions:
s: strong correlation
w: weak correlation
o: overlap

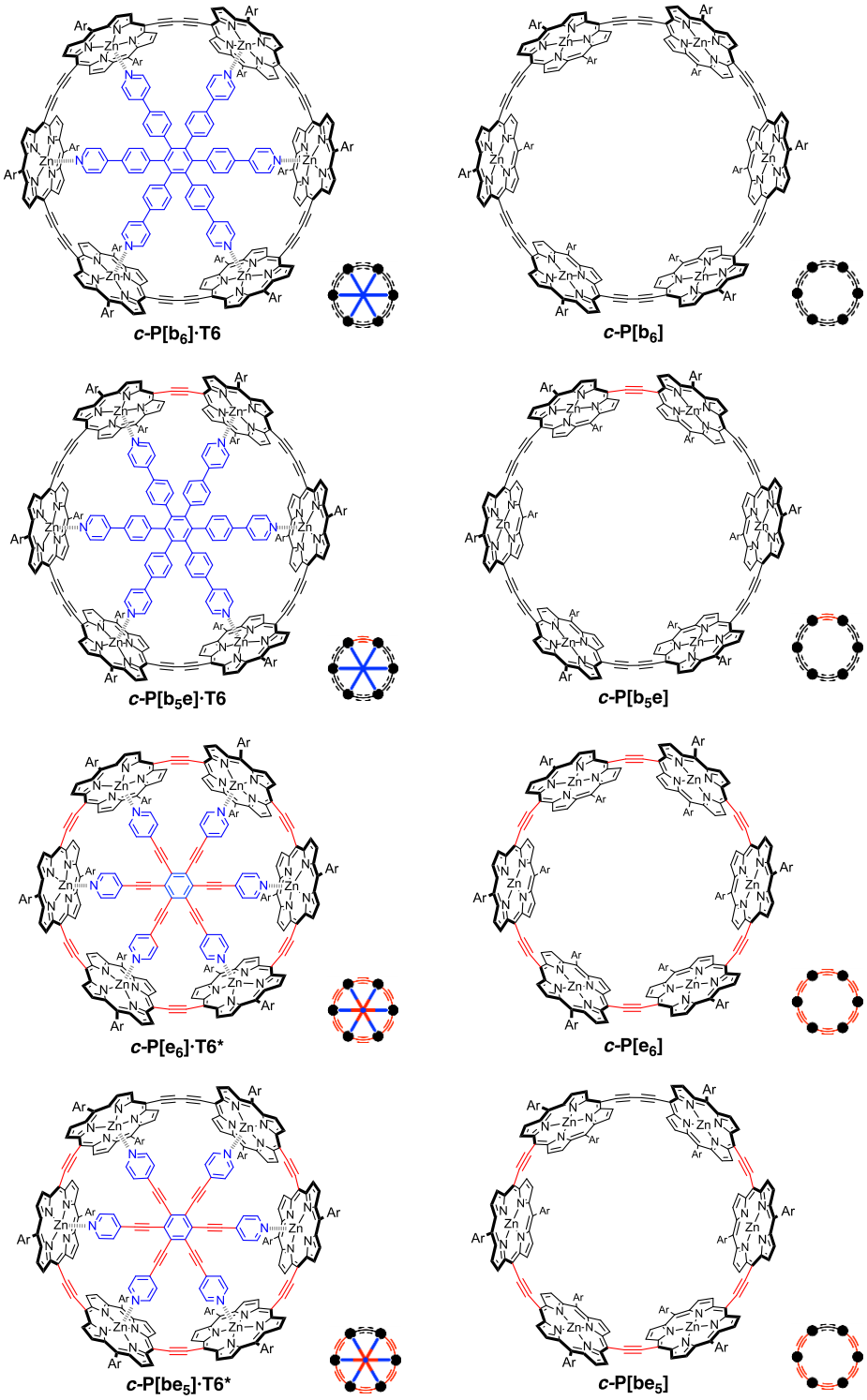

Figure S1: Chemical structures, compound labels and schematic representations of the compounds used in this study. Ar = 3,5-bis(trihexylsilyl)phenyl.

3 Synthetic Procedures

Monomers **Br-P1-Br**,[2] **Br-P1-H**,[3] **CPDIPS-P1-H**,[3] and **CPDIPS-P1-C$_2$H**,[4] templates **T6**,[5] and **T6***,[3] and porphyrin nanorings ***c*-P6[b$_6$]·T6**,[6] and ***c*-P6[e$_6$]·T6***,[3] were prepared as reported previously.

3.1 Synthesis of *c*-P6[b$_5$e]·T6 and *c*-P6[b$_5$e]

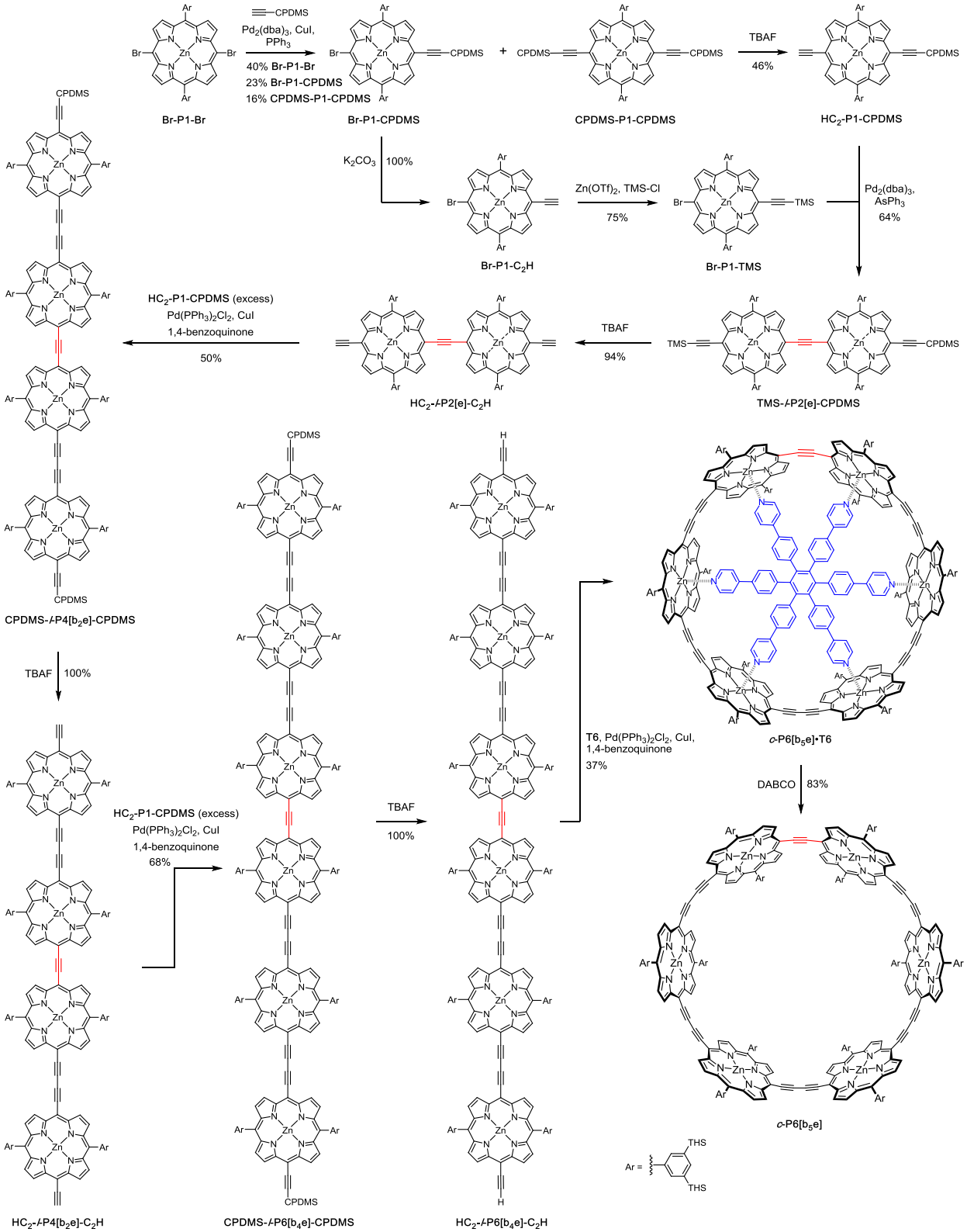

Scheme S1: Synthesis of ***c*-P6[b$_5$e]·T6.** We also prepared **CPDMS-*l*-P6[b$_4$e]-CPDMS** by coupling **H$_2$C-*l*-P2[e]-C$_2$H** with excess **H$_2$C-*l*-P2[b]-CPDMS** but we found that ***c*-P6[b$_5$e]·T6** prepared by this more direct route was always contaminated by small amounts of ***c*-P6[b$_6$]·T6**.

Br-P1-CPDMS:

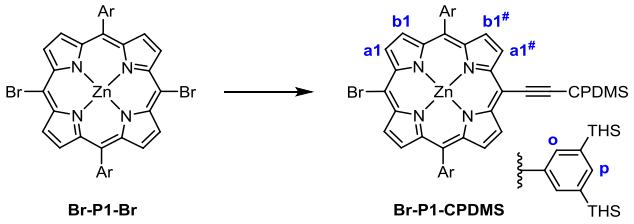

Br-P1-Br (1.40 g, 0.77 mmol), $Pd_2(dba)_3$ (70 mg, 0.077 mmol), CuI (15 mg, 0.077 mmol) and triphenylphosphine (40 mg, 0.15 mmol) were placed in a 250-mL two-necked flask. Dry toluene (36 mL) and *i*-Pr_2NH (36 mL) were added and the mixture was deoxygenated by freeze-pump-thaw cycles. Cyanopropyldimethylsilylacetylene (97 µL, 0.62 mmol) was added and the reaction mixture was stirred at 45 °C for 40 min after which TLC (PE_{40-60}/CH_2Cl_2 4:1) showed the desired statistical distribution of products. The volatiles were removed *in vacuo* and the residue was purified by column chromatography (SiO_2; gradient of PE_{40-60}/CH_2Cl_2 100:0 to 1:1) affording the desired product **Br-P1-CPDMS** (332 mg, 23%) as a green solid. Furthermore, starting material **Br-P1-Br** (559 mg, 40%) and the bis-acetylene substituted product **CPDMS-P1-CPDMS** (230 mg, 16%, for characterization see below) were obtained.

^{1}H NMR (400 MHz, $CDCl_3$, 298 K): δ_H 9.72 (d, *J* = 4.5 Hz, 2H, a1/a1$^{\#}$), 9.67 (d, *J* = 4.5 Hz, 2H, a1/a1$^{\#}$), 8.94 (d, *J* = 4.5 Hz, 2H, b1/b1$^{\#}$), 8.91 (d, *J* = 4.5 Hz, 2H, b1/b1$^{\#}$), 8.24 (d, *J* = 1.2 Hz, 4H, o), 8.01 (t, *J* = 1.2 Hz, 2H, p), 2.08 (t, *J* = 7.0 Hz, 2H, CPDMS-CH_2), 2.04 (m, 2H, CPDMS-CH_2), 1.49–0.90 (m, 156H, THS), 1.18 (m, 2H, CPDMS-CH_2), 0.61 (s, 6H, CPDMS-CH_3) ppm. **^{13}C NMR (125 MHz, $CDCl_3$, 298 K):** δ_C 153.0, 151.5, 150.6, 149.6, 140.6, 140.3, 139.4, 135.2, 133.7, 133.4, 133.2, 131.2, 124.0, 119.8, 108.9, 106.8, 99.9, 99.4, 33.7, 31.8, 24.2, 22.8, 21.1, 20.9, 16.3, 14.3, 13.0, 12.8, 12.6 ppm. **MALDI-ToF *m/z*** 1883.77 (calculated for $[C_{112}H_{182}BrN_5Si_5Zn]^+$: 1884.17).

CPDMS-P1-CPDMS:

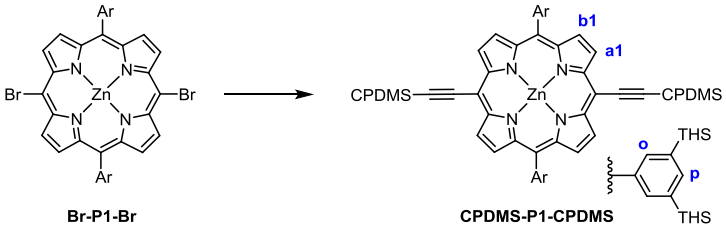

Br-P1-Br (454 mg, 0.25 mmol), $Pd(PPh_3)_2Cl_2$ (35 mg, 0.05 mmol) and CuI (9.5 mg, 0.05 mmol), were placed in a Schlenk tube, and placed under argon atmosphere by three vacuum-argon refill cycles. Dry toluene (25 mL), *i*-Pr_2NH (4.5 mL) and pyridine (0.6 mL) were injected to the Schlenk tube. 3-Cyanopropyldimethylsilylacetylene (151 mg, 0.16 mL, 1.00 mmol) was added by syringe. The reaction mixture was stirred at 50 °C under argon atmosphere for 2.5 h. The solvents were removed *in vacuo* and the residue was purified by column chromatography (SiO_2; gradient of PE_{40-60}/CH_2Cl_2 10:1 to 5:1 to 2:1) affording the desired product **CPDMS-P1-CPDMS** (419 mg, 79% yield) as an oily green solid.

^{1}H NMR (400 MHz, $CDCl_3$, 298 K): δ_H 9.63 (d, *J* = 4.5 Hz, 4H, a1), 8.88 (d, *J* = 4.5 Hz, 4H, b1), 8.22 (d, *J* = 1.2 Hz, 4H, o), 7.99 (t, *J* = 1.2 Hz, 2H, p), 2.55 (t, *J* = 7.0 Hz, 4H, CPDMS-CH_2), 2.13 (m, 4H, CPDMS-CH_2), 1.46–0.89 (m, 156H, THS), 1.19 (m, 4H, CPDMS-CH_2), 0.59 (s, 12H, CPDMS-CH_3) ppm. **^{13}C NMR (125 MHz, $CDCl_3$, 298 K):** δ_C 152.2, 150.8, 140.5, 140.2, 139.4, 135.2, 133.3, 131.1, 124.3, 119.8, 108.9, 101.0, 99.7, 77.4, 77.2, 76.9, 33.7, 31.8, 24.2, 22.8, 21.1, 20.9, 16.3, 14.3, 13.0, 12.8, 12.6, −1.3 ppm. **MALDI-ToF *m/z*** 1953.10 (calculated for $[C_{120}H_{194}N_6Si_6Zn]^+$: 1953.33).

Br-P1-C$_2$H:

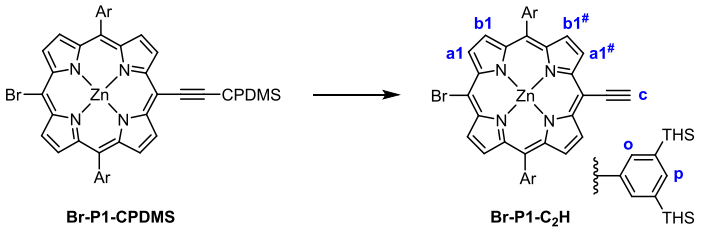

K_2CO_3 (140 mg, 1.0 mmol) was added to a solution of **Br-P1-CPDMS** (95 mg, 0.051 mmol) in THF (5 mL), MeOH (5 mL) and pyridine (0.1 mL). The suspension was stirred at room temperature for 30 min before the mixture was passed through a plug (SiO_2; $PE_{40\text{-}60}/CH_2Cl_2$ 2:1 + 1% pyridine). The volatiles were removed *in vacuo* yielding **Br-P1-C$_2$H** (90.3 mg 100%) as a green solid.

^{1}H NMR (400 MHz, $CDCl_3$, 298 K): δ_H 9.75 (t, *J* = 5.0 Hz, 4H, a1,1$^{\#}$), 8.97 (d, *J* = 4.7 Hz, 2H, b1/b1$^{\#}$), 8.94 (d, *J* = 4.7 Hz, 2H, b1/b1$^{\#}$), 8.26 (d, *J* = 0.8 Hz, 4H, o), 8.02 (t, *J* = 0.8 Hz, 2H, p), 4.19 (s, 1H, c), 1.51–0.91 (m, 156H, THS) ppm. **^{13}C NMR (100 MHz, $CDCl_3$, 298 K):** δ_C 153.2, 151.5, 150.7, 149.5, 140.7, 140.3, 139.4, 135.2, 133.7, 133.4, 133.2, 131.4, 123.9, 106.7, 99.2, 86.0, 83.9, 33.7, 31.8, 24.2, 22.8, 14.3, 12.8 ppm. **MALDI-ToF *m/z*** 1758.62 (calculated for $[C_{106}H_{171}BrN_4Si_4Zn]^+$: 1759.11).

Br-P1-TMS:

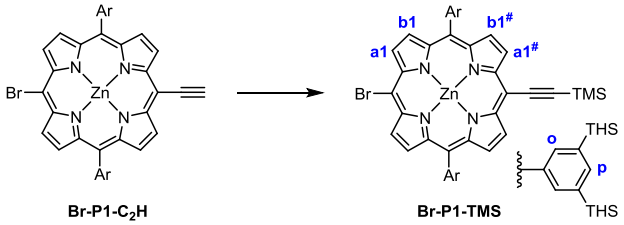

$Zn(OTf)_2$ (1.20 g, 3.3 mmol) was placed in a Schlenk flask under argon atmosphere. CH_2Cl_2 (7.5 mL) and NEt_3 (0.9 mL) were added and this mixture was stirred for 30 min. **Br-P1-C$_2$H** (287 mg, 0.16 mmol) in CH_2Cl_2 (3 mL) was added and the reaction mixture was stirred for 1 h before trimethylsilyl chloride (41 µL, 0.33 mmol) was added. The mixture was stirred overnight after which MALDI-ToF analysis confirmed completion. Saturated aqueous NH_4Cl was added and the organic layer was extracted and washed with H_2O. The organic layer was dried over $MgSO_4$ and the volatiles were removed *in vacuo*. The residue was purified by column chromatography (SiO_2; $PE_{40\text{-}60}/CH_2Cl_2$ 15:1) affording the desired product **Br-P1-TMS** (220 mg, 75%) as a green solid.

^{1}H NMR (400 MHz, $CDCl_3$ + 1% pyridine-d_5, 298 K): δ_H 9.63 (d, *J* = 1.2 Hz, 2H, a1/a1$^{\#}$), 9.62 (d, *J* = 1.2 Hz, 2H, a1/a1$^{\#}$), 8.84 (t, *J* = 4.8 Hz, 4H, b1,1$^{\#}$), 8.27 (d, *J* = 1.0 Hz, 4H, o), 7.97 (s, 2H, p), 1.49–0.87 (m, 156H, THS), 0.56 (s, 9H, TMS) ppm. **^{13}C NMR (100 MHz, $CDCl_3$ + 1% pyridine-d_5, 298 K):** δ_C 153.0, 151.2, 150.5, 149.3, 140.9, 140.8, 139.0, 134.7, 133.2, 132.9, 132.6, 131.0, 123.4, 106.2, 100.5, 99.3, 95.6, 33.7, 31.7, 24.2, 22.8, 14.3, 12.8, 0.44 ppm. **MALDI-ToF *m/z*** 1831.08 (calculated for $[C_{109}H_{179}BrN_4Si_5Zn]^+$: 1831.15).

HC_2-P1-CPDMS:

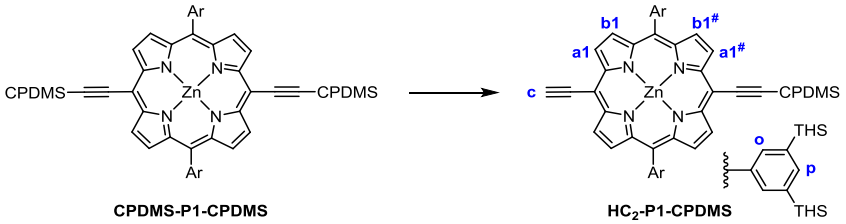

CPDMS-P1-CPDMS (980 mg, 0.50 mmol) was dissolved in $CHCl_3$ (130 mL, with 1.3 mL EtOH) and cooled to 0 °C. TBAF (1.0 M in THF, 0.25 mL, 0.25 mmol) was added and the reaction was monitored by TLC ($PE_{40\text{-}60}/CH_2Cl_2$ 4:1). After 20 min, the reaction was warmed to room temperature. After 50 min total reaction time, the reaction was quenched by adding acetic acid (0.05 mL, 0.9 mmol) and passed through a short plug (SiO_2; CH_2Cl_2 + 1% pyridine). Solvents were removed *in vacuo* and the residue was purified by column chromatography (SiO_2; gradient of $PE_{40\text{-}60}/CH_2Cl_2$ 4:1 to 1:1) to afford the bis-deprotected product[6] (214 mg, 25%) as a green solid, mono-deprotected product **HC_2-P1-CPDMS** (417 mg, 46%) as a green solid, and starting material **CPDMS-P1-CPDMS** (200 mg, 20%) as a green solid.

^{1}H NMR (400 MHz, $CDCl_3$, 298 K): δ_H 9.65 (d, *J* = 4.5 Hz, 2H, a1/a1$^{\#}$), 9.59 (d, *J* = 4.5 Hz, 2H, a1/a1$^{\#}$), 8.86 (d, *J* = 4.5 Hz, 4H, b1,1$^{\#}$), 8.21 (s, 4H, o), 7.97 (s, 2H, p), 4.14 (s, *J* = 1H, c), 2.55 (t, *J* = 7.0 Hz, 2H, CPDMS-CH_2), 2.13 (m, 2H, CPDMS-CH_2), 1.49–0.90 (m, 156H, THS), 1.18 (m, 2H, CPDMS-CH_2), 0.59 (s, 6H, CPDMS-CH_3) ppm. **^{13}C NMR (100 MHz, $CDCl_3$, 298 K):** δ_C 152.3, 152.1, 150.7, 150.6, 140.9, 140.7, 139.1, 136.0, 134.8, 133.0, 132.9, 130.9, 130.7, 123.9, 122.5, 119.9, 110.0, 100.0, 99.5, 98.6, 86.9, 83.3, 33.7, 31.8, 24.2, 22.8, 21.1, 20.9, 16.4, 14.3, 12.8, –1.27 ppm. **MALDI-ToF *m/z*** 1829.08 (calculated for $[C_{114}H_{183}N_5Si_5Zn]^+$: 1828.26).

TMS-*l*-P2[e]-CPDMS:

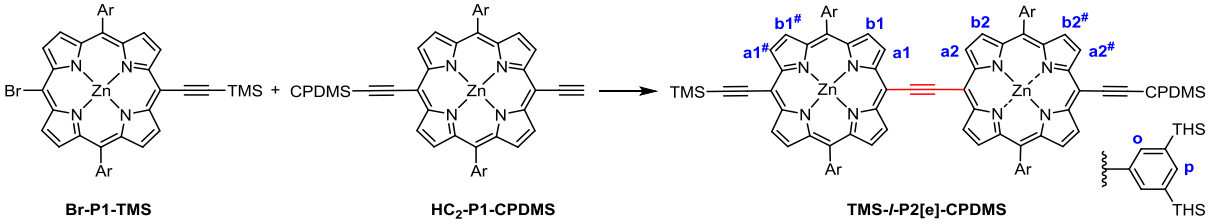

Br-P1-TMS (130 mg, 71.0 µmol), **HC_2-P1-CPDMS** (140 mg, 76.5 µmol), $Pd_2(dba)_3$ (14.6 mg, 14.2 µmol), $AsPh_3$ (17.3 mg, 56.8 µmol) were added into a flask, and placed under argon atmosphere by three vacuum-argon refill cycles. Dry THF (5 mL) and NEt_3 (1 mL) were injected to the flask. The reaction mixture was stirred at 60 °C for 17 h under argon atmosphere. The solvents were removed and the residue was purified by SEC (toluene + 1% pyridine) and further purified by column chromatography (SiO_2; gradient of $PE_{40\text{-}60}/CH_2Cl_2$ 10:1 to 10:3) to afford **TMS-*l*-P2[e]-CPDMS** (163 mg, 64%) as a green solid.

^{1}H NMR (400 MHz, $CDCl_3$, 298 K): δ_H 10.35 (d, *J* = 4.5 Hz, 2H, a1/a2), 10.33 (d, *J* = 4.5 Hz, 2H, a1/a2), 9.71 (d, *J* = 4.5 Hz, 2H, a1$^{\#}$/a2$^{\#}$), 9.66 (d, *J* = 4.5 Hz, 2H, a1$^{\#}$/a2$^{\#}$), 9.06 (d, *J* = 4.5 Hz, 2H, b1/b1$^{\#}$/b2/b2$^{\#}$), 9.05 (d, *J* = 4.5 Hz, 2H, b1/b1$^{\#}$/b2/b2$^{\#}$), 8.92 (d, *J* = 4.5 Hz, 2H, b1/b1$^{\#}$/b2/b2$^{\#}$), 8.90 (d, *J* = 4.5 Hz, 2H, b1/b1$^{\#}$/b2/b2$^{\#}$), 8.31 (m, 8H, o), 8.01 (m, 4H, p), 2.58 (t, *J* = 6.9 Hz, 2H, CPDMS-CH_2), 2.15 (m, 2H, CPDMS-CH_2), 1.50–0.82 (m, 312H, THS), 1.18 (m, 2H, CPDMS-CH_2), 0.62 (s, 6H, CPDMS-CH_3), 0.60 (s, 9H, TMS) ppm. **^{13}C NMR (125 MHz, $CDCl_3$, 298 K):** δ_C 152.6, 152.6, 152.5, 152.4, 150.6, 150.6, 150.6, 150.5, 144.6, 141.0, 140.9, 140.7, 140.6, 136.0, 134.8, 134.7, 133.0, 132.9, 130.9, 130.8, 130.7, 130.5, 129.2, 128.4, 124.3, 124.2, 122.7, 122.2, 119.9, 110.1, 108.6, 103.2, 102.7, 100.9, 100.6, 100.5, 99.7, 98.5, 53.6, 41.5, 33.7, 33.7, 31.8, 31.7, 29.2, 24.2, 22.8, 21.1, 20.9, 20.6, 19.6, 16.4, 14.3, 13.0, 12.8, 12.6, 11.6, 0.5, −1.2 ppm. **MALDI-ToF *m/z*** 3579.58 (calculated for $[C_{223}H_{361}N_9Si_{10}Zn_2]^+$: 3579.48). **UV-vis-NIR (toluene + 1% pyridine) λ_{max} (log ε):** 754 (4.92), 580 (4.28), 495 (5.51), 430 (5.28).

HC_2-*l*-P2[e]-C_2H:

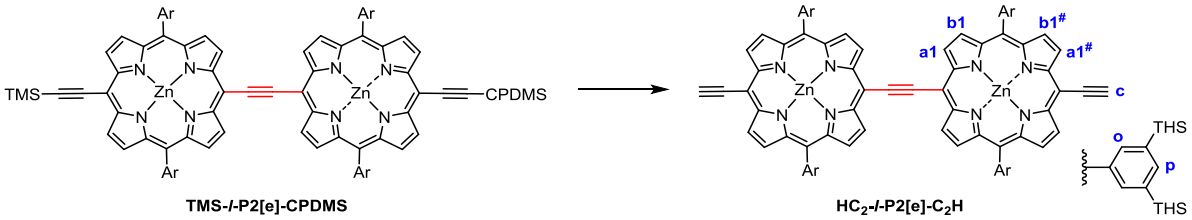

TMS-*l*-P2[e]-CPDMS (109 mg, 30.5 μmol) was dissolved in CH_2Cl_2 (10 mL) and pyridine (0.1 mL). TBAF (1.0 M in THF, 0.46 mL, 0.46 mmol) was added and the reaction was stirred for 20 min at room temperature before passing through a plug (SiO_2; $CHCl_3$ + 1% pyridine). The volatiles were removed *in vacuo* to afford **HC_2-*l*-P2[e]-C_2H** (97 mg, 94%) as a green solid.

^{1}H NMR (500 MHz, $CDCl_3$, 298 K): δ_H 10.31 (d, *J* = 4.5 Hz, 4H, a1), 9.66 (d, *J* = 4.5 Hz, 4H, a1$^{\#}$), 8.99 (d, *J* = 4.5 Hz, 4H, b1/b1$^{\#}$), 8.86 (d, *J* = 4.5 Hz, 4H, b1/b1$^{\#}$), 8.28 (s, 8H, o), 7.97 (s, 4H, p), 4.16 (s, 2H, c), 1.49–0.90 (m, 312H, THS) ppm. **^{13}C NMR (125 MHz, $CDCl_3$, 298 K):** δ_C 152.6, 150.7, 150.6, 145.5, 141.1, 140.7, 139.1, 136.0, 134.8, 133.05, 132.97, 130.8, 130.7, 124.1, 122.9, 102.9, 100.7, 98.9, 87.1, 83.2, 33.7, 31.8, 24.2, 22.8, 14.3, 12.8 ppm. **MALDI-ToF *m/z*** 3378.77 (calculated for $[C_{214}H_{342}N_8Si_8Zn_2]^+$: 3382.38).

CPDMS-*l*-P4[b_2e]-CPDMS:

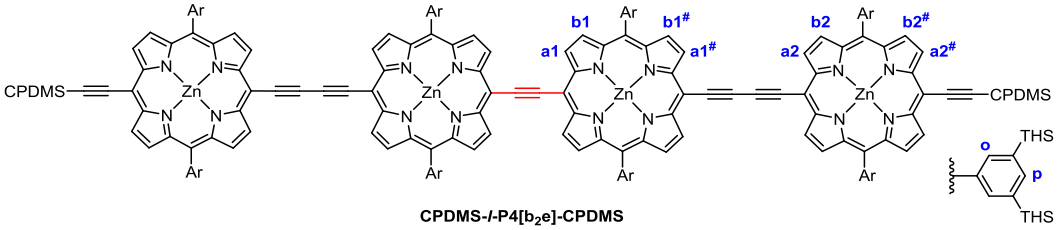

HC_2-*l*-P2[e]-C_2H (96 mg, 29 μmol) and **HC_2-P1-CPDMS** (417 mg, 0.23 mmol) were dissolved in dry toluene (25 mL). $Pd(PPh_3)_2Cl_2$ (10 mg, 14 μmol), CuI (27 mg, 0.14 mmol), and 1,4-benzoquinone (61 mg, 0.57 mmol) were dissolved in a mixture of dry toluene (25 mL) and dry *i*-Pr_2NH (5 mL) and this catalyst solution was added to the porphyrin solution. The reaction was stirred at room temperature and monitored by TLC. After 1 h, the mixture was passed through a plug (SiO_2; $CHCl_3$ + 1% pyridine). The solvents were removed and the residue was purified by SEC (toluene + 1% pyridine) and further purified by recycling GPC (toluene + 1% pyridine) to afford **CPDMS-*l*-P4[b_2e]-CPDMS** (103 mg, 50%) as a yellow-brown solid.

^{1}H NMR (400 MHz, $CDCl_3$, 298 K): δ_H 10.34 (d, *J* = 4.5 Hz, 4H, a1), 9.89 (overlapping doublets, *J* = 4.5 Hz, *J* = 4.5 Hz, 8H, a1$^{\#}$,2), 9.61 (d, *J* = 4.5 Hz, 4H, a2$^{\#}$), 9.01 (d, *J* = 4.5 Hz, 4H, b1), 8.96 (overlapping doublets, *J* = 4.5 Hz, *J* = 4.5 Hz, 8H, b1$^{\#}$,2), 8.87 (d, *J* = 4.5 Hz, 4H, b2$^{\#}$), 8.34 (s, 8H, o), 8.27 (s, 8H, o), 8.02 (m, 8H, p), 2.58 (t, *J* = 7.0 Hz, 4H, CPDMS-CH_2), 2.16 (m, 4H, CPDMS-CH_2), 1.52–0.83 (m, 624H), 1.22 (m, 4H, CPDMS-CH_2), 0.62 (s, 12H, CPDMS-CH_3) ppm. **^{13}C NMR (125 MHz, $CDCl_3$, 298 K):** δ_C 153.4, 153.1, 152.7,152.2, 150.8, 150.8, 150.5, 150.5, 143.8, 140.9, 140.7, 139.3, 136.1, 135.0, 134.9, 133.4, 133.3, 133.1, 133.0, 130.9, 130.8, 124.5, 122.6, 119.9, 109.9, 103.5, 101.1, 100.2, 99.5, 98.9, 88.5, 88.2, 82.7, 82.5, 33.7, 31.8, 24.2, 22.8, 21.1, 20.9, 16.4, 14.4, 14.3, 12.8, −1.3 ppm. **MALDI-ToF *m/z*** 7037.81 (calculated for $[C_{442}H_{704}N_{18}Si_{18}Zn_4]^+$: 7036.87). **UV-vis-NIR (toluene + 1% pyridine) λ_{max} (log ε):** 816 (5.28), 659 (4.75), 483 (5.53), 460 (5.61).

HC_2-*l*-P4[b_2e]-C_2H:

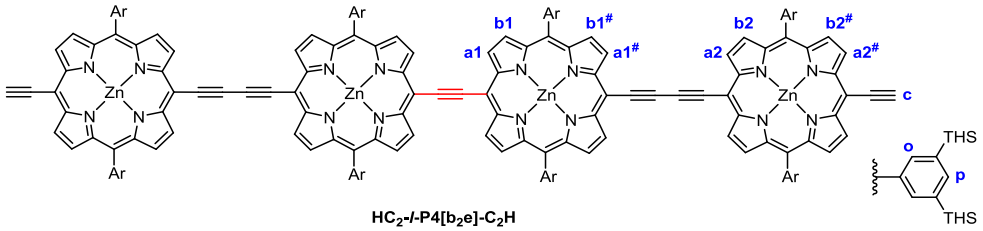

HC_2-*l*-P4[b_2e]-C_2H

CPDMS-*l*-P4[b_2e]-CPDMS (88 mg, 12 μmol) was dissolved in CH_2Cl_2 (5 mL) and pyridine (0.05 mL). TBAF (1.0 M in THF, 0.18 mL, 0.18 mmol) was added and the reaction was stirred for 20 min at room temperature before the mixture was passed through a plug (SiO_2; $CHCl_3$ + 1% pyridine). The solvents were removed to afford **HC_2-*l*-P4[b_2e]-C_2H** (84 mg, 100%) as a brown solid.

^{1}H NMR (400 MHz, $CDCl_3$, 298 K): δ_H 10.33 (d, *J* = 4.5 Hz, 4H, a1), 9.91 (d, *J* = 4.5 Hz, 4H, a1$^{\#}$/a2), 9.89 (d, *J* = 4.5 Hz, 4H, a1$^{\#}$/a2), 9.67 (d, *J* = 4.5 Hz, 4H, a2$^{\#}$), 9.01 (d, *J* = 4.5 Hz, 4H, b1), 8.96 (d, *J* = 4.5 Hz, 4H, b1$^{\#}$/b2), 8.95 (d, *J* = 4.5 Hz, 4H, b1$^{\#}$/b2), 8.88 (d, *J* = 4.5 Hz, 4H, b2$^{\#}$), 8.33 (s, 8H, o), 8.27 (s, 8H, o), 8.01 (m, 8H, p), 4.17 (s, 2H, c), 1.54–0.82 (m, 624H, THS) ppm. **MALDI-ToF *m/z*** 6785.39 (calculated for $[C_{430}H_{682}N_{16}Si_{16}Zn_4]^+$: 6786.74).

CPDMS-*l*-P6[b_4e]-CPDMS:

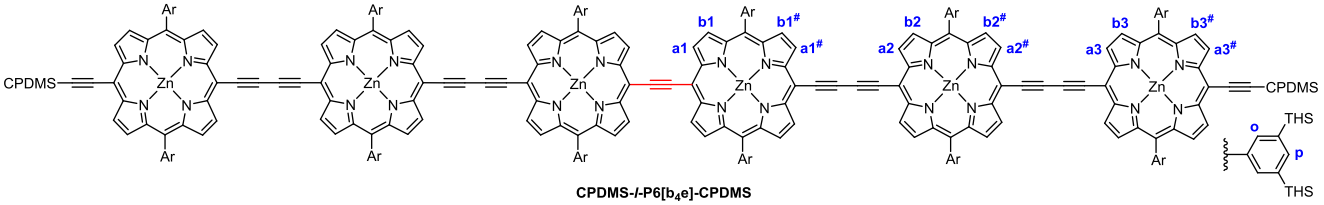

CPDMS-*l*-P6[b_4e]-CPDMS

HC_2-*l*-P4[b_2e]-C_2H· (60 mg, 7.8 μmol) and **HC_2-P1-CPDMS** (156 mg, 78 μmol) were dissolved in dry toluene (15 mL). $Pd(PPh_3)_2Cl_2$ (8.4 mg, 12 μmol), CuI (23 mg, 0.12 mmol), and 1,4-benzoquinone (92 mg, 0.85 mmol) were dissolved in a mixture of dry toluene (15 mL) and dry *i*-Pr_2NH (2 mL). The porphyrin solution was added to the catalyst solution. The mixture was stirred at room temperature and monitored by TLC. After 3 h, the mixture was filtered through a plug (SiO_2; $CHCl_3$ + 1% pyridine). The solvents were removed and the residue was purified by SEC (toluene + 1% pyridine) and further purified by recycling GPC (toluene + 1% pyridine) to afford **CPDMS-*l*-P6[b_4e]-CPDMS** (57 mg, 68%) as a brown solid.

^{1}H NMR (400 MHz, $CDCl_3$, 298 K): δ_H 10.38 (d, *J* = 4.5 Hz, 4H, a1), 9.98 (m, 16H, a1$^{\#}$,2,2$^{\#}$,3), 9.68 (d, *J* = 4.5 Hz, 4H, a3$^{\#}$), 9.10 (d, *J* = 4.5 Hz, 4H, b1), 9.03 (m, 16H, b1$^{\#}$,2,2$^{\#}$,3), 8.94 (d, *J* = 4.5 Hz, 4H, b3$^{\#}$), 8.39 (s, 8H, o), 8.37 (s, 8H, o), 8.31 (s, 8H, o), 8.05 (m, 12H, p), 2.58 (t, *J* = 6.9 Hz, 4H, CPDMS-CH_2), 2.15 (m, 4H, CPDMS-CH_2), 1.52–0.83 (m, 936H, THS), 1.21 (m, 4H, CPDMS-CH_2), 0.63 (s, 12H, CPDMS-CH_2) ppm. **^{13}C NMR (125 MHz, $CDCl_3$, 298 K):** δ_C 153.5, 13.2, 152.8,152.3, 151.0, 150.8, 150.7, 143.6, 140.9, 140.7, 140.3, 139.5, 135.4, 135.3, 133.6, 133.3, 131.2, 125.2, 124.7, 122.6, 119.8, 101.4, 100.9, 96.3, 87.6, 82.7, 33.7, 31.8, 24.2, 22.9, 21.1, 20.9, 16.3, 14.4, 14.3, 12.8, −1.3 ppm. **MALDI-ToF *m/z*** 10441 (calculated for $[C_{658}H_{1044}N_{26}Si_{26}Zn_6]^+$: 10441). **UV-vis-NIR (toluene + 1% pyridine) λ_{max} (log ε):** 832 (5.53), 593 (4.72), 493 (5.76), 464 (5.81).

HC_2-*l*-P6[b_4e]-C_2H:

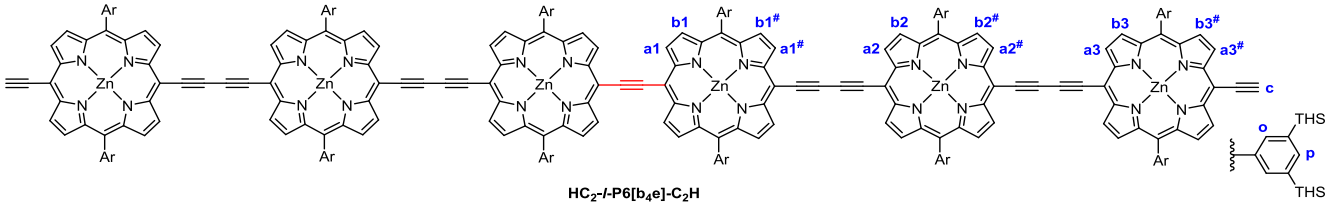

HC_2-*l*-P6[b_4e]-C_2H

CPDMS-*l*-P6[b_4e]-CPDMS (18 mg, 1.7 μmol) was dissolved in CH_2Cl_2 (2 mL) and pyridine (0.05 mL). TBAF (1.0 M in THF, 26 μL, 26 μmol) was added. The reaction mixture was stirred for 20 min at room temperature before it was passed through a plug (SiO_2; $PE_{40\text{-}60}/CH_2Cl_2$ 3:1 + 1% pyridine). The solvents were removed *in vacuo* to afford **HC_2-*l*-P6[b_4e]-C_2H** (17 mg, 100%) as a brown solid.

^{1}H NMR (400 MHz, $CDCl_3$, 298 K): δ_H 10.34 (d, *J* = 4.5 Hz, 4H, a1), 9.90 (m, 16H, a1#,2,2#,3), 9.67 (d, *J* = 4.5 Hz, 4H, a3#), 9.03 (d, *J* = 4.5 Hz, 4H, b1), 8.97 (m, 16H, b1#,2,2#,3), 8.89 (d, *J* = 4.5 Hz, 4H, b3#), 8.35 (s, 8H, o), 8.32 (s, 8H, o), 8.28 (s, 8H, o), 8.01 (m, 12H, p), 4.18 (s, 2H, c), 1.53–0.83 (m, 936H) ppm. **MALDI-ToF *m/z*** 10191.76 (calculated for $[C_{646}H_{1022}N_{24}Si_{24}Zn_6]^+$: 10191.10)

***c*-P6[b_5e]·T6:**

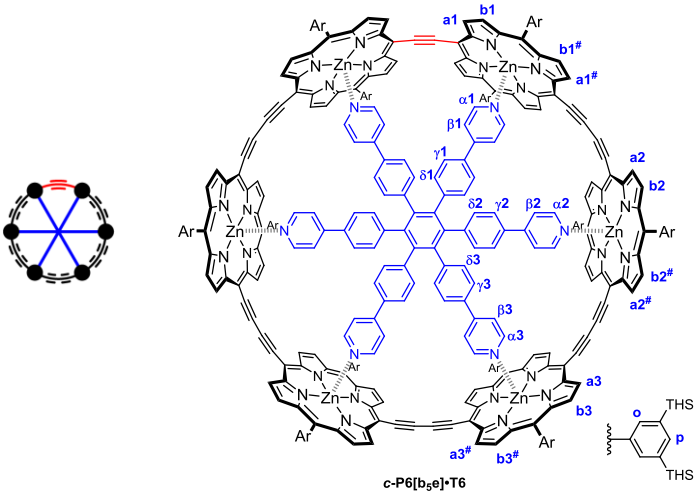

c-P6[b_5e]•T6

HC_2-*l*-P6[b_4e]-C_2H (13 mg, 1.3 μmol) was dissolved in dry $CHCl_3$ (14 mL) and dry *i*-Pr_2NH (1.2 mL). **T6** (2.6 mg, 2.6 μmol) was dissolved in $CHCl_3$ (3 mL) and added to the porphyrin hexamer solution under inert atmosphere. Complex formation was confirmed by UV-vis-NIR spectroscopy. A catalyst mixture of $Pd(PPh_3)_2Cl_2$ (90 mg, 0.13 mmol), CuI (24 mg, 0.13 mmol) and 1,4-benzoquinone (14 mg, 0.13 mmol) was added as solids and the reaction progress was monitored by UV-vis-NIR spectroscopy. After 4 h, the mixture was passed through a plug (SiO_2; $CHCl_3$ + 1% pyridine). The solvents were removed and the residue was purified by SEC (toluene + 1% pyridine) and further purified by recycling GPC (toluene + 1% pyridine) to afford ***c*-P6[b_5e]·T6** (5.4 mg, 37%) as a red-brown solid.

^{1}H NMR (500 MHz, $CDCl_3$, 298 K): δ_H 10.02 (d, *J* = 4.4 Hz, 4H, a1), 9.43 (m, 16H, a2–3), 9.37 (d, *J* = 4.4 Hz, 4H, a1#), 8.79 (d, *J* = 4.4 Hz, 4H, b1), 8.67 (m, 16H, b2–3), 8.59 (d, *J* = 4.4 Hz, 4H, b1#), 8.31 (s, 8H, o'2,3), 8.28 (s, 4H, o'1), 7.96 (s, 4H, p1/p2/p3), 7.95 (shoulder, 4H, o1), 7.94 (s, 8H, p1/p2/p3), 7.91 (br s, 8H, o2,3), 5.50 (d, *J* = 8.7 Hz, 4H, δ3), 5.44 (d, *J* = 8.4 Hz, 4H, δ2), 5.35 (d, *J* = 8.7 Hz, 4H, γ3), 5.33 (d, *J* = 8.7 Hz, 4H, γ2), 5.25 (d, *J* = 8.7 Hz, 4H, δ1), 5.16 (d, *J* = 8.1 Hz, 4H, γ 1), 4.81 (m, 8H, β2,3), 4.68 (d, *J* = 6.4 Hz, 4H, β1), 2.06 (d, *J* = 5.8 Hz, 4H, α1), 1.95 (m, 8H, α2,3), 1.47–0.72 (m, 936H, THS) ppm. **MALDI-ToF *m/z*** 11184 (calculated for $[C_{718}H_{1068}N_{30}Si_{24}Zn_6]^+$: 11186). **UV-vis-NIR (toluene) λ_{max} (log ε):** 967 (4.88), 874 (5.78), 831 (5.83), 790 (5.69), 505 (6.04), 441 (5.77).

***c*-P6[b$_5$e]:**

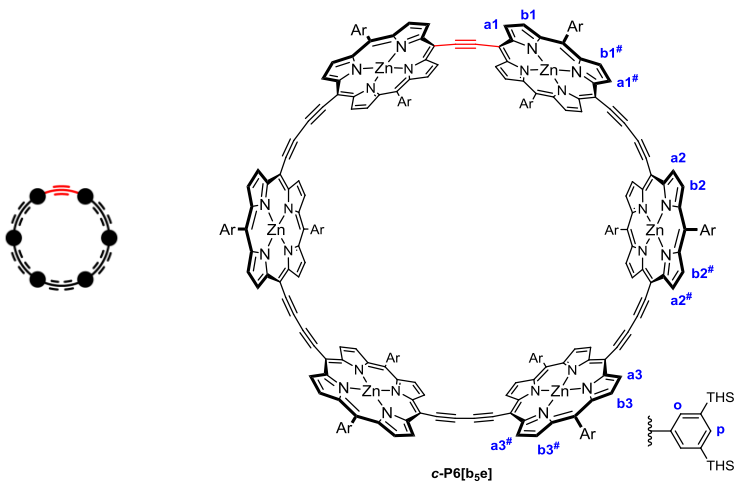

A solution of freshly recrystallized DABCO in toluene (260 mg/mL) was prepared. A SEC column (toluene) was eluted with DABCO solution (20 mL) such that the top of the column was saturated with DABCO. ***c*-P6[b$_5$e]·T6** (4.0 mg, 0.36 µmol) was dissolved in DABCO solution (0.5 mL) and loaded onto the SEC column. The column was eluted with DABCO solution (8 mL) and subsequently with toluene. The collected material was diluted to 40 mL in toluene and washed with water (4 × 50 mL). The toluene fraction was dried over $MgSO_4$ and concentrated. The material was purified on a short plug (SiO_2; $PE_{40\text{-}60}/CH_2Cl_2$ 4:1 + 1% pyridine). This procedure was repeated twice to ensure complete template removal from the nanoring to yield ***c*-P6[b$_5$e]** (3.0 mg, 83%) as a brown solid.

^{1}H NMR (500 MHz, $CDCl_3$ + 1% pyridine-d$_5$, 298 K): δ_H 10.01 (d, *J* = 4.4 Hz, 4H, a1), 9.52 (m, 20H, a1$^{\#}$,a2–3), 8.74 (d, *J* = 4.4 Hz, 4H, b1), 8.67 (m, 20H, b1$^{\#}$,b2–3), 8.07 (s, 24H, o1–3,o'1–3), 7.91 (s, 12H, p1–3), 1.47–0.72 (m, 936H, THS) ppm. **MALDI-ToF *m/z*** 10192.86 (calculated for $[C_{646}H_{1020}N_{24}Si_{24}Zn_6]^+$: 10189.09). UV-vis-NIR (toluene + 1% pyridine) λ_{max} (log ε): 803 (5.62), 610 (4.68), 502 (5.93), 442 (5.73).

3.2 Synthesis of *c*-P6[be$_5$]·T6* and *c*-P6[be$_5$]

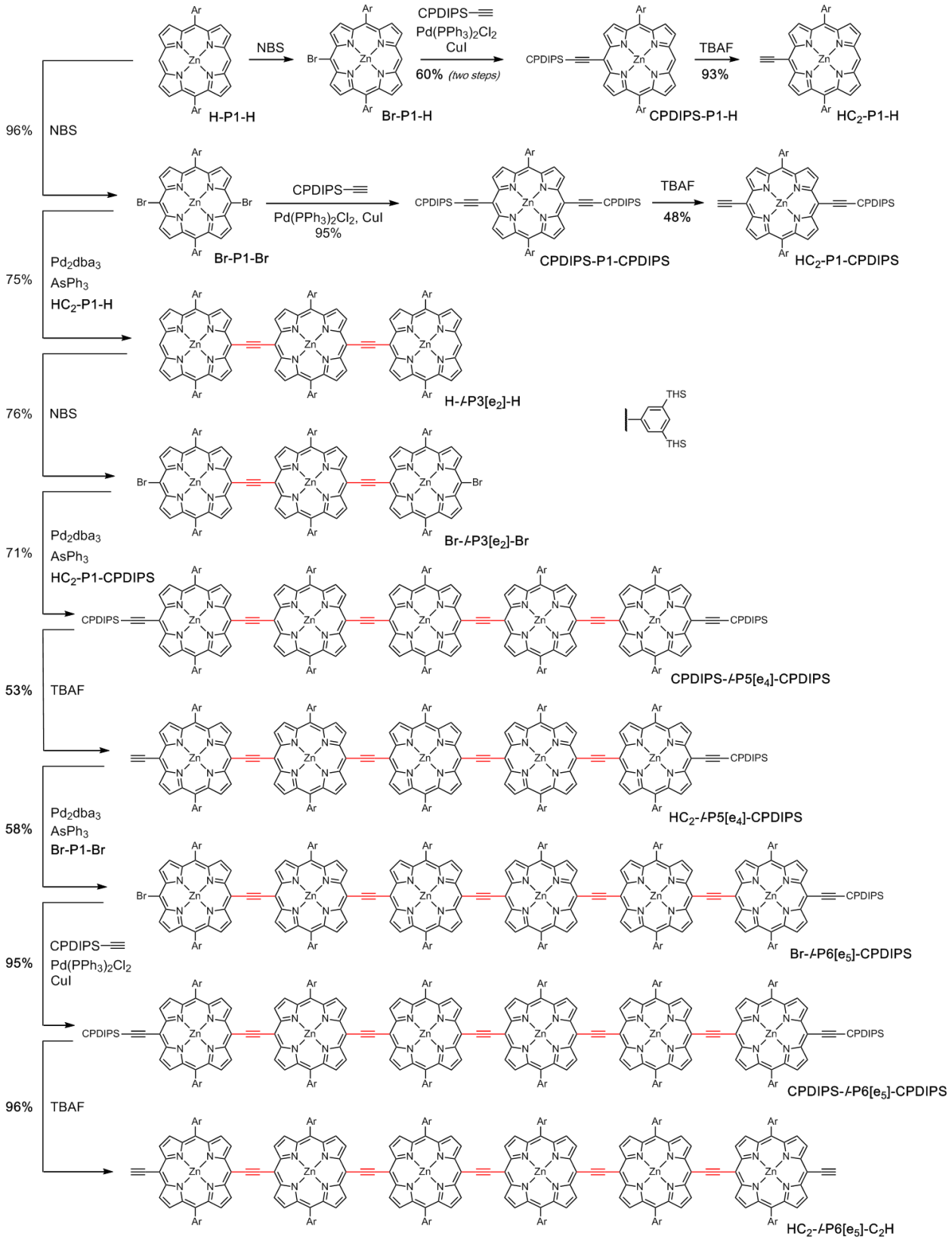

Scheme S2: Synthetic overview of linear precursor **HC$_2$-*l*-P6[e$_5$]-C$_2$H**

Br-P1-Br:

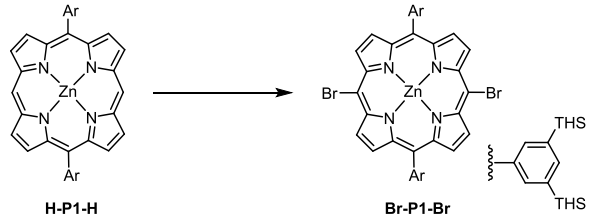

A solution of NBS (0.35 g, 2.0 mmol) in dry $CHCl_3$ (76 mL) was added to a solution of porphyrin **H-P1-H** (1.5 g, 0.9 mmol) in dry pyridine (14 mL) and dry $CHCl_3$ (60 mL) at –78 °C under inert atmosphere. The reaction mixture was stirred at –41 °C for 1 h before acetone (10 mL) was added to quench the excess of NBS. The solution was concentrated under reduced pressure, and passed through a short plug (SiO_2; $PE_{40–60}/CH_2Cl_2$ 5:1). The solvent was removed under reduced pressure to give **Br-P1-Br** (1.58 g, 96%) as a red oil.

Characterization data matched those previously reported.[2]

CPDIPS-P1-CPDIPS:

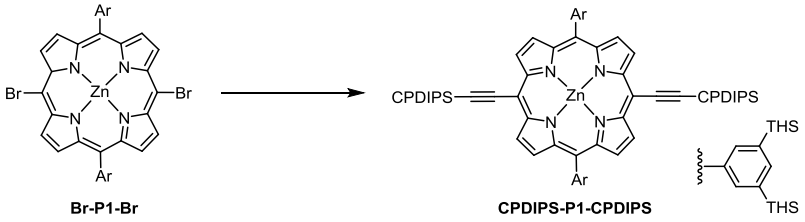

Porphyrin **Br-P1-Br** (0.83 g, 0.46 mmol) was placed in an argon flushed Schlenk flask. Dry toluene (7 mL) and dry *i*-Pr_2NH (7 mL) were added. 3-Cyanopropyldiisopropylsilylacetylene (0.48 g, 0.49 mL, 2.3 mmol) was added. The solution was freeze-pump-thaw degassed (3 cycles). While frozen, catalysts $Pd(PPh_3)_2Cl_2$ (65 mg, 0.093 mmol) and CuI (9.0 mg, 0.046 mmol) were added under a stream of argon, before performing three additional freeze-pump-thaw cycles. The solution was stirred at 50 °C for 2 h before cooling to room temperature and removing the solvents under reduced pressure. The residue was subjected to a plug (SiO_2; gradient of $PE_{40–60}/CH_2Cl_2$ 5:1 to 1:1) giving target porphyrin **CPDIPS-P1-CPDIPS** (0.90 g, 95%) as a green-purple oily solid.

Characterization data matched those previously reported.[4]

HC_2-P1-H:

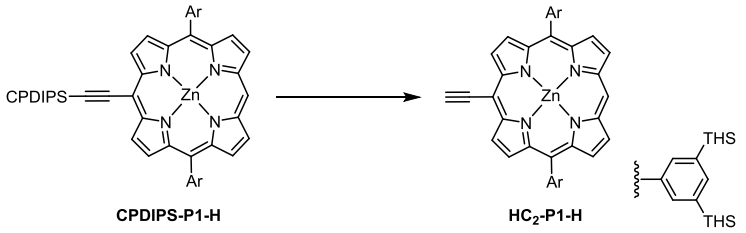

To a solution of **CPDIPS-P1-H** (1.35 g, 0.72 mmol) in dry CH_2Cl_2 (13 mL) was progressively added TBAF (1.0 M in THF, 2.50 mL, 2.50 mmol) under inert atmosphere over 15 min at room temperature until full deprotection was indicated by TLC. The reaction mixture was directly passed through a short plug (NEt_3-deactivated SiO_2; CH_2Cl_2) and the solvents removed under reduced pressure. Purification by SEC (toluene) yielded **HC_2-P1-H** (1.13 g, 93%) as a dark green oily solid.

Characterization data matched those previously reported.[3]

H-*l*-P3[e_2]-H:

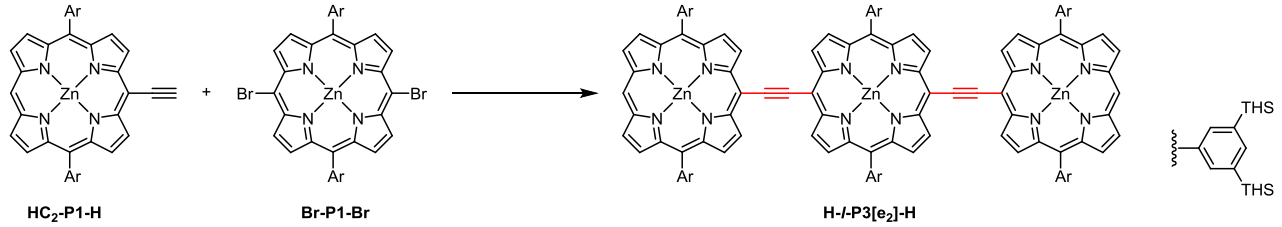

To a dried, argon flushed Schlenk-tube was added **Br-P1-Br** (0.28 mg, 0.15 mmol) and **HC_2-P1-H** (0.65 mg, 0.38 mmol) together with dry THF (40 mL) and dry NEt_3 (5 mL) before performing two consecutive freeze-pump-thaw cycles. While frozen, $Pd_2(dba)_3$ (13.5 mg, 15 µmol) and $AsPh_3$ (69 mg, 0.22 mmol) were added under a stream of argon, before performing three additional freeze-pump-thaw cycles. The solution was heated to 60 °C for 2 d before cooling to room temperature and removing the solvents under reduced pressure. A short plug (SiO_2; $PE_{40–60}/CH_2Cl_2$ 5:1) followed by SEC (toluene + 1% pyridine) yielded **H-*l*-P3[e_2]-H** (580 mg, 75%) as a dark brown oily solid.

Characterization data matched those previously reported.[3]

Br-*l*-P3[e_2]-Br:

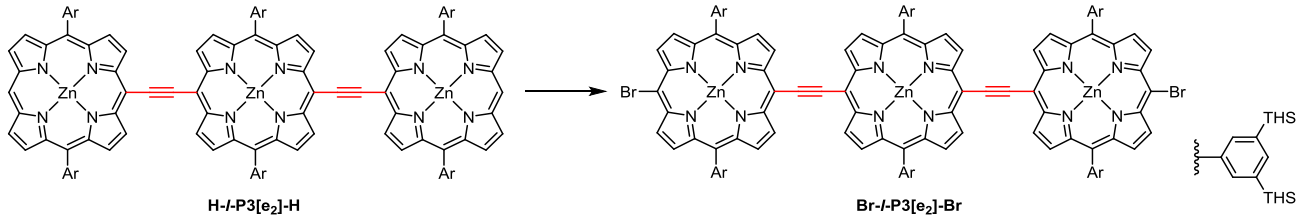

H-*l*-P3[e_2]-H (100 mg, 20 µmol) was placed in a round-bottom flask. Argon-degassed dry ethanol-stabilized $CHCl_3$ (4 mL), and dry pyridine (1.5 mL) were added before cooling to –78 °C. In a second flask, a solution of NBS (8.0 mg, 44 µmol) in argon-degassed dry ethanol-stabilized $CHCl_3$ (9 mL) was prepared and subsequently added to the first solution over 30 min at –78 °C. Stirring was continued for an additional 10 min at –78 °C. The solution was allowed to warm to –41 °C in a dry ice/MeCN bath, and stirred for 1 h. Finally, the reaction mixture was placed in an ice bath at 0 °C for 45 min. The course of the reaction was monitored by ^{1}H NMR of reaction aliquots. The reaction mixture was subjected directly to a short plug (SiO_2; $PE_{40–60}/CH_2Cl_2$ 5:1) yielding **Br-*l*-P3[e_2]-Br** (78 mg, 76%) as a dark brown oily solid.

Characterization data matched those previously reported.[3]

CPDIPS-*l*-P5[e_4]-CPDIPS:

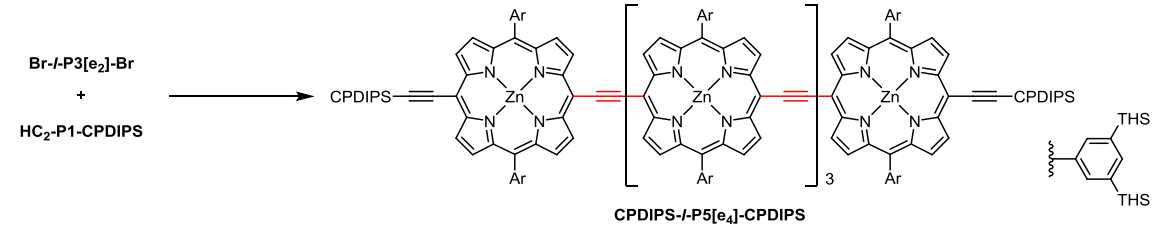

To a dried, argon flushed Schlenk-tube was added **Br-*l*-P3[e_2]-Br** (68 mg, 13 µmol) and **HC_2-P1-CPDIPS** (100 mg, 53 µmol) together with dry THF (3.5 mL) and dry NEt_3 (0.5 mL) before performing two consecutive freeze-pump-thaw cycles. While frozen, $Pd_2(dba)_3$ (1.2 mg, 1.3 µmol) and $AsPh_3$ (6.0 mg, 19.5 µmol) were added under a stream of argon, before performing three additional freeze-pump-thaw cycles. The solution was heated to 60 °C for 2 d before cooling to room temperature and removing the solvents under reduced pressure. A short plug (NEt_3-deactivated SiO_2; gradient of $PE_{40–60}/CH_2Cl_2$ 50:1 to 5:1), and subsequent short SEC (toluene + 1% pyridine) and recycling GPC (toluene + 1% pyridine) yielded **CPDIPS-*l*-P5[e_4]-CPDIPS** (82 mg, 71%) as a dark brown oily solid.

Characterization data matched those previously reported.[3]

HC_2-*l*-P5[e_4]-CPDIPS:

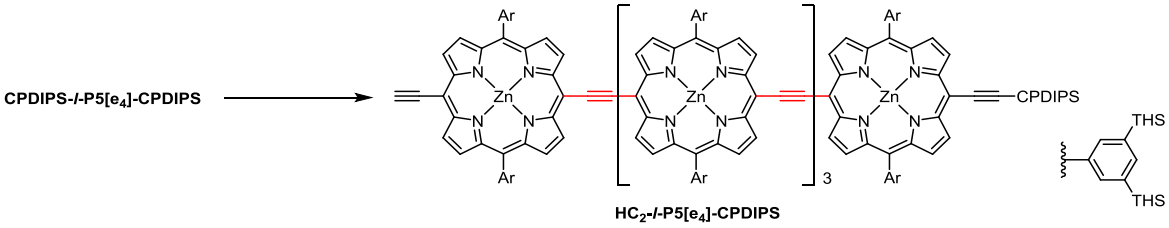

To a solution of **CPDIPS-*l*-P5[e_4]-CPDIPS** (0.151 g, 17.2 µmol) in dry CH_2Cl_2 (9 mL), dry ethanol-stabilized $CHCl_3$ (4.5 mL) and dry pyridine (0.1 mL) was progressively added TBAF (1.0 M in THF, 0.17 mL, 0.17 mmol) under inert atmosphere over 15 min at 0 °C. The course of the reaction was monitored by TLC. The reaction mixture was subjected directly to a short plug (NEt_3-deactivated SiO_2; $CHCl_3$) to quench the excess of TBAF and purified by flash column chromatography (NEt_3-deactivated SiO_2; gradient: $PE_{40–60}$, $PE_{40–60}/CH_2Cl_2$ 40:1 to 10:1) yielding **HC_2-*l*-P5[e_4]-CPDIPS** (78 mg, 53%) as a dark brown oily solid.

Characterization data matched those previously reported.[3]

Br-*l*-P6[e_5]-CPDIPS:

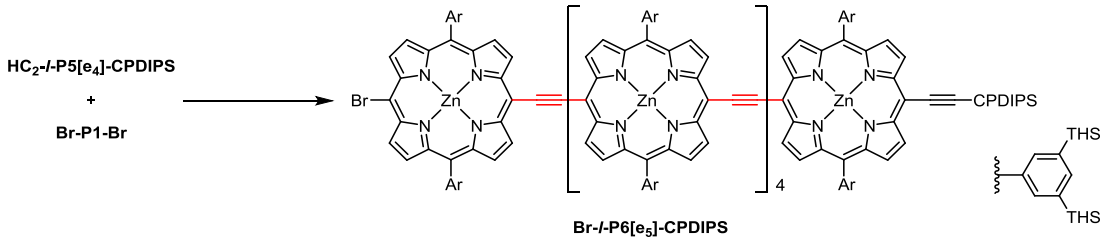

To a dried, argon flushed Schlenk-tube was added **HC_2-*l*-P5[e_4]-CPDIPS** (97 mg, 11.3 µmol) and **Br-P1-Br** (102 mg, 56.4 µmol) together with dry THF (3.5 mL) and dry NEt_3 (0.5 mL) before performing two consecutive freeze-pump-thaw cycles. While frozen, $Pd_2(dba)_3$ (1.0 mg, 1.1 µmol) and $AsPh_3$ (5.2 mg, 17 µmol) were added under a stream of argon, before performing three additional freeze-pump-thaw cycles. The solution was heated to 60 °C for 3 d before cooling to room temperature and removing the solvents under reduced pressure. A short plug (NEt_3-deactivated SiO_2; CH_2Cl_2), and subsequent short SEC (toluene) and recycling GPC (toluene + 1% pyridine) yielded **Br-*l*-P6[e_5]-CPDIPS** (67 mg, 58%) as a dark brown oily solid.

Characterization data matched those previously reported.[3]

CPDIPS-*l*-P6[e_5]-CPDIPS:

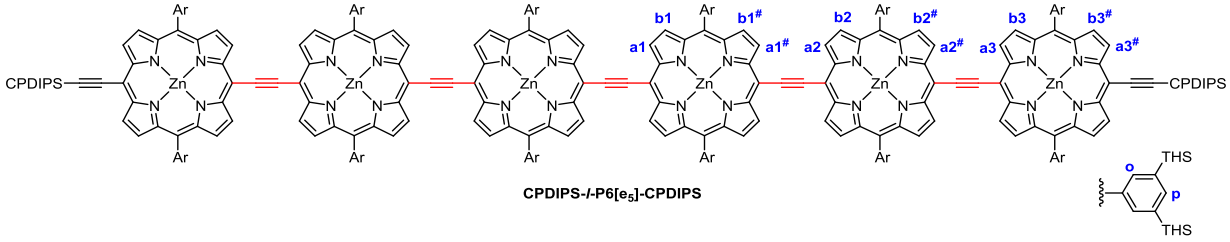

To a dried, argon flushed Schlenk-tube was added **Br-*l*-P6[e_5]-CPDIPS** (13.0 mg, 1.26 µmol) and acetylene-CPDIPS (1.30 mg, 6.29 µmol) together with dry toluene (2 mL) and dry *i*-Pr_2NH (1 mL) before performing three consecutive freeze-pump-thaw cycles. While frozen, $Pd(PPh_3)_2Cl_2$ (177 µg, 20 mol%), and CuI (30 µg, 10 mol%) were added under a stream of argon, before performing three additional freeze-pump-thaw cycles. The solution was heated to 50 °C for 2 h before cooling to room temperature and removing the solvents under reduced pressure. The residue was subjected to a plug (NEt_3-deactivated SiO_2; $PE_{40–60}/CH_2Cl_2$ 1:1) giving target **CPDIPS-*l*-P6[e_5]-CPDIPS** (12.5 mg, 95%) which was directly used in the next step.

^{1}H NMR (400 MHz, $CDCl_3$, 298 K): δ_H 10.36–10.31 (m, 20H, a1–2,a3), 9.64 (d, *J* = 4.4 Hz, 4H, a3$^{\#}$), 9.03–8.99 (m, 20H, b1–2,b3), 8.87 (d, *J* = 4.4 Hz, 4H, b3$^{\#}$), 8.38 (s, 8H, o), 8.36 (s, 8H, o), 8.29 (s, 8H, o), 8.02–8.00 (m, 12H, p), 2.57 (t, *J* = 7.2 Hz, 4H, CPDIPS-CH_2), 2.26–2.18 (m, 4H, CPDIPS-CH), 1.54–0.70 (m, 968H, THS, CPDIPS) ppm. **MALDI-ToF *m/z*** 10453 (calculated for $[C_{658}H_{1060}N_{26}Si_{26}Zn_6]^+$: 10458). **UV-vis-NIR (toluene + 1% pyridine) λ_{max} (log ε):** 873 (4.88), 498 (5.15), 440 (5.01).

HC_2-*l*-P6[e_5]-C_2H:

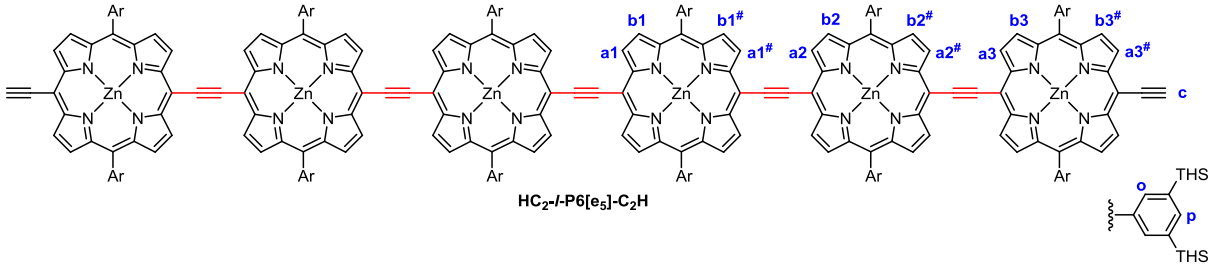

To a solution of **CPDIPS-*l*-P6[e_5]-CPDIPS** (12.5 mg, 1.20 µmol) in dry CH_2Cl_2 (2.0 mL) and dry pyridine (20 µL) was progressively added TBAF (1.0 M in THF, 7.2 µL, 7.2 µmol) at room temperature and stirred for 15 min. The course of the reaction was monitored by TLC. The reaction mixture was subjected directly to a short plug (NEt_3-deactivated SiO_2; CH_2Cl_2) yielding **HC_2-*l*-P6[e_5]-C_2H** (12 mg, 96%) as a dark brown meta-solid. Due to the tendency to homo-couple in the presence of oxygen, the target is best directly subjected to cyclization.

^{1}H NMR (400 MHz, $CDCl_3$, 298 K): δ_H 10.37–10.33 (m, 20H, a1–2,a3), 9.68 (d, *J* = 4.4 Hz, 4H, a3$^{\#}$), 9.04–9.01 (m, 20H, b1–2,b3), 8.89 (d, *J* = 4.4 Hz, 4H, b3$^{\#}$), 8.38 (s, 8H, o), 8.37 (s, 8H, o), 8.31 (s, 8H, o), 8.03–8.01 (m, 12H, p), 4.18 (s, 2H, c), 1.56–0.71 (m, 936H, THS) ppm.

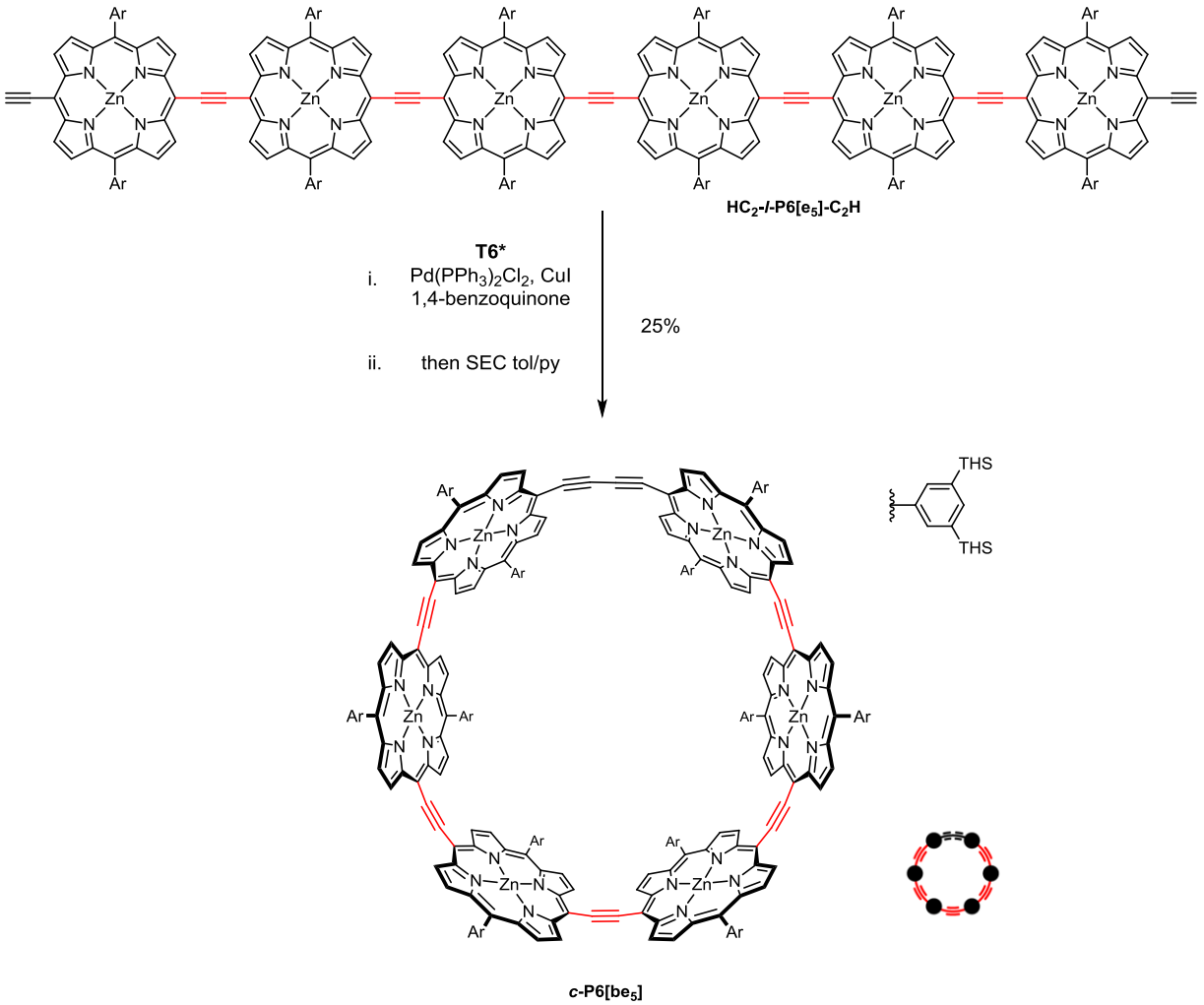

Scheme S3: Synthetic overview of ***c*-P6[be$_5$]**.

***c*-P6[be$_5$]·T6*:**

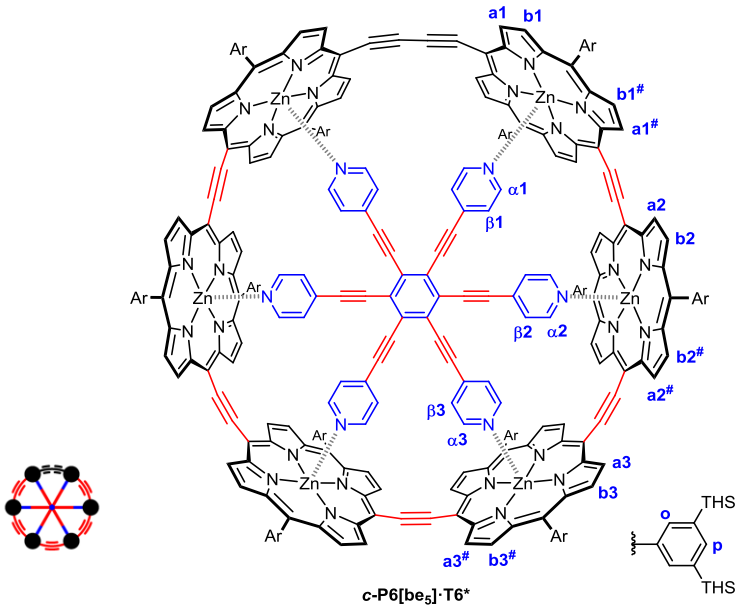

To a dried, argon flushed Schlenk-tube was added **HC$_2$-*l*-P6[e$_5$]-C$_2$H** (12.0 mg, 1.19 µmol) and **T6*** (2.44 mg, 3.57 µmol) together with dry, ethanol-stabilized $CHCl_3$ (10 mL) and dry *i*-Pr_2NH (0.5 mL) before degassing by a stream of argon and stirring for 15 min at room temperature. Under counter-flow, 1,4-benzoquinone (10 mg, 92 µmol), $Pd(PPh_3)_2Cl_2$ (10 mg, 14 µmol) and CuI (10 mg, 52 µmol) were added and degassing continued for 5 min. The solution stirred at room temperature for 1.5 h before removing the solvents under reduced pressure. The residue was subjected to a short plug (NEt_3-deactivated SiO_2, $PE_{40–60}/CH_2Cl_2$ 1:1), and subsequent short SEC (toluene) and recycling GPC (toluene + 1% pyridine) giving target ring ***c*-P6[be$_5$]·T6*** (3.2 mg, 25%) as a brown solid.

^{1}H NMR (700 MHz, $CDCl_3$, 298 K): δ_H 9.93 (d, J = 4.2 Hz, 4H, a1$^{\#}$), 9.90 (dd, *J* = 8.9, 4.4 Hz, 16H, a2–3), 9.36 (d, *J* = 4.3 Hz, 4H, a1), 8.66 (d, *J* = 4.2 Hz, 4H, b1$^{\#}$), 8.61 (d, *J* = 4.8 Hz, 16H, b2–3), 8.49 (d, *J* = 4.3 Hz, 4H, b1), 8.06 (s, 8H, o'2,3), 8.02 (s, 4H, o'1), 7.92–7.90 (m, 20H, o1–3,p2,3), 7.88 (s, 4H, p1), 4.40 (d, *J* = 6.1 Hz, 4H, β1), 4.21 (d, *J* = 6.4 Hz, 8H, β2,3), 2.00 (t, *J* = 6.1 Hz, 8H, α2,3), 1.94 (d, *J* = 5.8 Hz, 4H, α1), 1.58–0.46 (m, 936H, THS) ppm. **MALDI-ToF *m/z*** 10774 (calculated for $[C_{686}H_{1044}N_{30}Si_{24}Zn_6]^+$: 10778). **UV-vis-NIR (toluene + 1% pyridine) λ_{max} (log ε):** 436 (5.39), 500 (5.74), 853 (5.45), 899 (5.40), 955 (5.15).

***c*-P6[be$_5$]:**

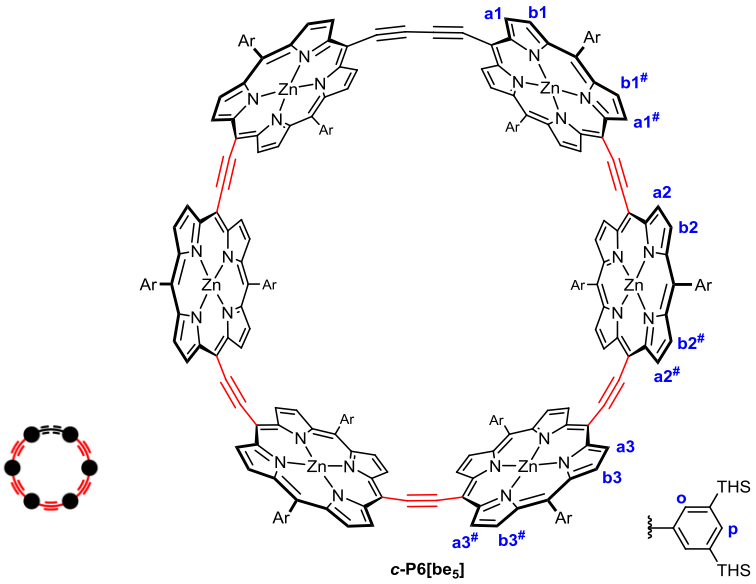

To remove the template, ***c*-P6[be$_5$]·T6*** (3.2 mg, 0.30 µmol) was dissolved in pyridine/toluene (100:1) and subjected to repeated SEC (pre-saturated with pyridine/toluene 100:1, 4×) and another plug (NEt_3-deactivated SiO_2; $PE_{40–60}/CH_2Cl_2$ 1:1) yielding desired template-free ***c*-P6[be$_5$]** (2.9 mg, 99 %) as a brown solid.

^{1}H NMR (700 MHz, $CDCl_3$, 298 K): δ_H 9.94–9.90 (m, 20H, a1$^{\#}$,a2–3), 9.43 (d, *J* = 4.3 Hz, 4H, a1), 8.71–8.69 (m, 20H, b1$^{\#}$,b2–3), 8.62 (d, *J* = 4.4 Hz, 4H, b1), 8.02 (br s, 24H, o), 7.91–7.90 (m, 12H, p), 1.48–0.38 (m, 936H, THS) ppm. **MALDI-ToF *m/z*** 10097 (calculated for $[C_{638}H_{1020}N_{24}Si_{24}Zn_6]^+$: 10094). **UV-vis-NIR (toluene + 1% pyridine) λ_{max} (log ε):** 428 (5.45), 494 (5.81), 780 (5.36).

4 ^{1}H-NMR Assignment of *c*-P6[b$_5$e]·T6, *c*-P6[b$_5$e], *c*-P6[be$_5$]·T6* and *c*-P6[be$_5$]

In the following section, the full assignments of the ^{1}H-NMR spectra of the nanorings ***c*-P6[b$_5$e]** and ***c*-P6[be$_5$]**, with and without the template **T6(*)**, are described. All ^{1}H-NMR spectra were recorded at 298 K using a Bruker AVIII 700 instrument with $CDCl_3$ as the solvent. The 2D-NMR techniques COSY and NOESY were used to achieve full assignment of the signals. COSY correlations are indicated in blue, NOESY correlations are indicated in red. The assignment of the nanostructure will be discussed systematically.

4.1 Assignment of *c*-P6[b$_5$e]·T6

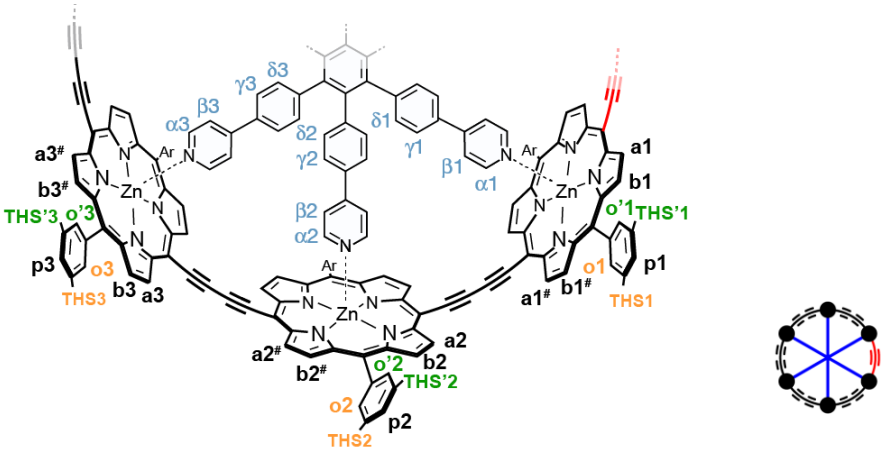

Assignment of Porphyrin 1

We can assign the 4H-doublet at 10.02 ppm with confidence to proton **a1**, on the basis of its unusual chemical shift; this enables us to assign **b1** through a COSY correlation (Figure S2). The other distinct COSY correlation in this region between two 4H-doublets is assigned to **a1$^{\#}$** and **b1$^{\#}$** (supported by NOE correlations as discussed below).

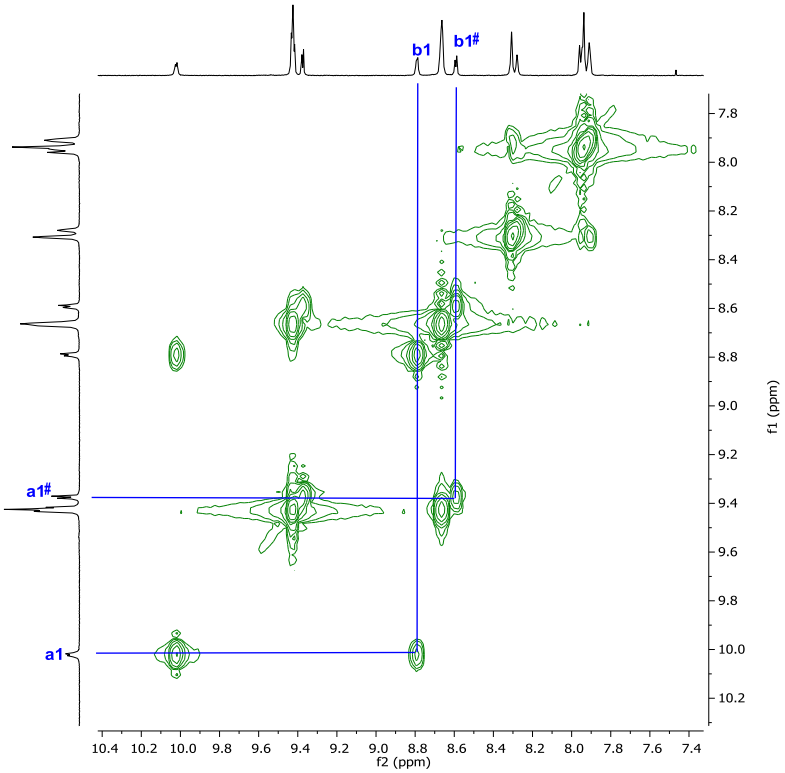

Figure S2: Region of the COSY correlation spectrum (500 MHz, $CDCl_3$, 298 K) of ***c*-P6[b_5e]·T6**, indicating the COSY correlation between proton **a1** and proton **b1** and proton **a1#** and **b1#**.

NOESY correlations from proton **a1** to **o1**, **o'1**, **α1** and **β1** (Figures S3 and S4) enable the assignment of these protons. Protons **α1** and **β1** exhibit a COSY correlation (not shown), confirming their assignment.

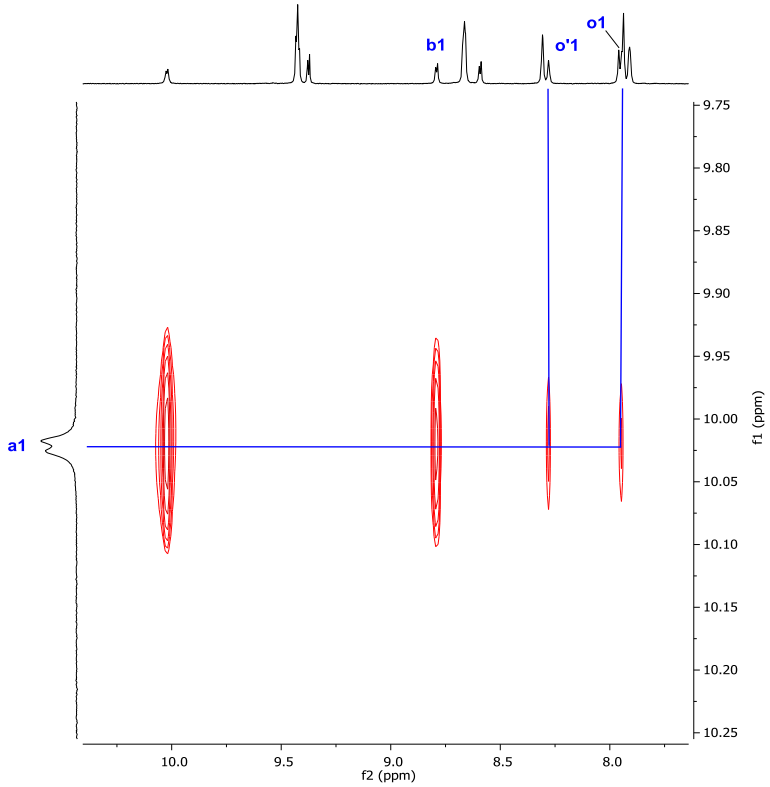

Figure S3: Region of the NOESY spectrum (500 MHz, $CDCl_3$, 298 K) of ***c*-P6[b_5e]·T6**, indicating the NOEs between proton **a1** and protons **o1** and **o'1**.

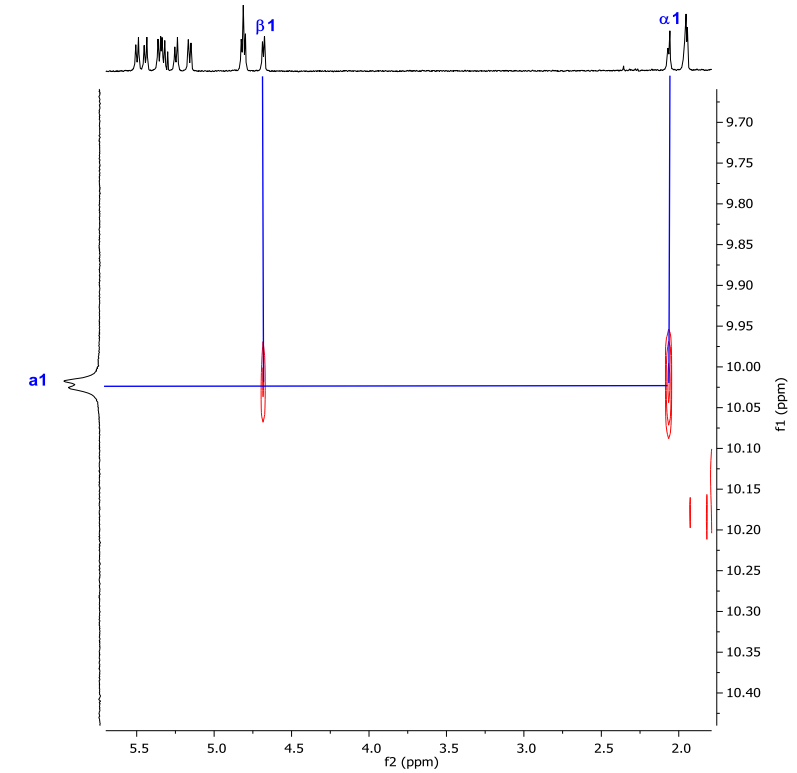

Figure S4: Region of the NOESY spectrum (500 MHz, $CDCl_3$, 298 K) of ***c*-P6[b_5e]·T6**, indicating the NOEs between proton **a1** and protons **α1** and **β1**.

NOE cross-peaks correlating **o1**/**o1'** and **a1**$^{\#}$ and **b1**$^{\#}$ confirm their assignment (Figure S5). NOEs between **o1**/**o'1** and **p1** could not be distinguished due to the overlap between **o1** and **p1**.

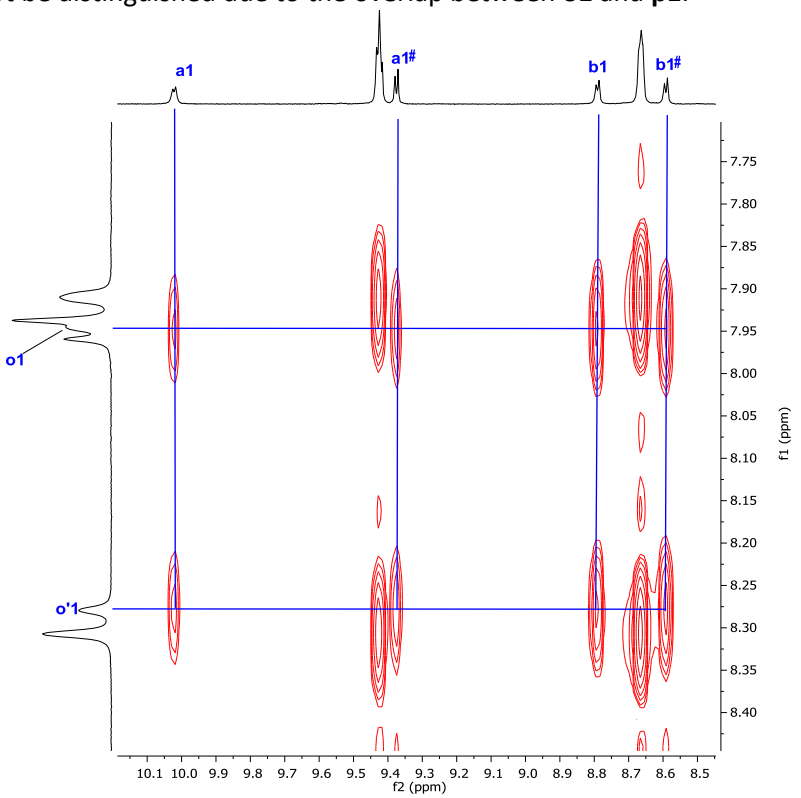

Figure S5: Region of the NOESY spectrum (500 MHz, $CDCl_3$, 298 K) of ***c*-P6[b_5e]·T6**, indicating the NOEs between protons **o1**/**o'1** and protons **a1**, **a1**$^{\#}$, **b1** and **b1**$^{\#}$.

Finally, NOEs from **α1** and **β1** to **γ1** and **δ1** (Figure S6) (and a COSY correlation from **γ1** to **δ1;** not shown), complete the assignment of porphyrin 1.

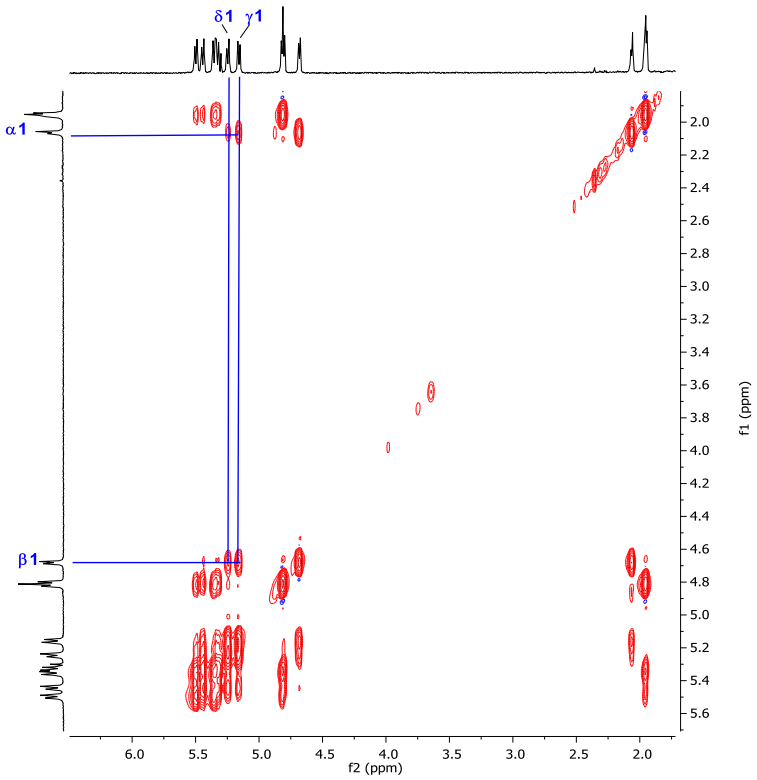

Figure S6: Region of the NOESY spectrum (500 MHz, $CDCl_3$, 298 K) of ***c*-P6[b_5e]·T6**, indicating the NOEs between protons **α1** and **β1** and protons **γ1** and **δ1**.

Assignment of Porphyrins 2 and 3

The assignment of porphyrins 2 and 3 follows from the assignment of porphyrin 1 using the COSY correlations and NOEs from the template. There are NOEs from **δ1** to **δ2** (Figure S7) enabling the identification of **δ2**, which has NOEs to **β2**,**3** and **α2**,**3** (both the **α** and **β** signals for porphyrins 2 and 3 overlap at 1.95 ppm and 4.81 ppm, respectively).

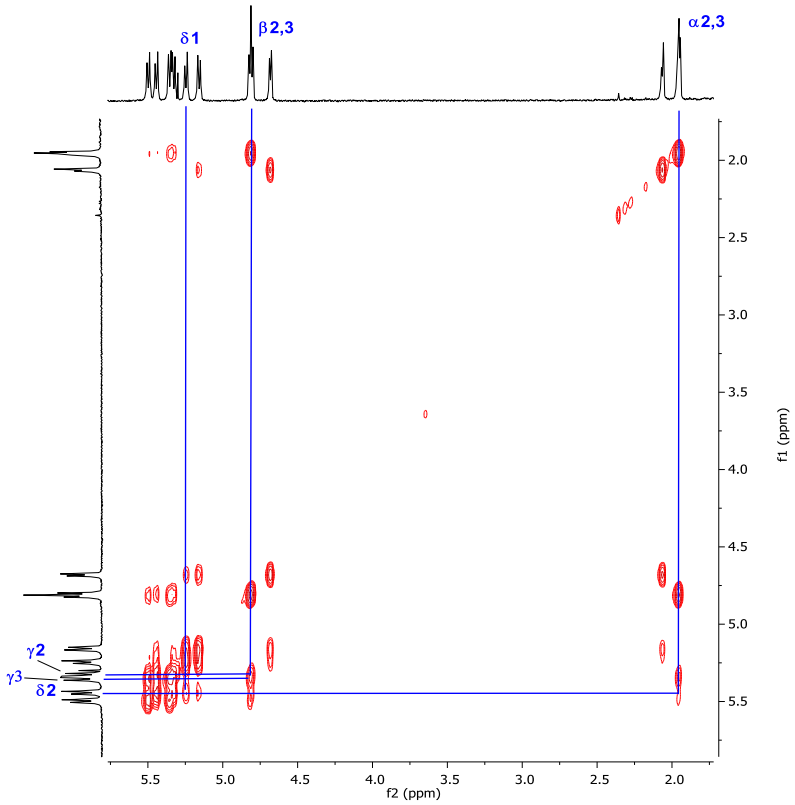

Figure S7: Region of the NOESY spectrum (500 MHz, $CDCl_3$, 298 K) of ***c*-P6[b_5e]·T6**, indicating the NOEs between protons **δ1** and **δ2** and subsequently protons **δ2** and **β2**,**3** and **α2**,**3**.

Proton **δ2** has a COSY correlation to **γ2** at 5.33 ppm (Figure S8). There is another pair of template protons displaying a COSY correlation which is assigned to **δ3** (5.50 ppm) and **γ3** (5.35 ppm). This assignment is further confirmed by NOEs from **γ2** and **γ3** to the overlapping signal **β2**,**3** (Figure S7).

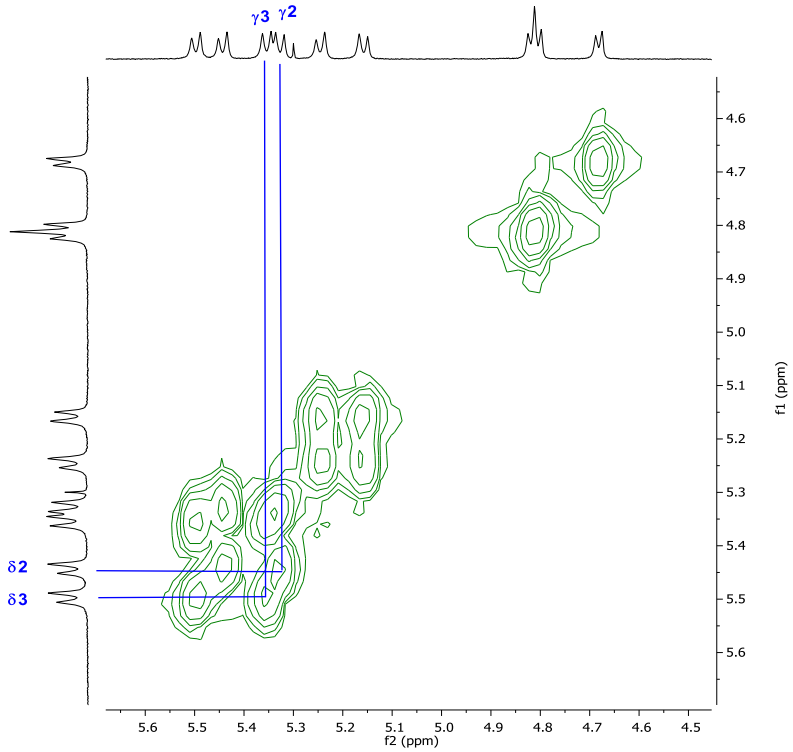

Figure S8: Region of the COSY correlation spectrum (500 MHz, $CDCl_3$, 298 K) of ***c*-P6[b$_5$e]·T6**, indicating the COSY correlation between proton **δ3** and proton **γ3** and proton **δ2** and **γ2**.

The signal at 8.31 ppm can be assigned to **o'2** and **o'3** as there is a strong NOE between the signal at 8.31 ppm and the **α2,3** signal at 1.95 ppm and a very weak NOE between the signal at 8.31 ppm and the **β2,3** signal at 4.81 ppm (Figure S9).

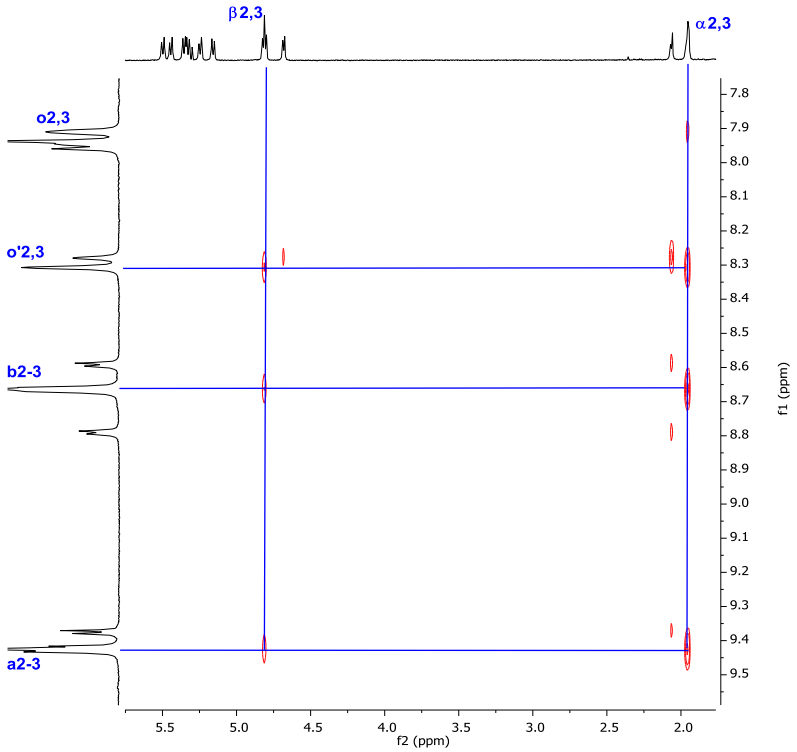

Figure S9: Region of the NOESY spectrum (500 MHz, $CDCl_3$, 298 K) of ***c*-P6[b_5e]·T6**, indicating the NOEs between protons **o'2,3** and **α2,3** and **β2,3** and NOEs between protons **α2,3** and **β2,3** to **a2–3** and **b2–3**.

The NOE between the signal at 8.31 ppm and the signal at 9.43 ppm identifies the latter as **a2–3** which itself displays a NOE to the signal at 7.91, identifying this signal as **o2**,**3** (Figure S10). This also enables the assignment of the multiplet at 8.67 as **b2–3** as this signal shows strong NOEs to **α2**,**3**, weak NOEs to **β2**,**3** (Figure S9), strong NOEs to **a2–3**, and strong NOEs to **o2**,**3** and **o'2**,**3** (Figure S10).

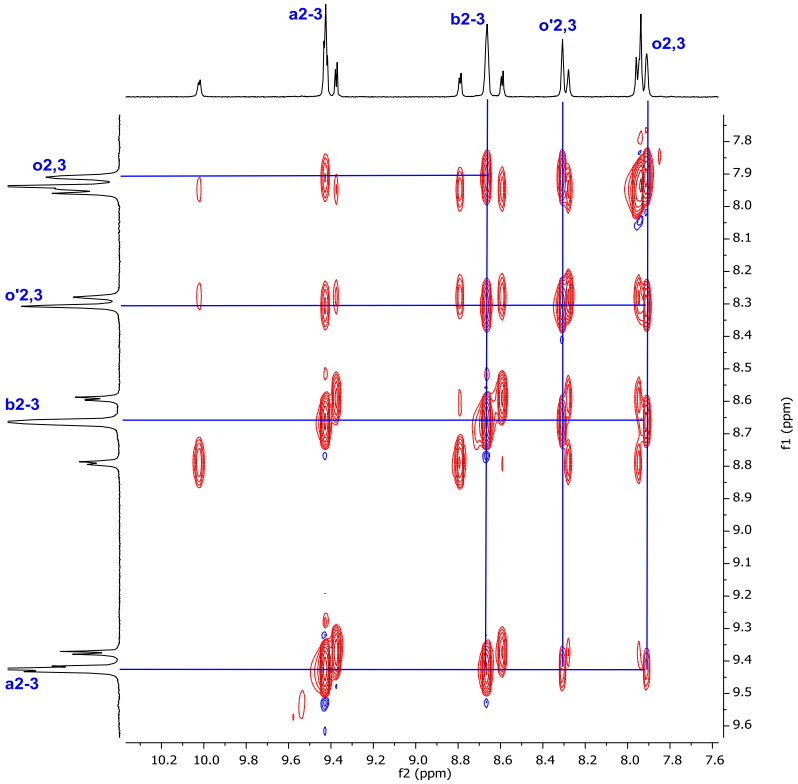

Figure S10: Region of the NOESY spectrum (500 MHz, $CDCl_3$, 298 K) of ***c*-P6[b$_5$e]·T6**, indicating the NOEs between protons **o'2**,**3** and **a2-3** which subsequently shows NOEs to **o2**,**3**, and indicating the NOEs between **b2-3** to **a2-3**, **o2**,**3** and **o'2**,**3**.

The remaining signals at 7.96 ppm and 7.94 ppm are assigned to **p1–3**. Since these signals don't display any NOE or COSY correlations, a specific assignment is not possible.

Table S1: Correlation matrix depicting the COSY and NOE correlations in the ^{1}H NMR spectrum of ***c*-P6[b$_5$e]·T6** (labels; **s**: strong correlation, **w**: weak correlation, **o**: overlapping signals).

		beta 1				aryl 1			template 1				THS 1		beta 2				aryl 2			template 2				THS 2		beta 3				aryl 3			template 3				THS 3	
		a	a#	b	b#	o	o′	p	α	β	γ	δ	T	T'	a	a#	b	b#	o	o′	p	α	β	γ	δ	T	T'	a	a#	b	b#	o	o′	p	α	β	γ	δ	T	T'
beta 1	a		-	S	-	-	-	-	-	-	-	-	-	-																										
	a#	-		-	S	-	-	-	-	-	-	-	-	-																										
	b	S	-		-	-	-	-	-	-	-	-	-	-																										
	b#	-	S	-		-	-	-	-	-	-	-	-	-																										
aryl 1	o	w	w	S	S				-	-	-	-																												
	o′	S	w	S	S	S			-	-	-	-																												
	p	-	-	-	-	-	-		-	-	-	-																												
template 1	α	S	S	S	S	-	S	-		S	-	-	-	-																										
	β	w	w	-	w	-	w	-	S		-	-	-	-																										
	γ	-	-	-	-	-	-	-	S	S		S	-	-																										
	δ	-	-	-	-	-	-	-	w	S	S		-	-																										
THS 1	T	S	S	S	S	O	O	O	-	-	-	-		-																										
	T'	S	S	S	S	O	O	O	-	-	-	-	O																												
beta 2	a												O	O		-	O	O	-	-	-	-	-	-	-	-	-													
	a#												O	O	-		O	O	-	-	-	-	-	-	-	-	-													
	b												O	O	O	O		-	-	-	-	-	-	-	-	-	-													
	b#												O	O	O	O	-		-	-	-	-	-	-	-	-	-													
aryl 2	o												O	O	O	O	O	O			-	-	-	-	-	-	-													
	o′												O	O	O	O	O	O	O		-	-	-	-	-	-	-													
	p												O	O	-	-	-	-	-	-		-	-	-	-	-	-													
template 2	α														O	O	O	O	O	O	-		S	-	-	-	-													
	β														O	O	O	O	-	O	-	S		-	-	-	-													
	γ														-	-	-	-	-	-	-	w	S		S	-	-													
	δ										w	S			-	-	-	-	-	-	-	w	S	S		-	-													
THS 2	T					O	O	O							O	O	O	O	O	O	O	-	-	-	-		-													
	T'					O	O	O							O	O	O	O	O	O	O	-	-	-	-	-														
beta 3	a												O	O			O	O	O	O		O	O			O	O		-	O	O	-	-	-	-	-	-	-	-
	a#												O	O			O	O	O	O		O	O			O	O	-		O	O	-	-	-	-	-	-	-	-
	b												O	O	O	O			O	O		O	O			O	O	O	O		-	-	-	-	-	-	-	-	-
	b#												O	O	O	O			O	O		O	O			O	O	O	O	-		-	-	-	-	-	-	-	-
aryl 3	o												O	O	O	O	O	O		O		O	-			O	O	O	O	O	O		-	-	-	-	-	-	-
	o′												O	O	O	O	O	O	O			O	O			O	O	O	O	O	O	O		-	-	-	-	-	-
	p												O	O												O	O	-	-	-	-	-	-		-	-	-	-	-
template 3	α														O	O	O	O	O	O			O	O	O			O	O	O	O	O	S	-		S	-	-	-	-
	β														O	O	O	O	-	O		O		O	O			O	O	O	O	-	w	-	S		-	-	-	-
	γ																					O	O		O			-	-	-	-	-	-	-	w	S		S	-	-
	δ																					O	O	O				-	-	-	-	-	-	-	w	S	S		-	-
THS 3	T	O	O	O	O	O	O	O							O	O	O	O	O	O	O							O	O	O	O	O	O	O	-	-	-	-		-
	T'	O	O	O	O	O	O	O							O	O	O	O	O	O	O							O	O	O	O	O	O	O	-	-	-	-	-	

4.2 Assignment of *c*-P6[b_5e]

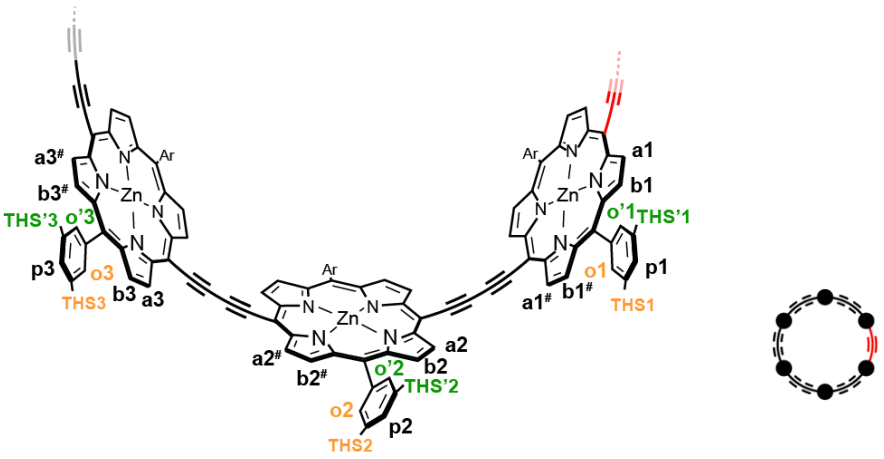

Assignment of Porphyrins 1, 2 and 3

The ^{1}H NMR spectrum of ***c*-P6[b_5e]** has more overlapping signals than its template-complex counterpart ***c*-P6[b_5e]·T6** and hence most of the individual signals cannot be assigned. We can assign the 4H-doublet at 10.01 ppm with confidence to proton **a1**; this enables us to assign **b1** through a COSY correlation (Figure S11). There is only one other distinct COSY correlation in this region between two 20H-multiplets which are overlapping signals for **a1**$^{\#}$,**a2–3** at 9.52 ppm and **b1**$^{\#}$,**b2–3** at 8.67 ppm.

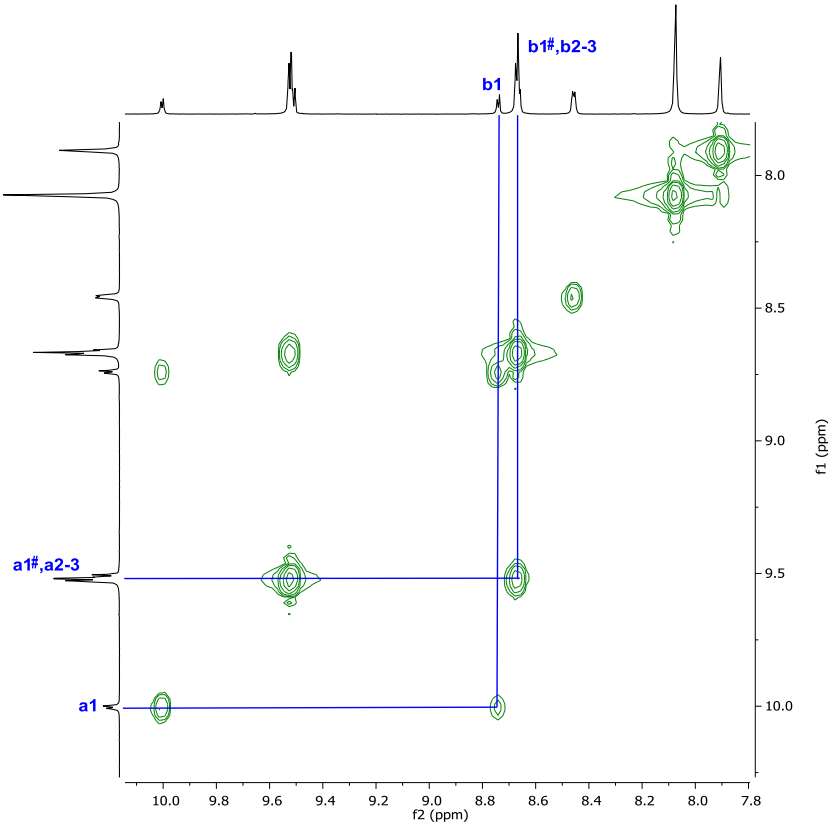

Figure S11: Region of the COSY correlation spectrum (500 MHz, $CDCl_3$ + 1% pyridine-d_5, 298 K) of ***c*-P6[b_5e]**, indicating the COSY correlation between proton **a1** and **b1** and protons **a1**$^{\#}$,**a2–3** and **b1**$^{\#}$,**b2–3**.

NOESY correlations from the 20H multiplets at 9.52 ppm and 8.67 ppm to the 24H singlet at 8.07 ppm confirms the assignment of the latter as **o1–3**, **o'1–3** (denoted in Figure S12 as **o**). A weak NOESY correlation between this singlet and the 12H singlet at 7.91 enables the assignment of this signal as **p1–3** (denoted as **p**) and completes the assignment of ***c*-P6[b$_5$e]**.

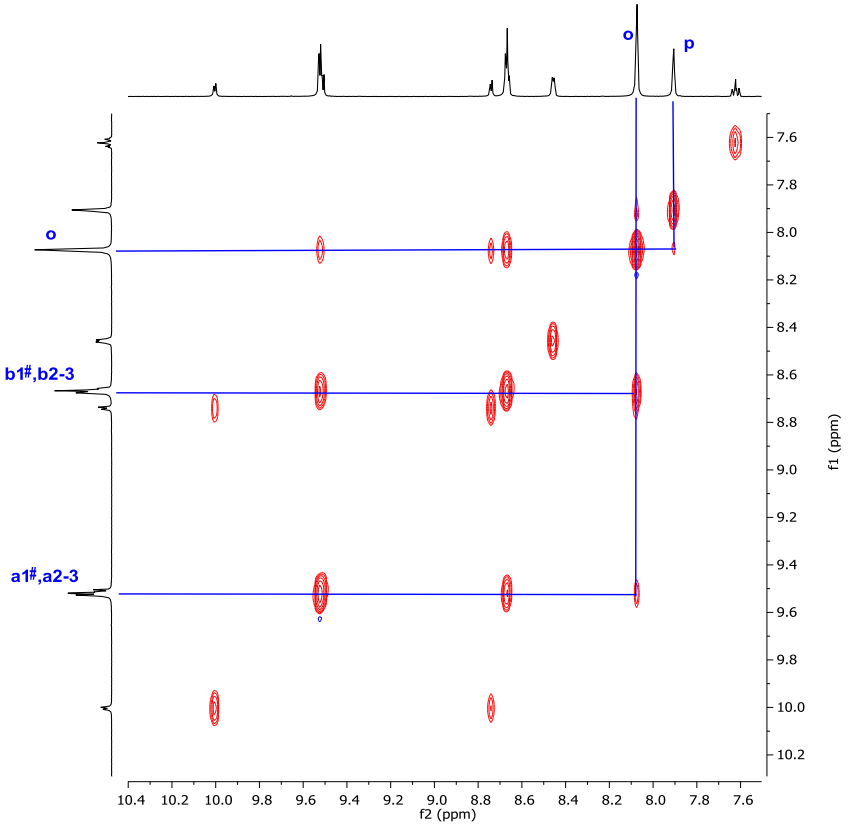

Figure S12: Region of the NOESY spectrum (500 MHz, $CDCl_3$ + 1% pyridine-d_5, 298 K) of ***c*-P6[b$_5$e]**, indicating the NOEs between protons **a1$^{\#}$,a2–3** and **b1$^{\#}$,b2–3** to **o**, and the weak NOE from **o** to **p**.

Table S2: Correlation matrix depicting the COSY and NOE correlations in the ^{1}H NMR spectrum of ***c*-P6[b$_5$e]** (labels; **s**: strong correlation, **w**: weak correlation, **o**: overlapping signals).

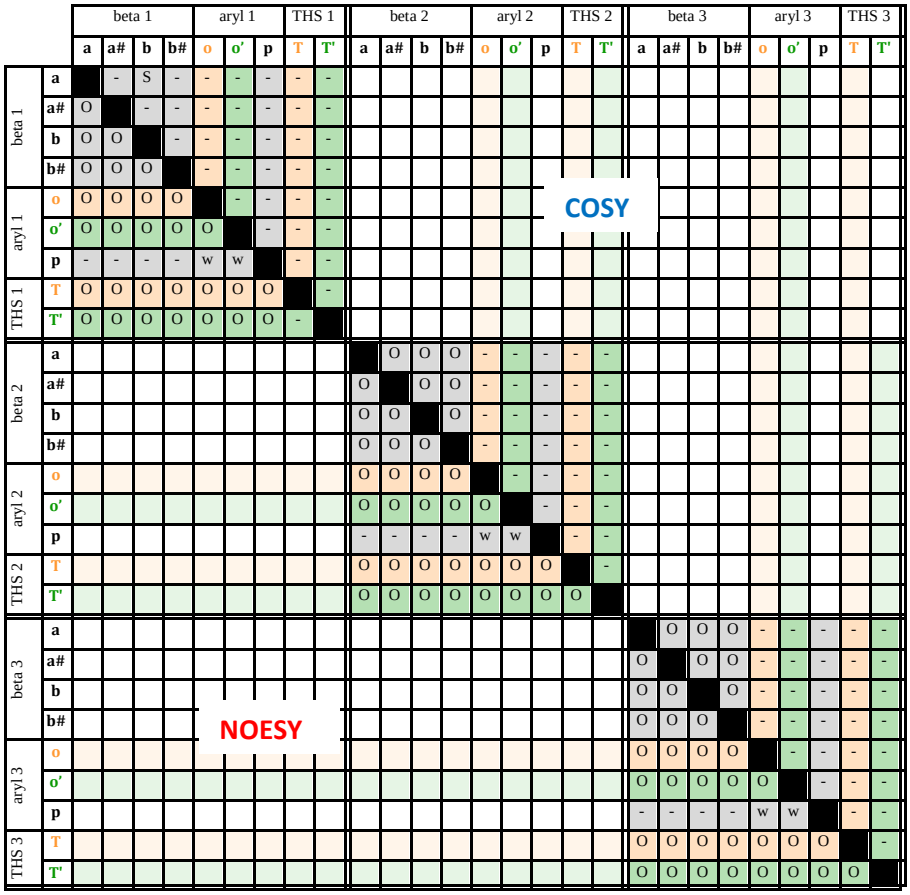

4.3 Assignment of *c*-P6[be$_5$]·T6*

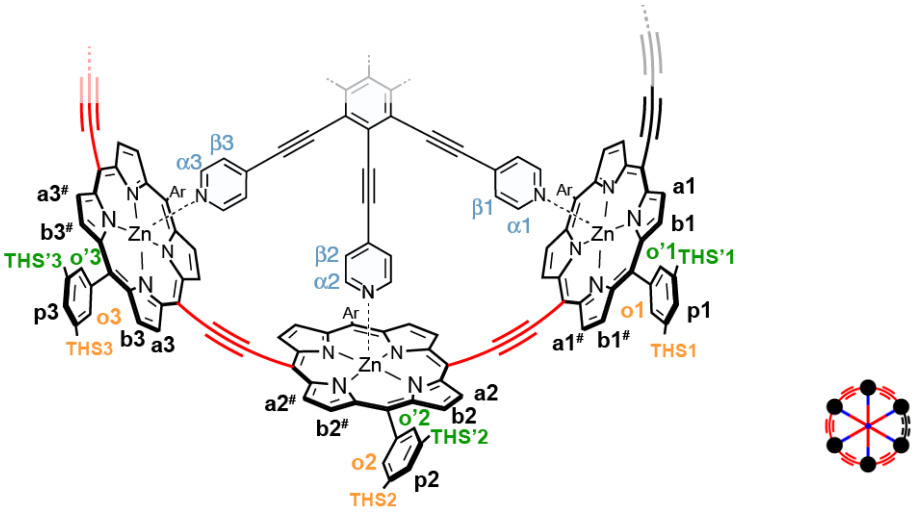

Assignment of Porphyrin 1

As we can assign the 4H-doublet at 9.36 ppm with confidence to proton **a1**, this enables us to assign **b1** through a COSY correlation as the 4H-doublet at 8.49 ppm (Figure S13). The other distinct COSY correlation in this region between two 4H doublets is assigned to **a1**$^{\#}$ and **b1**$^{\#}$ (supported by NOE correlations; Figure S14). Unlike the COSY spectrum, the NOESY also shows a weak correlation between the near *beta* protons **b1** and **b1**$^{\#}$ (Figure S14).

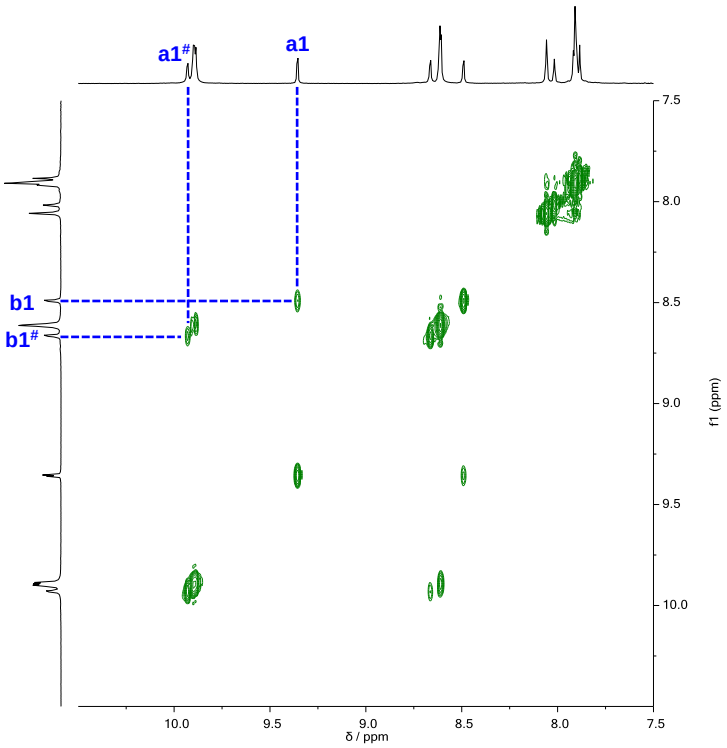

Figure S13: Region of the COSY spectrum (700 MHz, $CDCl_3$, 298 K) of ***c*-P6[be$_5$]·T6***, indicating the COSY correlations between protons **a1** and **b1**, and protons **a1**$^{\#}$ and **b1**$^{\#}$.

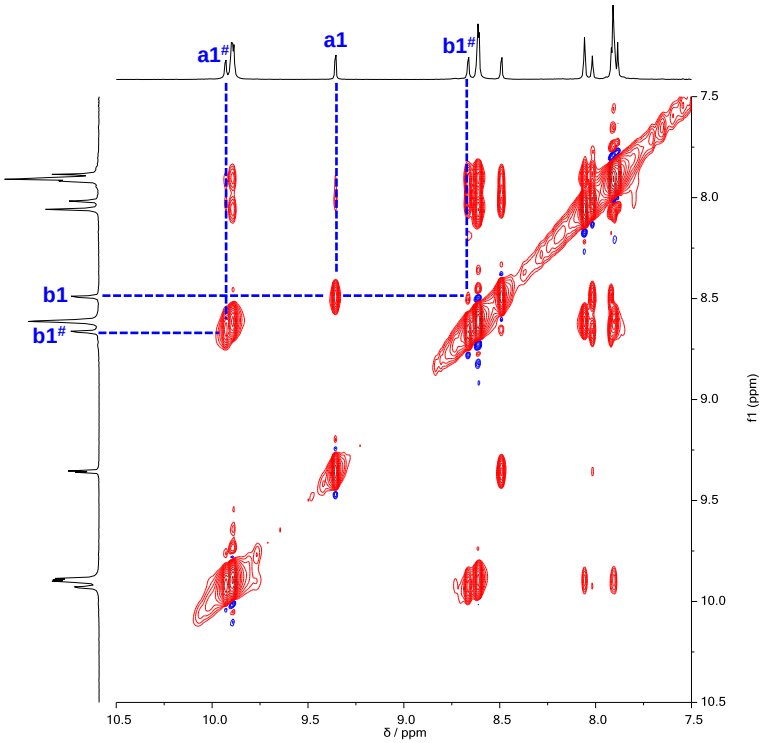

Figure S14: Region of the NOESY spectrum (700 MHz, $CDCl_3$, 298 K) of ***c*-P6[be$_5$]·T6***, indicating the NOE cross peaks correlating *beta* protons **a1** and **b1**, **a1**$^{\#}$ and **b1**$^{\#}$, and **b1** and **b1**$^{\#}$.

The signals for the aryl protons *ortho* to the porphyrin are split due to the different environments inside and outside the nanoring. The NOE cross peaks correlating the *beta* protons (**b1** and **b1**$^{\#}$) and the downfield shifted *ortho* proton at 8.02 ppm allow us to identify this 4H-singlet as **o'1**. Along the same lines, the NOE cross peaks correlating the *beta* protons (**b1** and **b1**$^{\#}$) and the upfield shifted *ortho* proton lead us to locate the proton **o1** as part of a 20H-multiplet between 7.92–7.90 ppm. In addition, the NOE cross peak correlating the proton **o'1** and the corresponding *para* proton **p1** allowed us to identify the latter as a 4H-singlet at 7.88 ppm (Figure S15).

Figure S16 shows the NOE cross peaks correlating proton **o'1** and the template resonances which enables us to identify protons **α1** at 1.94 ppm (strong correlation) and **β1** at 4.40 ppm (weak correlation). Moreover, the correlation between the template protons, namely **α1** and **β1**, is easily observable in both COSY and NOESY spectra (Figure S17).

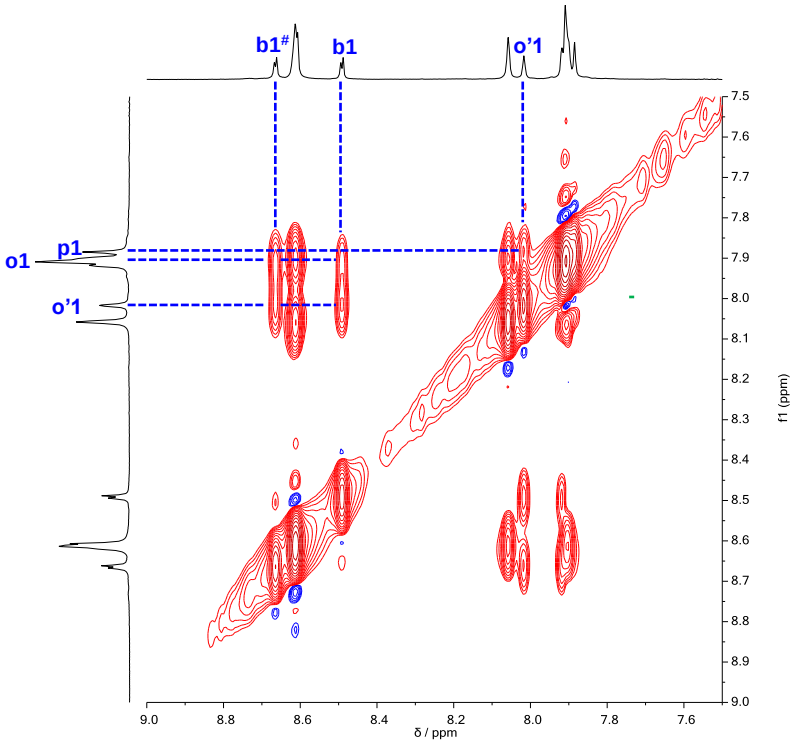

Figure S15: Region of the NOESY spectrum (700 MHz, $CDCl_3$, 298 K) of ***c*-P6[be$_5$]·T6***, indicating the NOE cross peaks correlating the *beta* (**b1** and **b1**$^{\#}$) and the *ortho* protons (**o1** and **o'1**). The proton **o'1** also correlates with the **p1**.

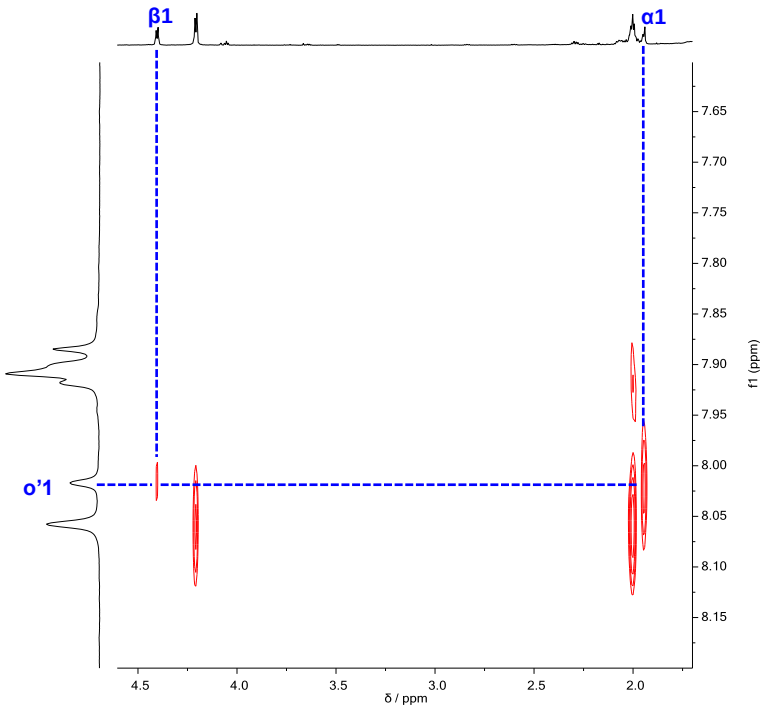

Figure S16: Region of the NOESY spectrum (700 MHz, $CDCl_3$, 298 K) of ***c*-P6[be$_5$]·T6***, indicating the NOE cross peaks correlating proton **o'1** and template resonances (**α1** and **β1**).

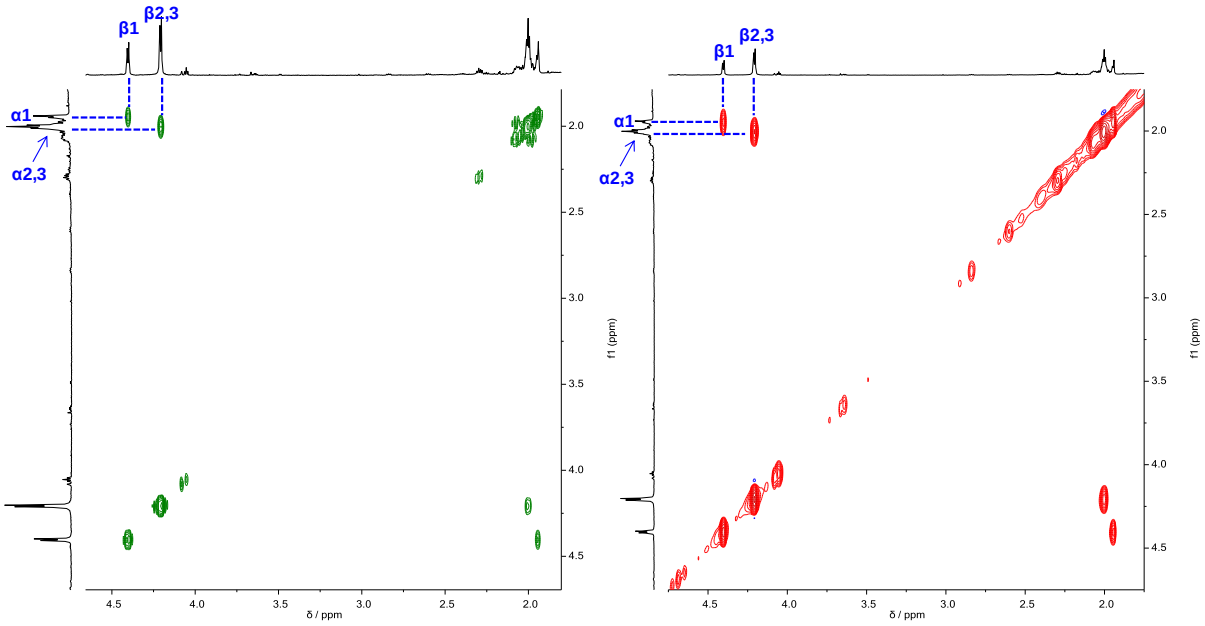

Figure S17: Region of the COSY (left) and NOESY (right) spectra (700 MHz, $CDCl_3$, 298 K) of ***c*-P6[be$_5$]·T6***, indicating the correlations between template protons **α** and **β**.

Assignment of Porphyrins 2 and 3

The assignment of porphyrins 2 and 3 follows from the assignment of porphyrin 1. We can assign the 16H-doublet of doublets at 9.90 ppm with confidence to protons **a2–3**, which enables us to assign protons **b2–3** through a COSY correlation as a 16H-doublet at 8.61 ppm (Figure S18). Figure S19 shows the NOE cross peaks correlating the *beta* protons (**a2–3** and **b2–3**) and the aryl protons *ortho* to the porphyrin. Thus, we easily identified the downfield shifted protons **o'2**,**3** as the 8H-singlet at 8.06 ppm and the upfield shifted protons **o2**,**3** along with **p2**,**3** as part of a 20H-multiplet between 7.92–7.90 ppm.

Figure S20 depicts the NOE cross peaks correlating the aryl *ortho* protons and the template resonances. Specifically, the protons **o'2**,**3** strongly correlates to protons **α2**,**3** at 2.00 ppm and **β2**,**3** at 4.21 ppm, whereas protons **o2**,**3** weakly correlates only to protons **α2**,**3**. As also commented earlier for porphyrin 1, the correlation between the template protons, namely **α2**,**3** and **β2**,**3**, is easily observable in both COSY and NOESY spectra (Figure S17).

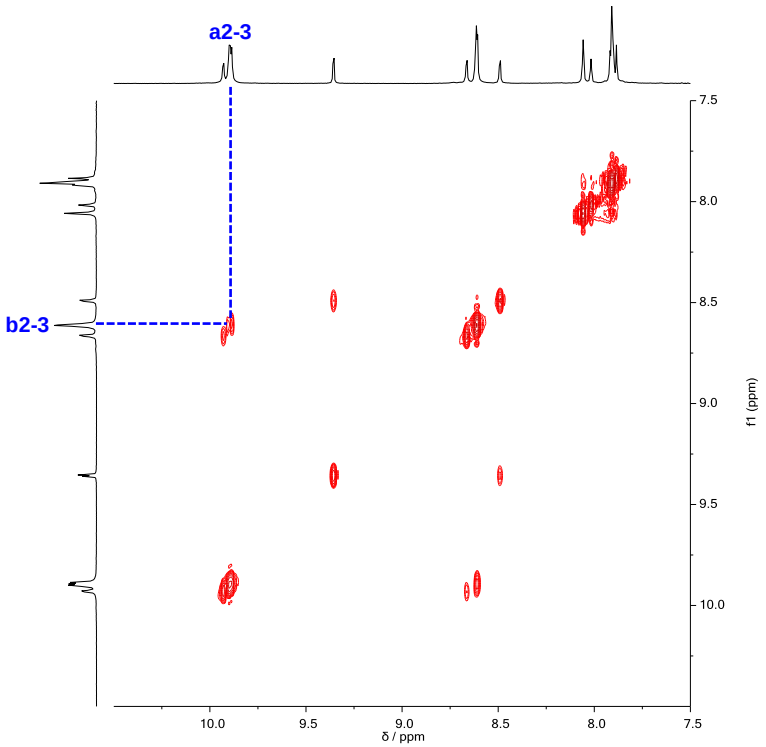

Figure S18: Region of the COSY spectrum (700 MHz, $CDCl_3$, 298 K) of ***c*-P6[be$_5$]·T6***, indicating the COSY correlations between protons **a2–3** and **b2–3**.

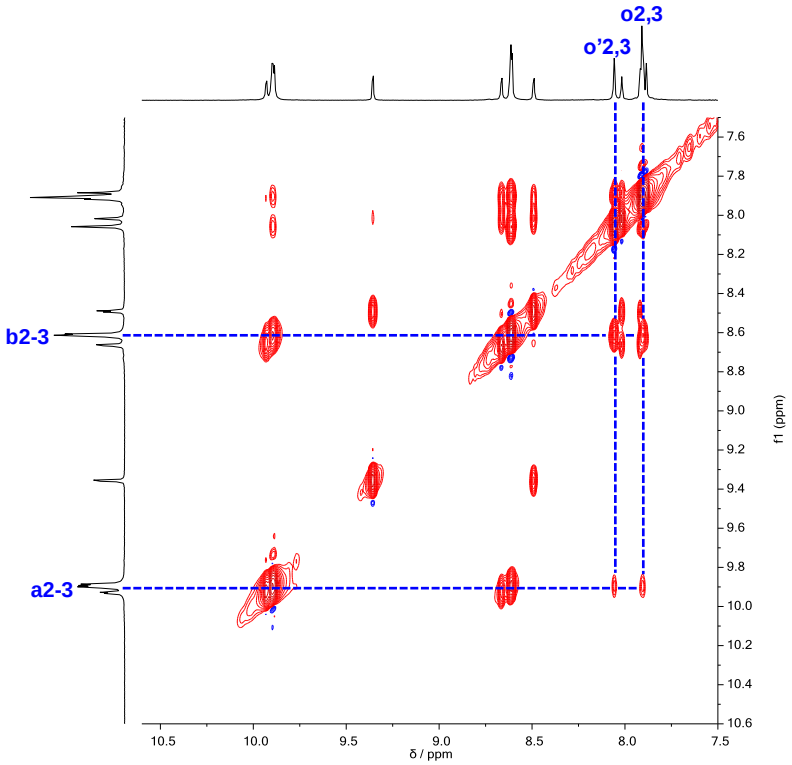

Figure S19: Region of the NOESY spectrum (700 MHz, $CDCl_3$, 298 K) of ***c*-P6[be$_5$]·T6***, indicating the NOE cross peaks correlating the *beta* protons (**a2–3** and **b2–3**) and the aryl *ortho* protons (**o'2,3** and **o2,3**).

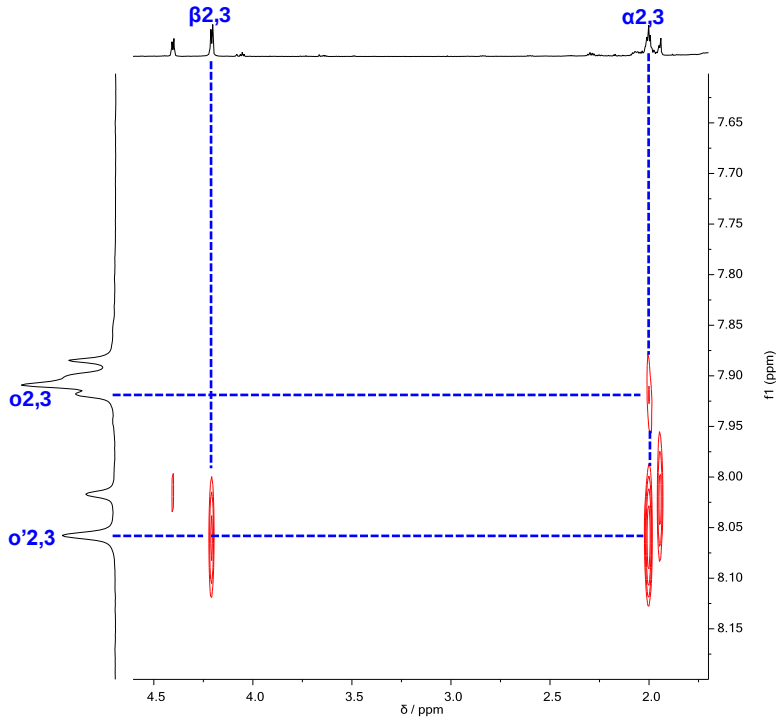

Figure S20: Region of the NOESY spectrum (700 MHz, $CDCl_3$, 298 K) of ***c*-P6[be$_5$]·T6***, indicating the NOE cross peaks correlating the aryl *ortho* protons (**o'2,3** and **o2,3**) and the template resonances (**α2,3** and **β2,3**).

Table S3: Correlation matrix depicting the COSY and NOE correlations in the ^{1}H NMR spectrum of ***c*-P6[be$_5$]·T6*** (labels; **s**: strong correlation, **w**: weak correlation, **o**: overlapping signals).

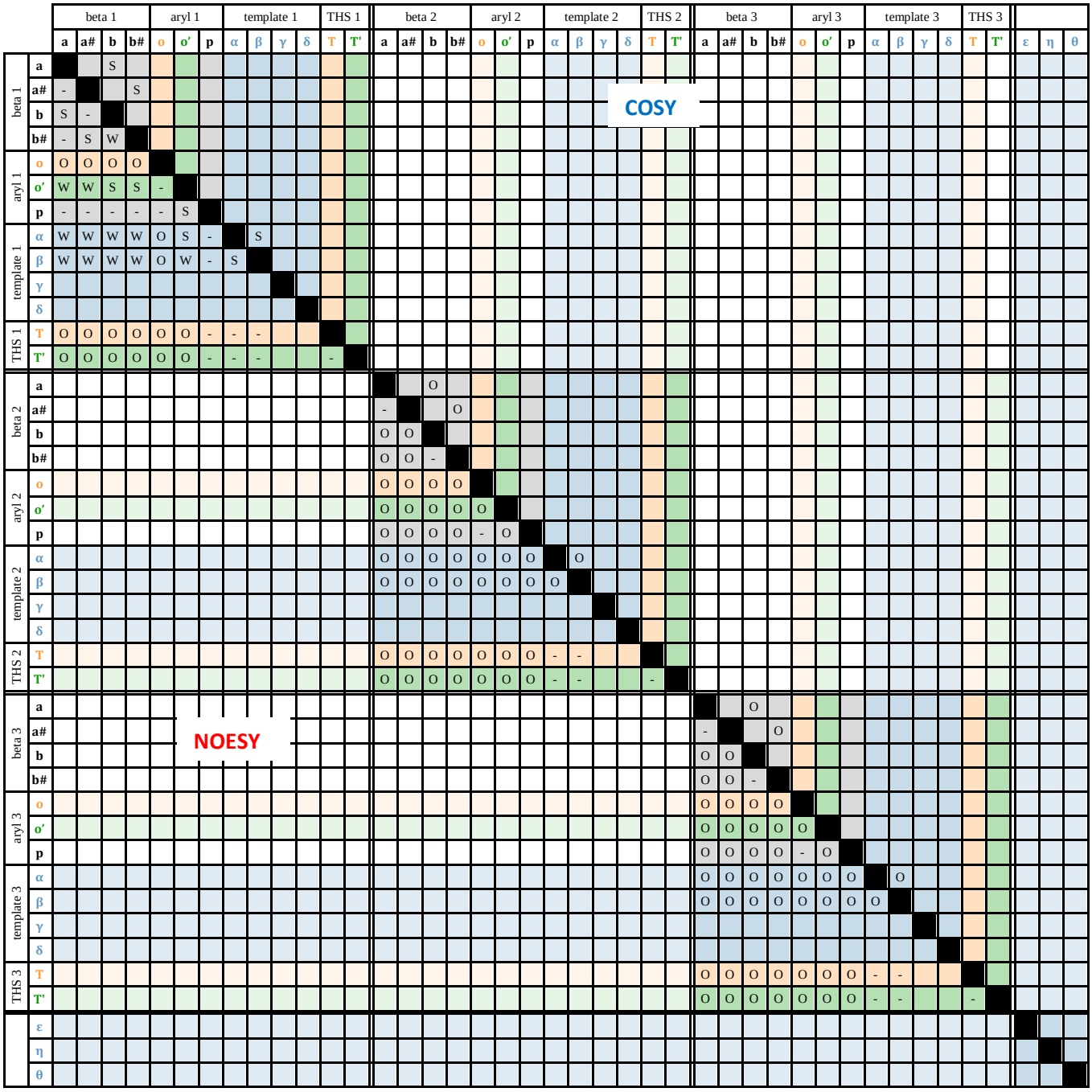

4.4 Assignment of *c*-P6[be$_5$]

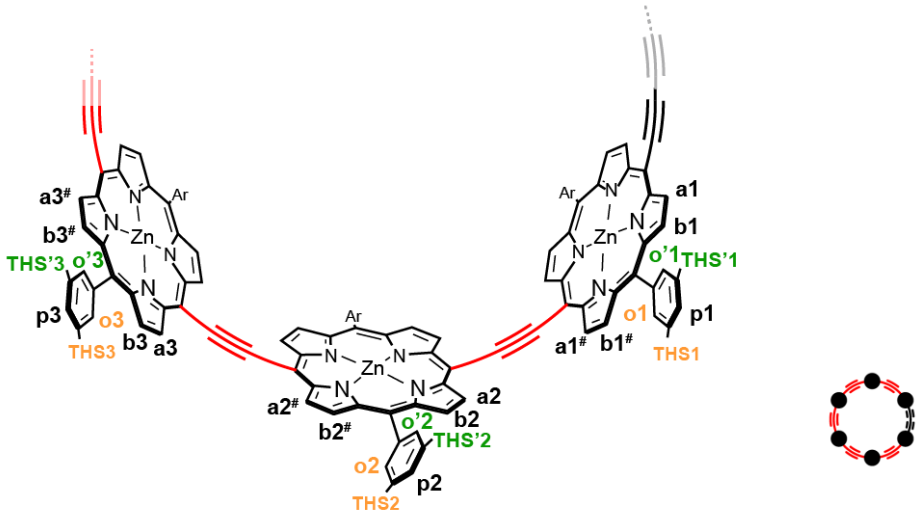

Assignment of Porphyrin 1

As we can assign the 4H-doublet at 9.43 ppm with confidence to proton **a1**, this enables us to assign **b1** through a NOESY correlation as the 4H-doublet at 8.62 ppm (Figure S21). Unlike the template-based system, here the protons **a1**$^{\#}$ and **b1**$^{\#}$ resonate together with the rest of *beta* protons of the nanoring, namely **a2–3** and **b2–3**, respectively.

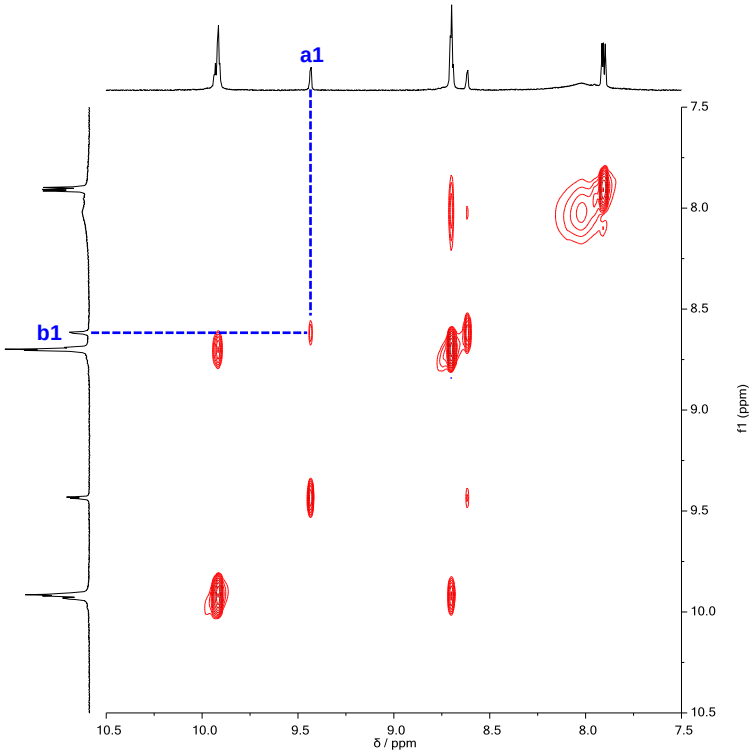

Figure S21: Region of the NOESY spectrum (700 MHz, $CDCl_3$, 298 K) of ***c*-P6[be$_5$]**, indicating the NOE cross peak correlating protons **a1** and **b1**.

Assignment of Porphyrins 2 and 3

We can assign the 20H-multiplet between 9.94–9.90 ppm with confidence to protons **a1**$^{\#}$ and **a2–3**, which enables us to assign protons **b1**$^{\#}$ and **b2–3** through a NOESY correlation as the 20H-multiplet between 8.71–8.69 ppm (Figure S22).

The signals for the aryl protons *ortho* to the porphyrin are broader than for the template-based system, thus indicating conformational exchange. Figure S22 also depicts the NOE cross peaks correlating the *beta* protons (**a1**, **a1**$^{\#}$,**a2–3**, **b1** and **b1**$^{\#}$,**b2–3**) and the aryl *ortho* protons **o** as a 24H-broad singlet at 8.02 ppm. Finally, the 12H-multiplet between 7.91–7.90 ppm is assigned to all the aryl *para* protons **p** of the system.

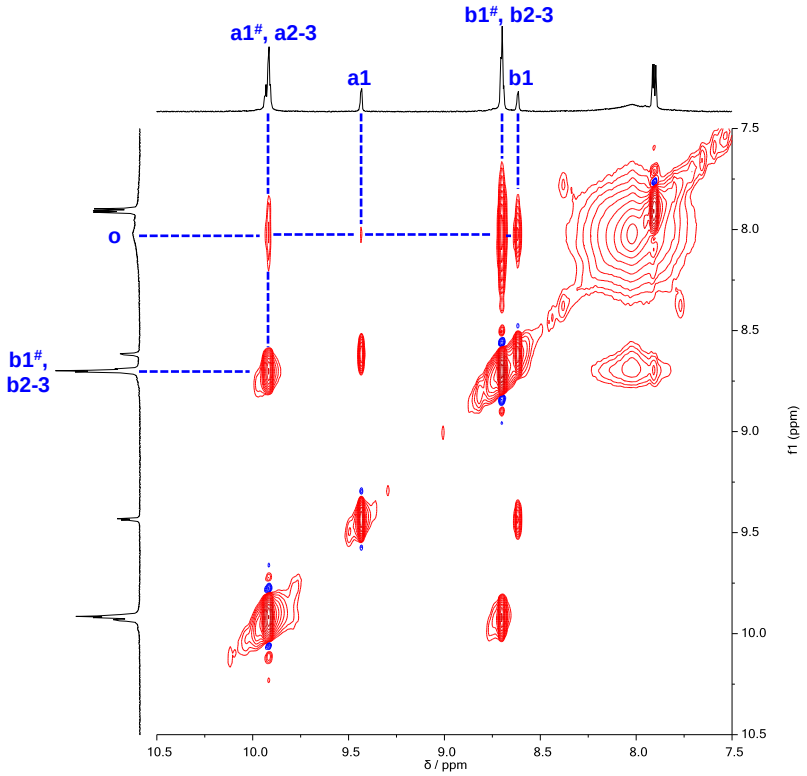

Figure S22: Region of the NOESY spectrum (700 MHz, $CDCl_3$, 298 K) of ***c*-P6[be$_5$]**, indicating the NOE cross peaks correlating the *beta* protons (**a1**, **a1**$^{\#}$,**a2–3**, **b1** and **b1**$^{\#}$,**b2–3**) and the *ortho* protons **o**. The protons **a1**$^{\#}$,**a2–3** also correlate to **b1**$^{\#}$,**b2–3**.

Table S4: Correlation matrix depicting the NOE correlations in the ^{1}H NMR spectrum of ***c*-P6[be$_5$]** (labels; **s**: strong correlation, **w**: weak correlation, **o**: overlapping signals).

		beta 1				aryl 1			THS 1		beta 2				aryl 2			THS 2		beta 3				aryl 3			THS 3	
		a	**a#**	**b**	**b#**	**o**	**o'**	**p**	**T**	**T'**	**a**	**a#**	**b**	**b#**	**o**	**o'**	**p**	**T**	**T'**	**a**	**a#**	**b**	**b#**	**o**	**o'**	**p**	**T**	**T'**
beta 1	**a**																											
	a#	-																										
	b	S	-																									
	b#	-	O	-																								
aryl 1	**o**	O	O	O	O																							
	o'	O	O	O	O	-																						
	p	-	-	-	-	-	-																					
THS 1	**T**	-	O	O	O	-	-	O																				
	T'	-	O	O	O	-	-	O	-																			
beta 2	**a**																											
	a#										-																	
	b										O	O																
	b#										O	O	-															
aryl 2	**o**										O	O	O	O														
	o'										O	O	O	O	-													
	p										-	-	-	-	-	-												
THS 2	**T**										O	O	O	O	-	-	O											
	T'										O	O	O	O	-	-	O	-										
beta 3	**a**																											
	a#																			-								
	b																			O	O							
	b#																			O	O	-						
aryl 3	**o**																			O	O	O	O					
	o'																			O	O	O	O	-				
	p																			-	-	-	-	-	-			
THS 3	**T**																			O	O	O	O	-	-	O		
	T'																			O	O	O	O	-	-	O	-	

NOESY

5 Spectra Confirming Identity of New Compounds

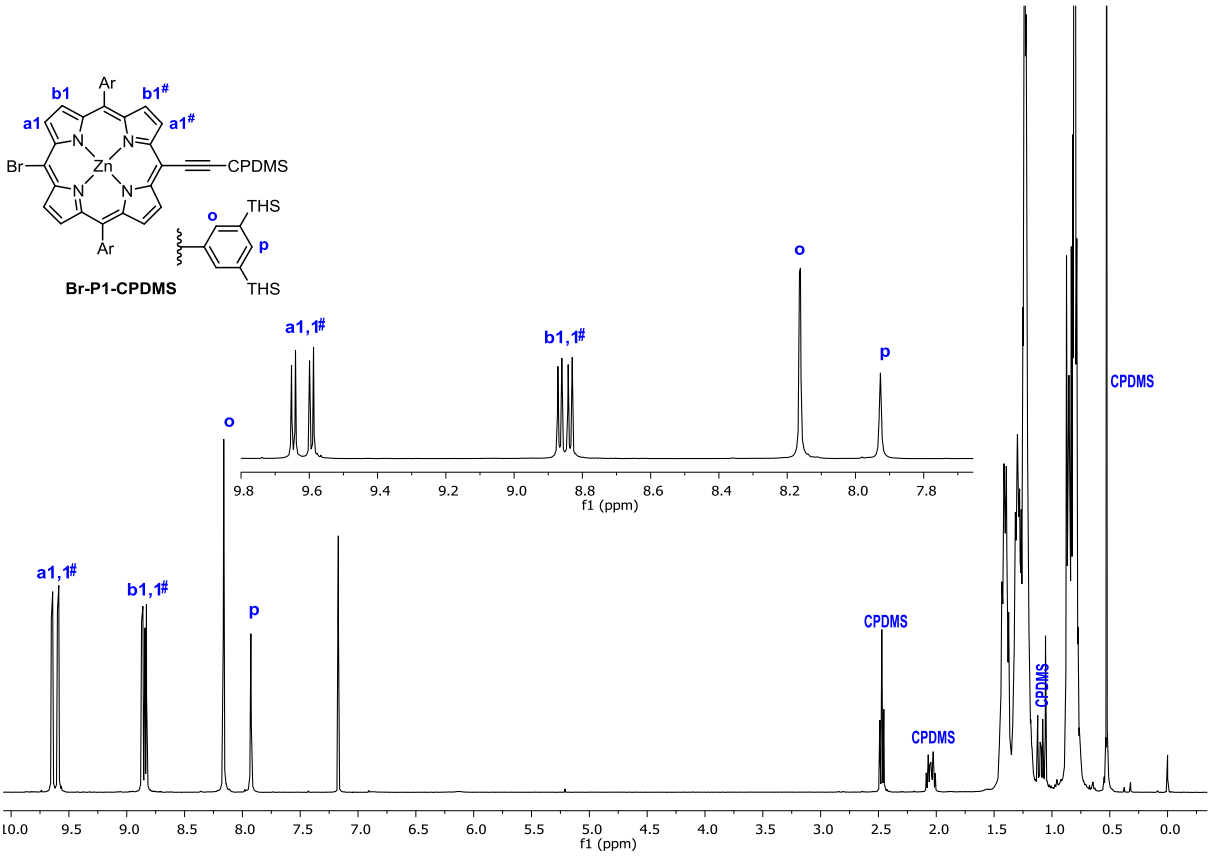

Figure S23: ^{1}H NMR spectrum of compound **Br-P1-CPDMS** (400 MHz, $CDCl_3$, 298 K).

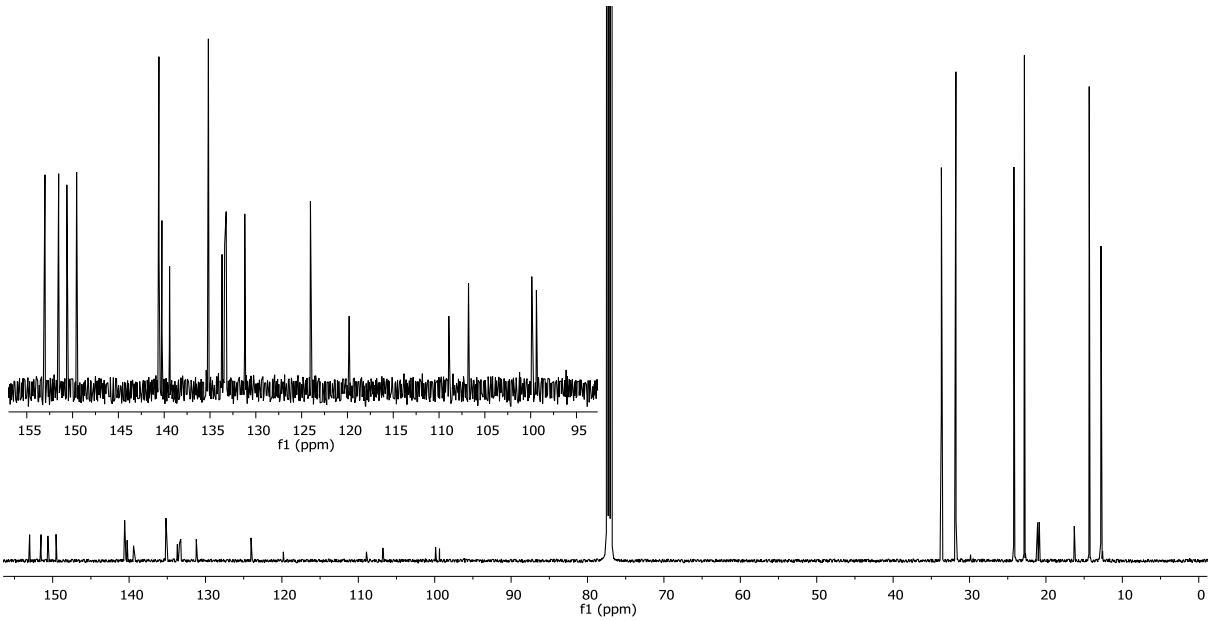

Figure S24: ^{13}C NMR spectrum of compound **Br-P1-CPDMS** (125 MHz, $CDCl_3$, 298 K).

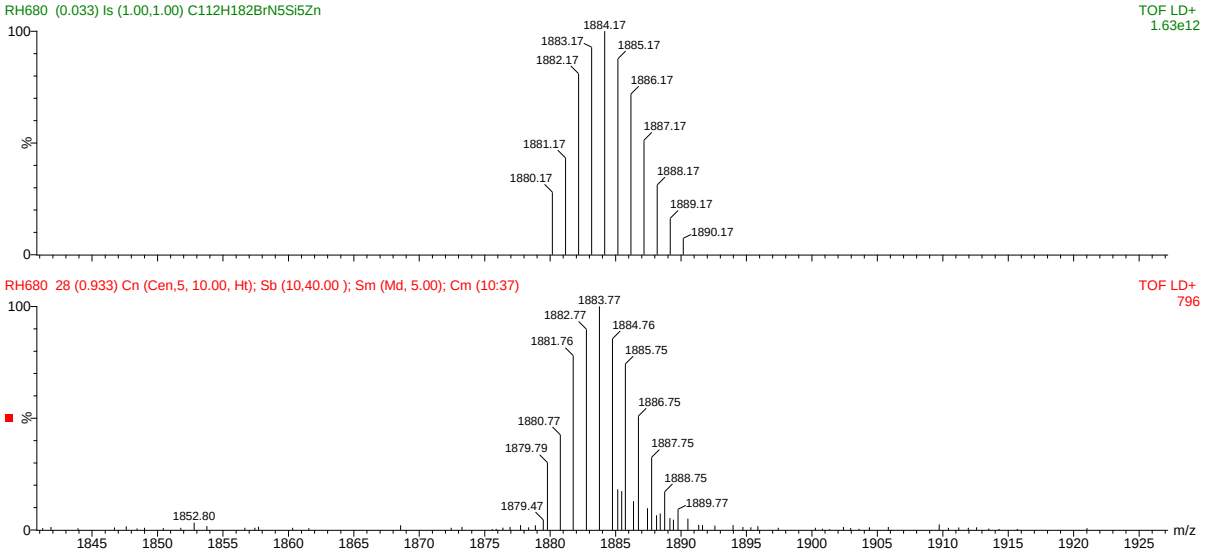

Figure S25: (top) Simulated MALDI-ToF spectrum of compound **Br-P1-CPDMS** ($[C_{112}H_{182}BrN_5Si_5Zn]^+$). (bottom) Measured MALDI-ToF spectrum of compound **Br-P1-CPDMS** (matrix: DCTB)**.**

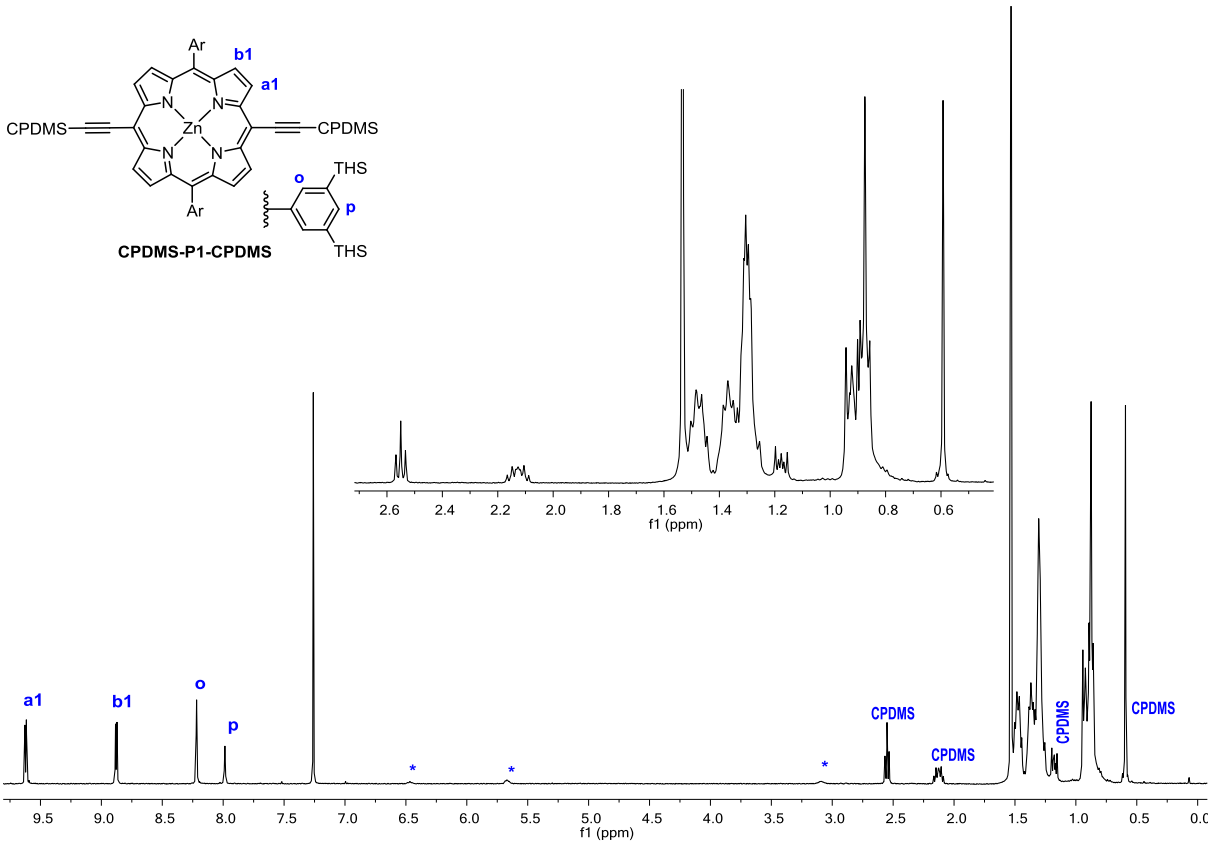

Figure S26: ^{1}H NMR spectrum of compound **CPDMS-P1-CPDMS** (400 MHz, $CDCl_3$, 298 K, * denotes coordinated pyridine).

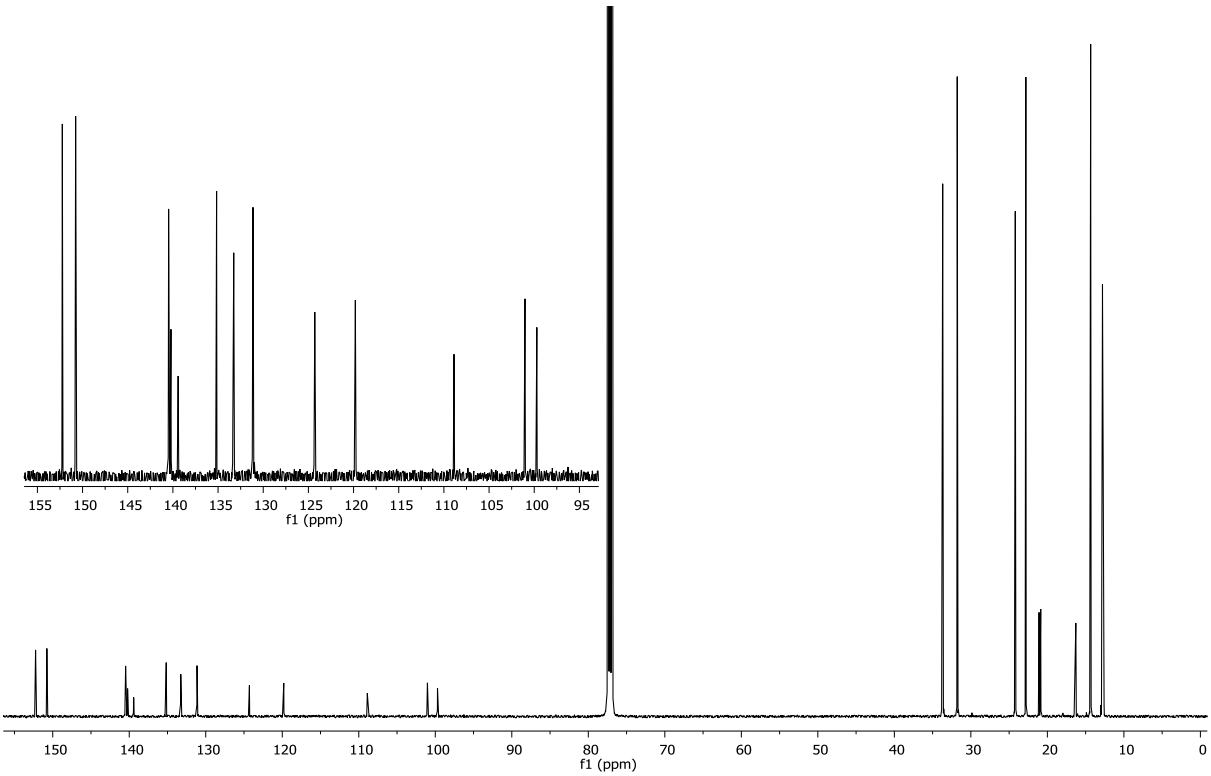

Figure S27: ^{13}C NMR spectrum of compound **CPDMS-P1-CPDMS** (125 MHz, $CDCl_3$, 298 K).

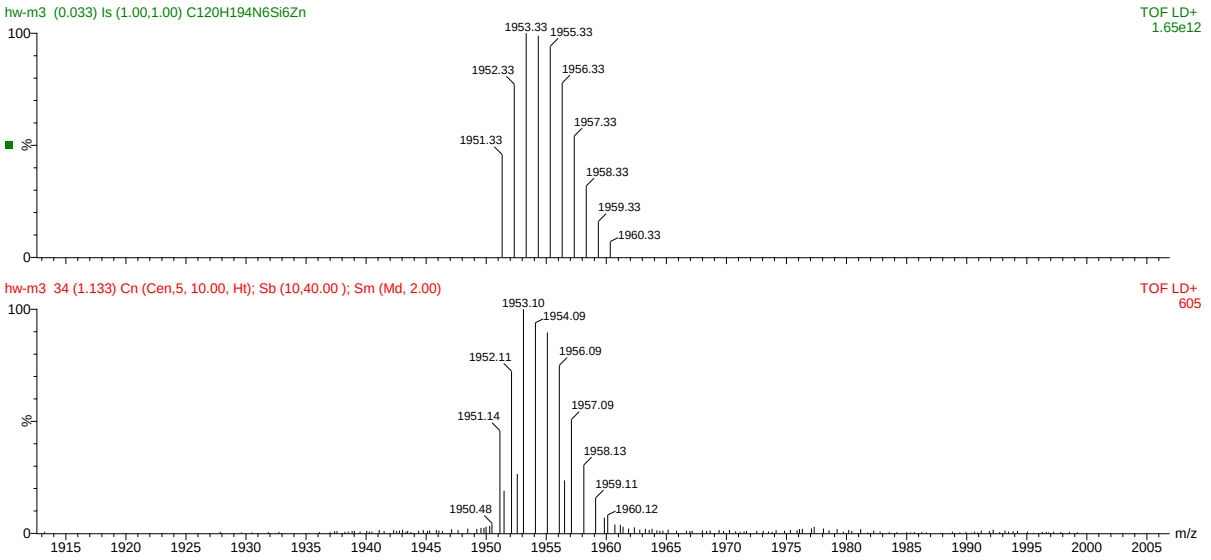

Figure S28: (top) Simulated MALDI-ToF spectrum of compound **CPDMS-P1-CPDMS** ($[C_{120}H_{194}N_6Si_6Zn]^+$). (bottom) Measured MALDI-ToF spectrum of compound **CPDMS-P1-CPDMS** (matrix: DCTB)**.**

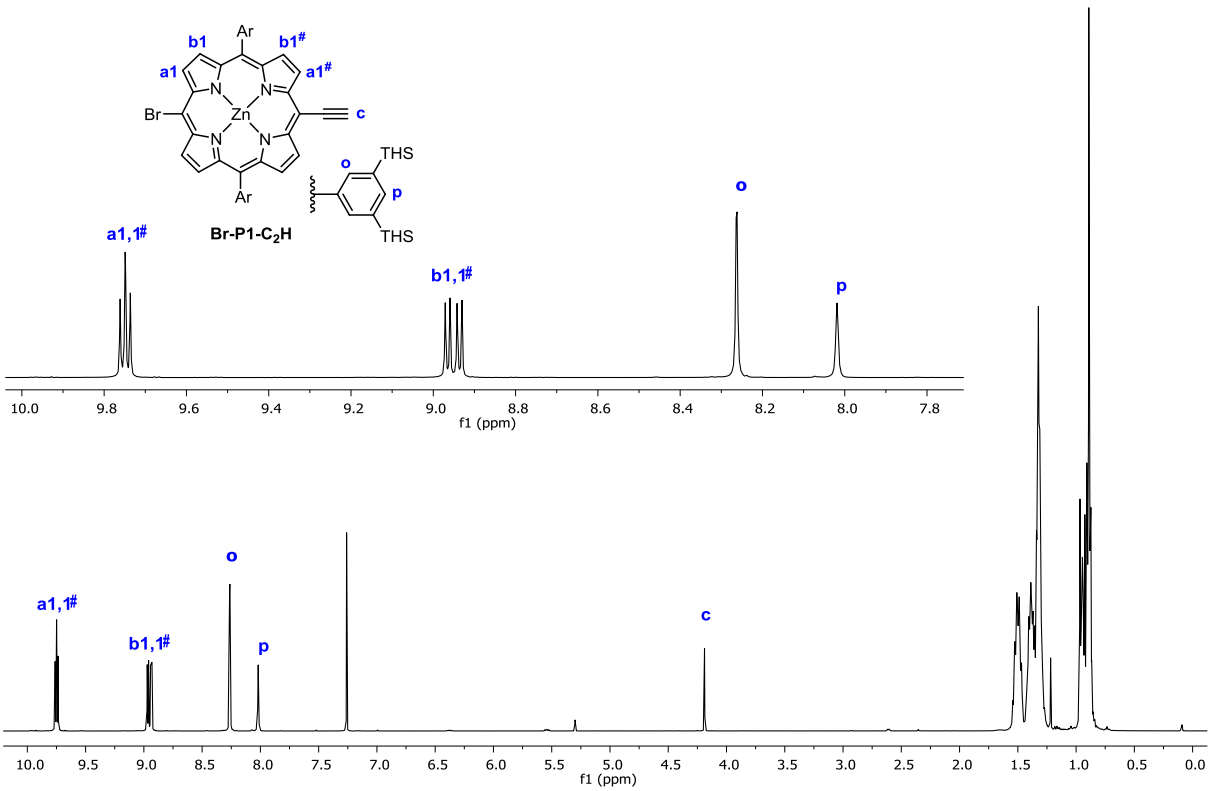

Figure S29: ^{1}H NMR spectrum of compound **Br-P1-C$_2$H** (400 MHz, $CDCl_3$, 298 K).

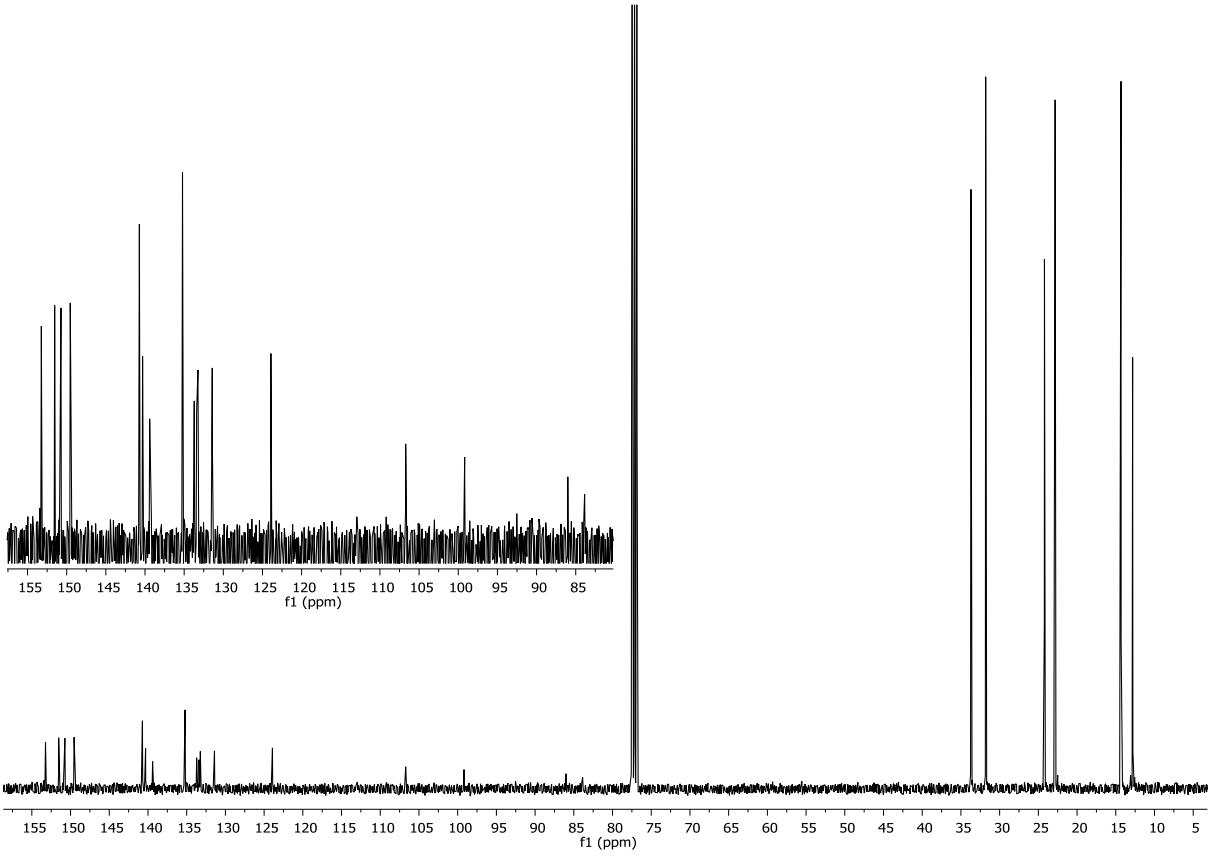

Figure S30: ^{13}C NMR spectrum of compound **Br-P1-C$_2$H** (100 MHz, $CDCl_3$, 298 K).

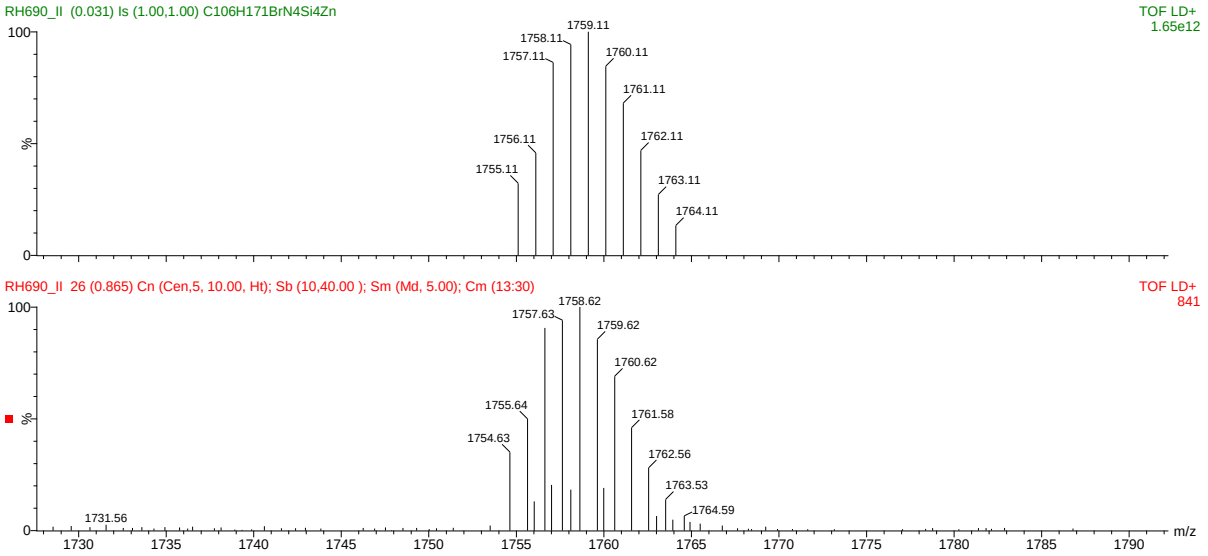

Figure S31: (top) Simulated MALDI-ToF spectrum of compound **Br-P1-C$_2$H** ([$C_{106}H_{171}BrN_4Si_4Zn$]$^+$). (bottom) Measured MALDI-ToF spectrum of compound **Br-P1-C$_2$H** (matrix: DCTB)**.**

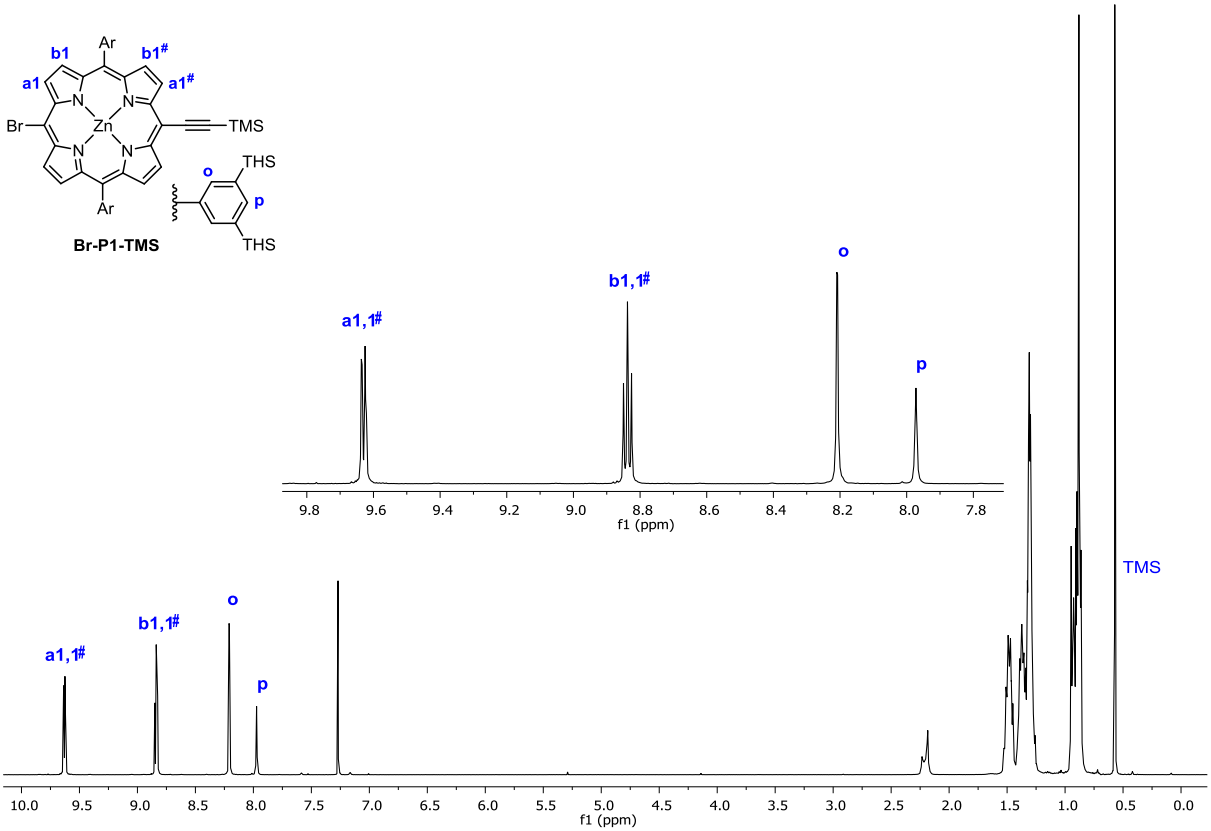

Figure S32: ^{1}H NMR spectrum of compound **Br-P1-TMS** (400 MHz, $CDCl_3$ + 1% pyridine-d_5, 298 K).

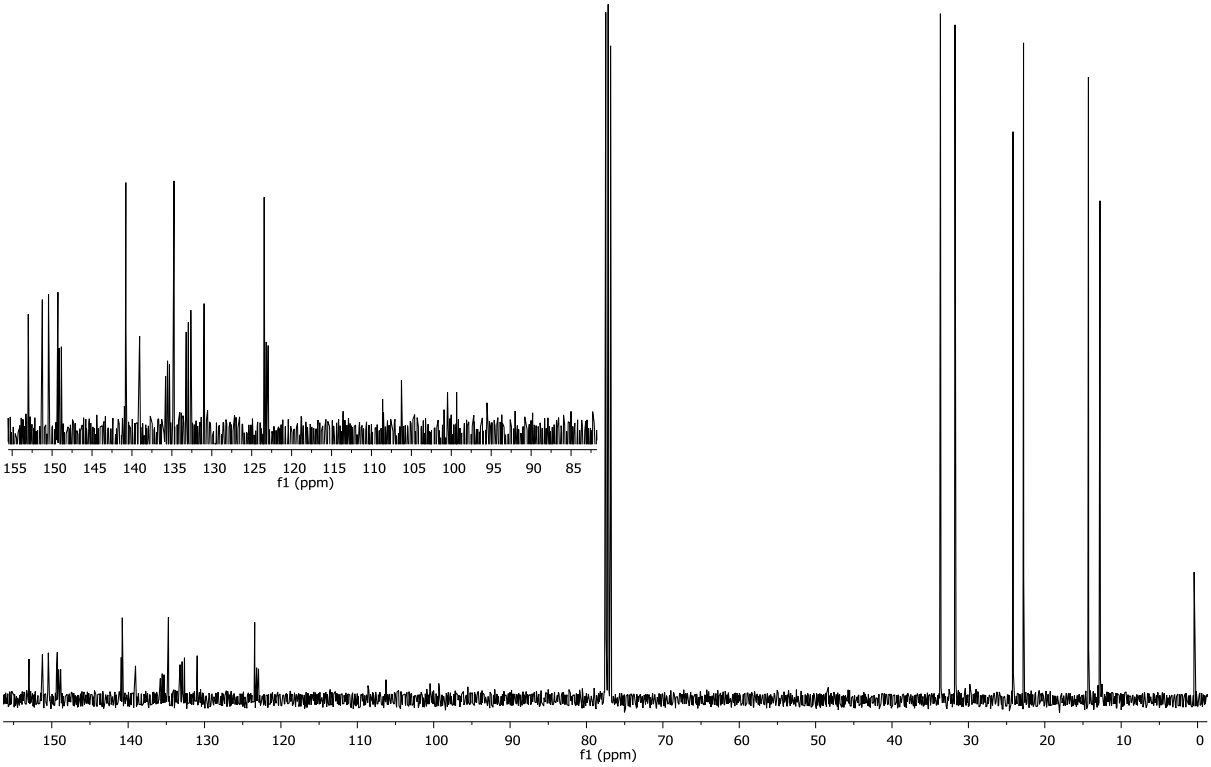

Figure S33: ^{13}C NMR spectrum of compound **Br-P1-TMS** (100 MHz, $CDCl_3$ + 1% pyridine-d_5, 298 K).

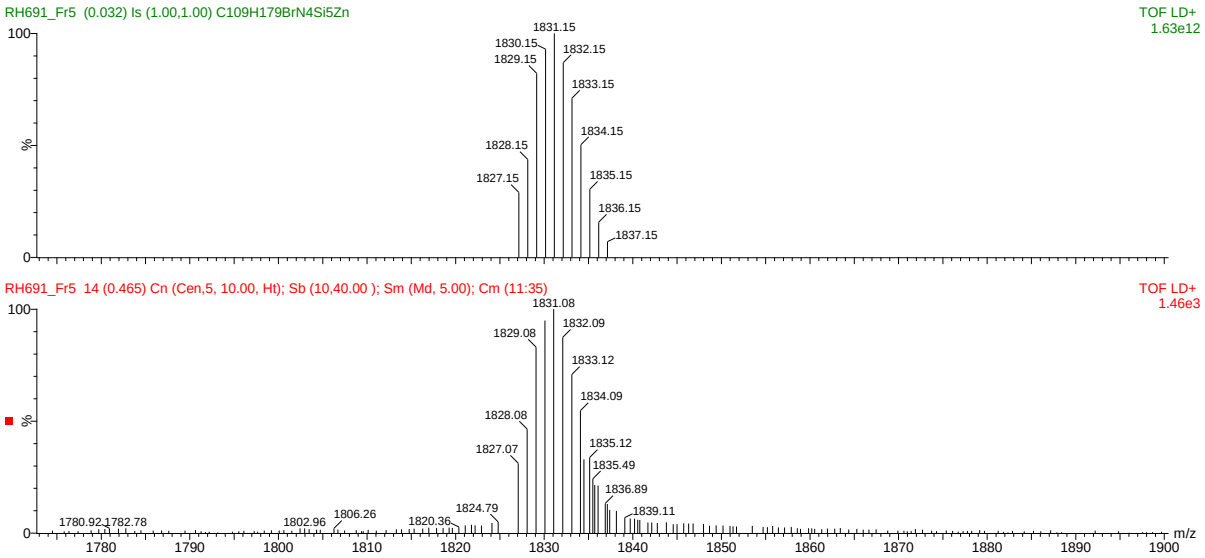

Figure S34: (top) Simulated MALDI-ToF spectrum of compound **Br-P1-TMS** ($[C_{109}H_{179}BrN_4Si_4Zn]^+$). (bottom) Measured MALDI-ToF spectrum of compound **Br-P1-TMS** (matrix: DCTB)**.**

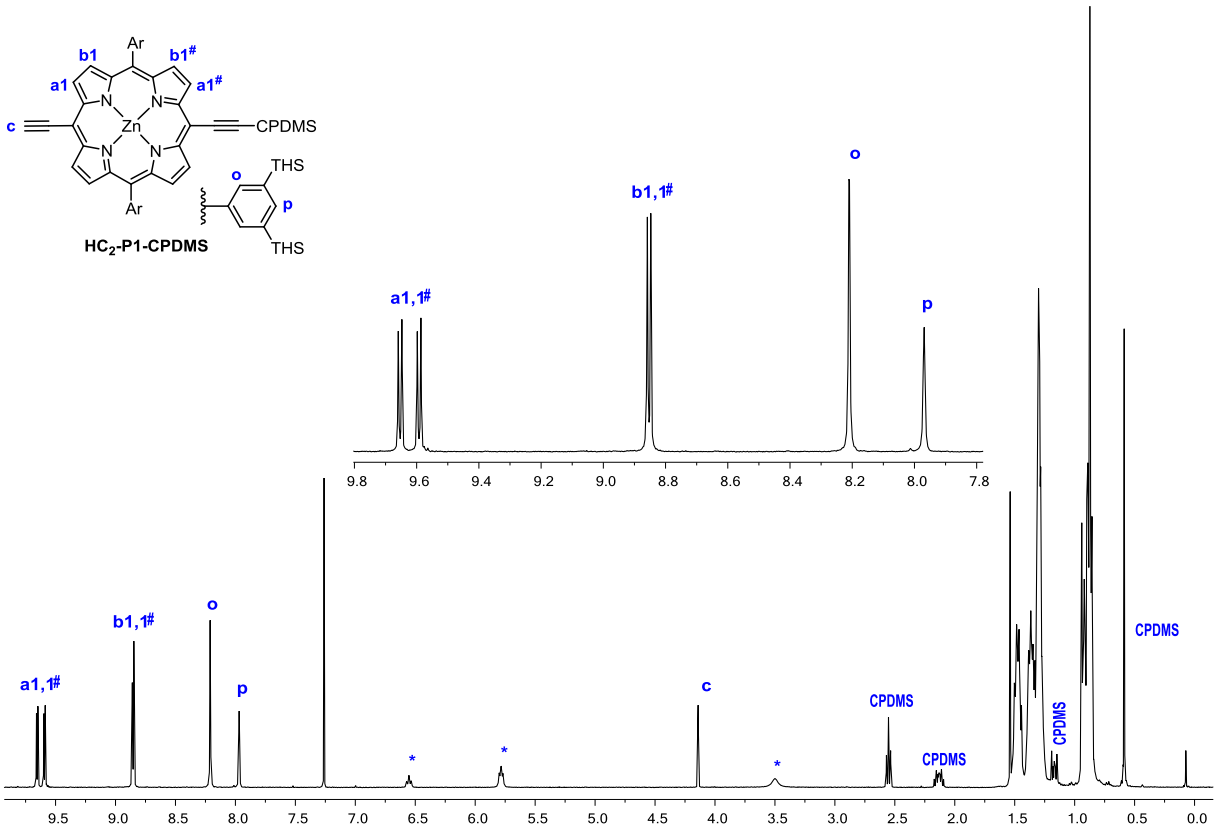

Figure S35: ^{1}H NMR spectrum of compound **HC_2-P1-CPDMS** (400 MHz, $CDCl_3$, 298 K, * denotes coordinated pyridine).

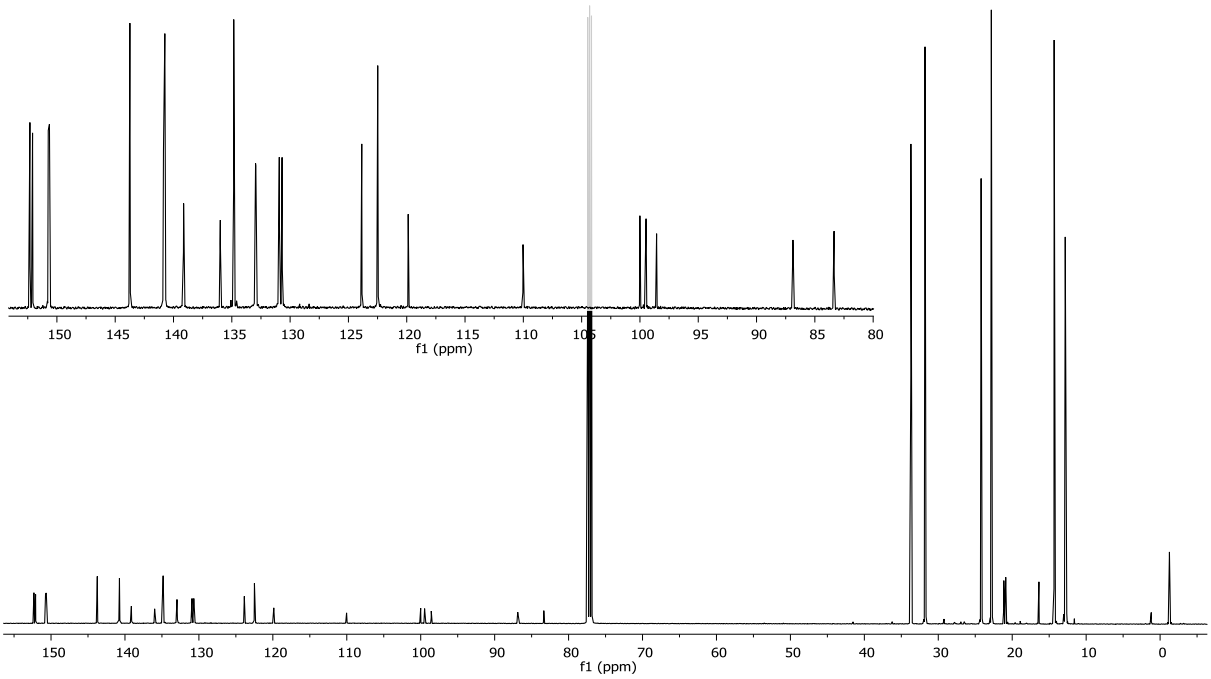

Figure S36: ^{13}C NMR spectrum of compound **HC_2-P1-CPDMS** (125 MHz, $CDCl_3$, 298 K).

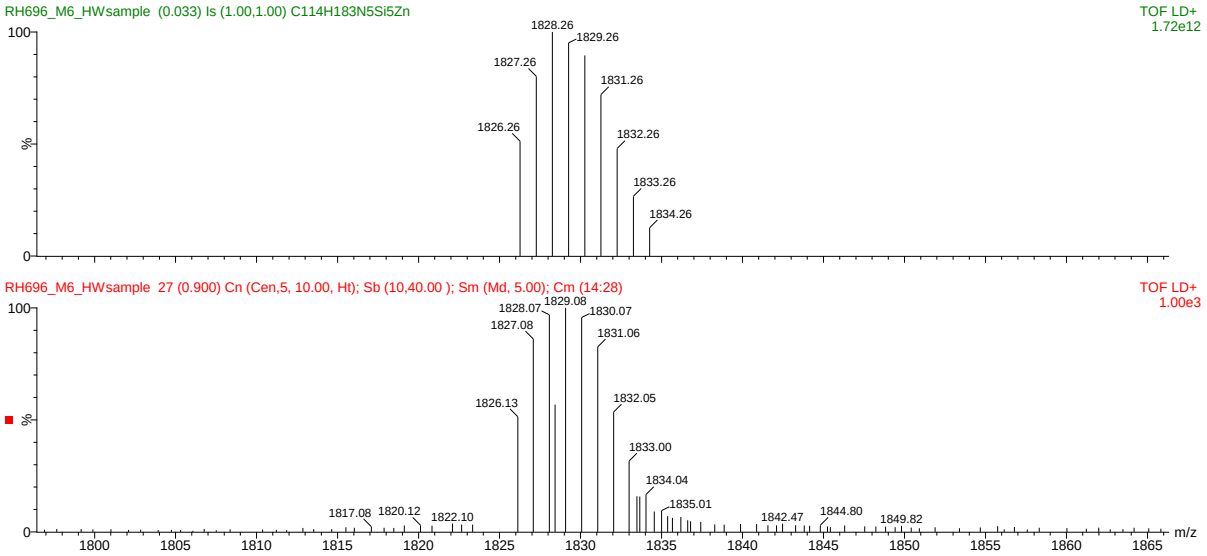

Figure S37: (top) Simulated MALDI-ToF spectrum of compound **HC$_2$-P1-CPDMS** ([$C_{114}H_{183}N_5Si_5Zn$]$^+$). (bottom) Measured MALDI-ToF spectrum of compound **HC$_2$-P1-CPDMS** (matrix: DCTB)**.**

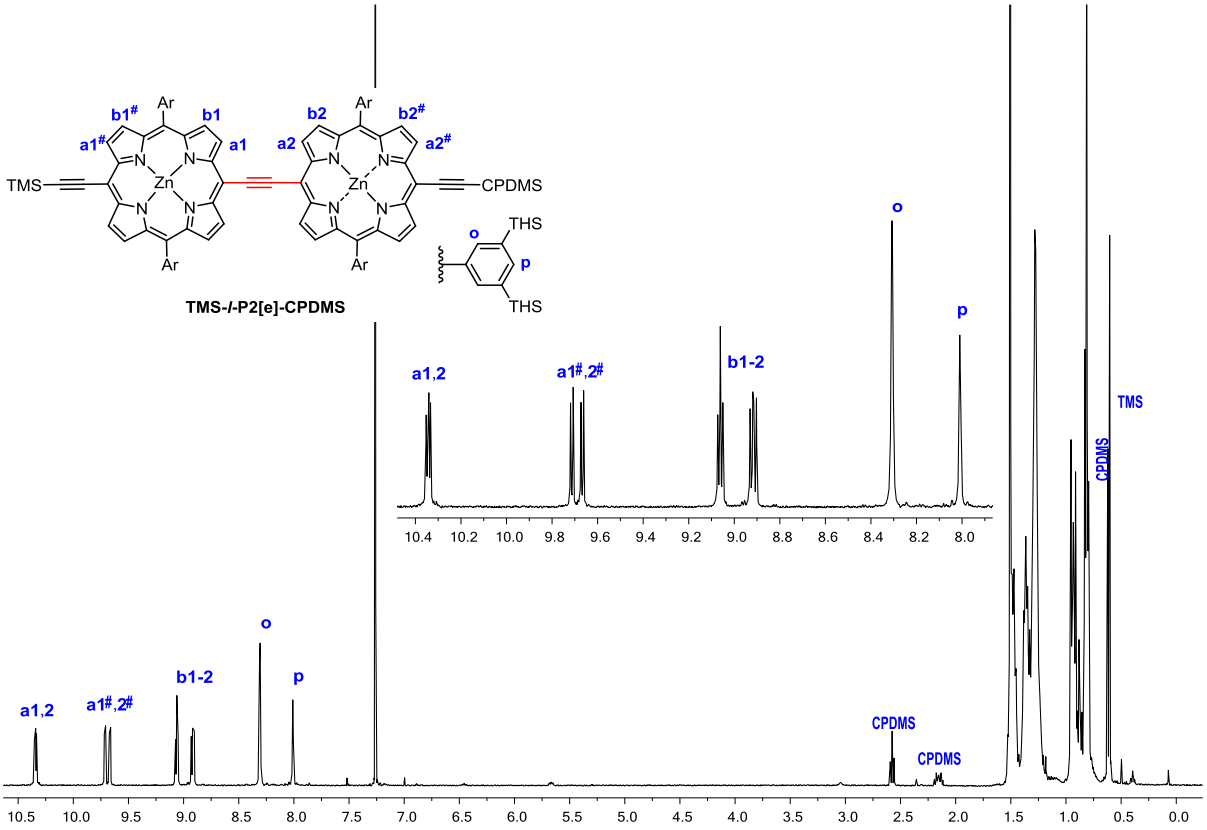

Figure S38: ^{1}H NMR spectrum of compound **TMS-*l*-P2[e]-CPDMS** (400 MHz, $CDCl_3$, 298 K).

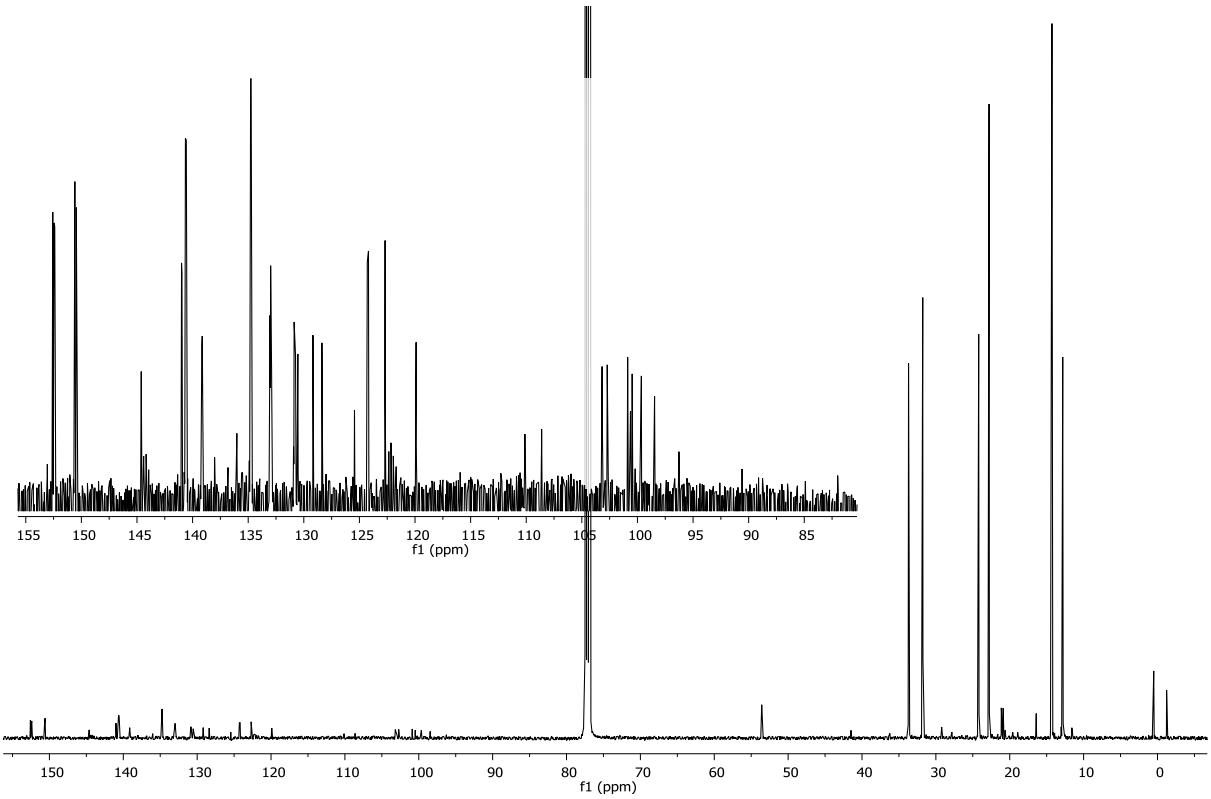

Figure S39: ^{13}C NMR spectrum of compound **TMS-*l*-P2[e]-CPDMS** (125 MHz, $CDCl_3$, 298 K).

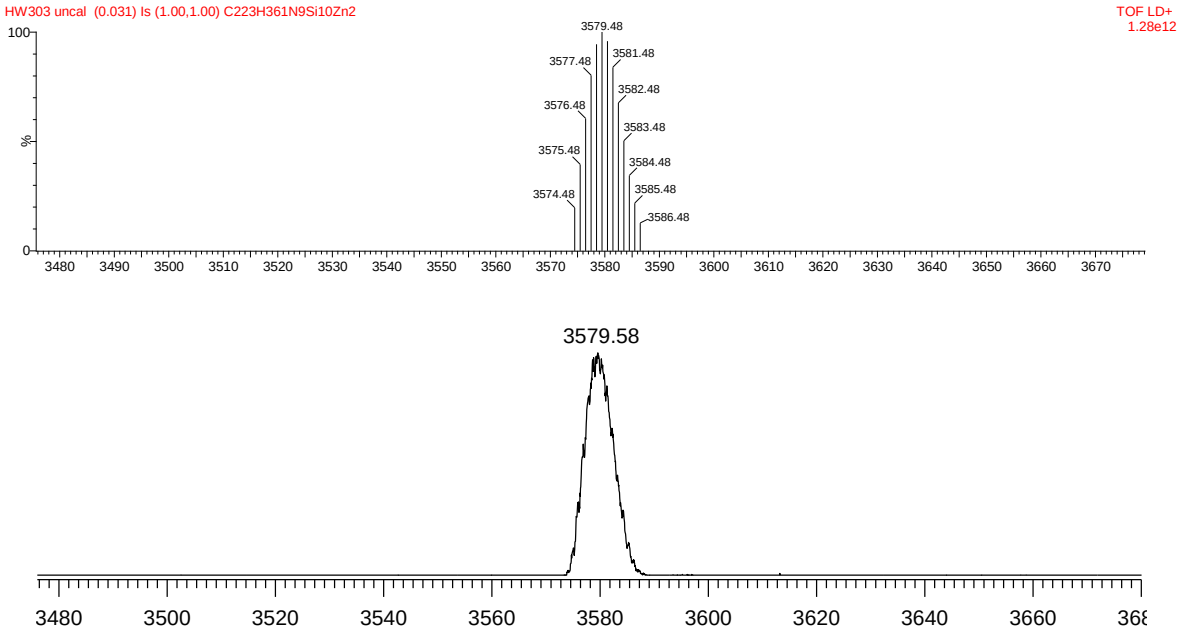

Figure S40: (top) Simulated MALDI-ToF spectrum of compound **TMS-*l*-P2[e]-CPDMS** ($[C_{223}H_{361}N_9Si_{10}Zn_2]^+$). (bottom) Measured MALDI-ToF spectrum of compound **TMS-*l*-P2[e]-CPDMS** (matrix: DCTB)**.**

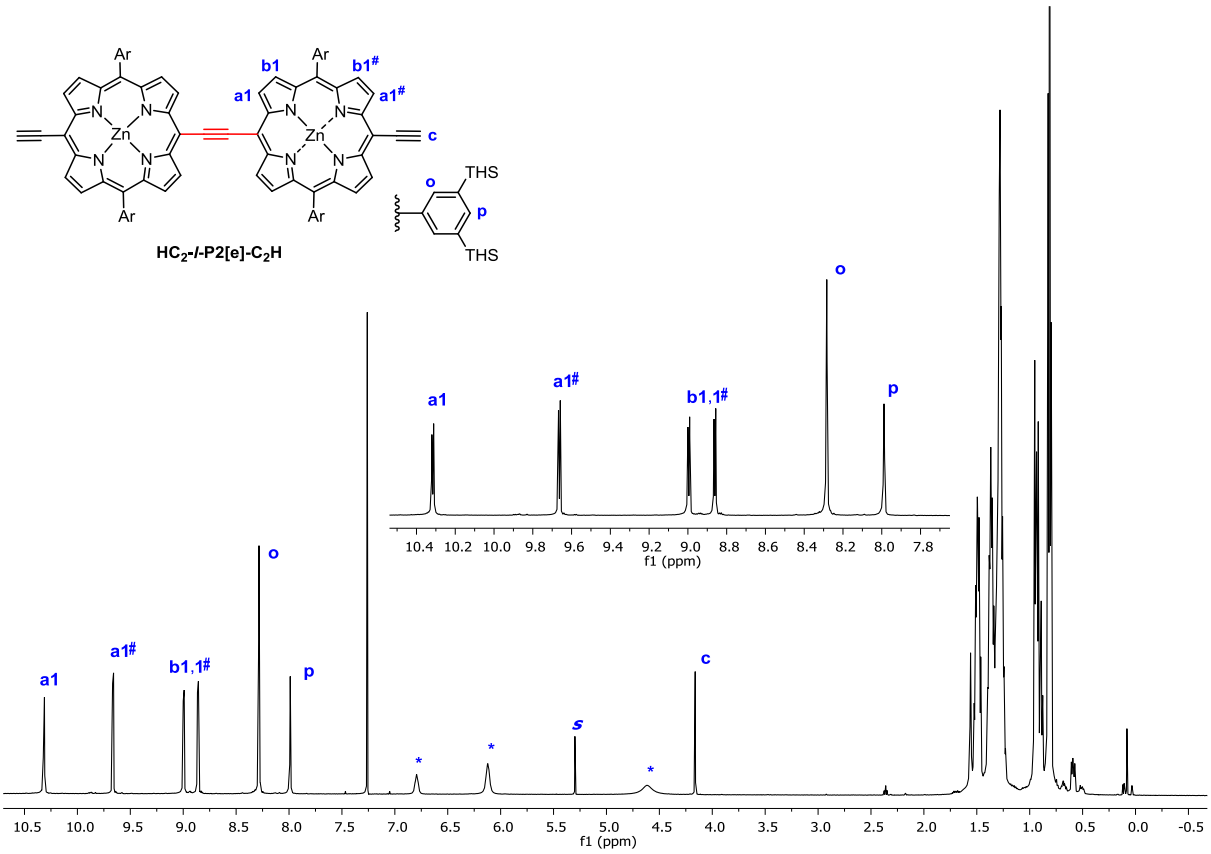

Figure S41: ^{1}H NMR spectrum of compound **HC_2-*l*-P2[e]-C_2H** (500 MHz, $CDCl_3$, 298 K, * denotes coordinated pyridine.

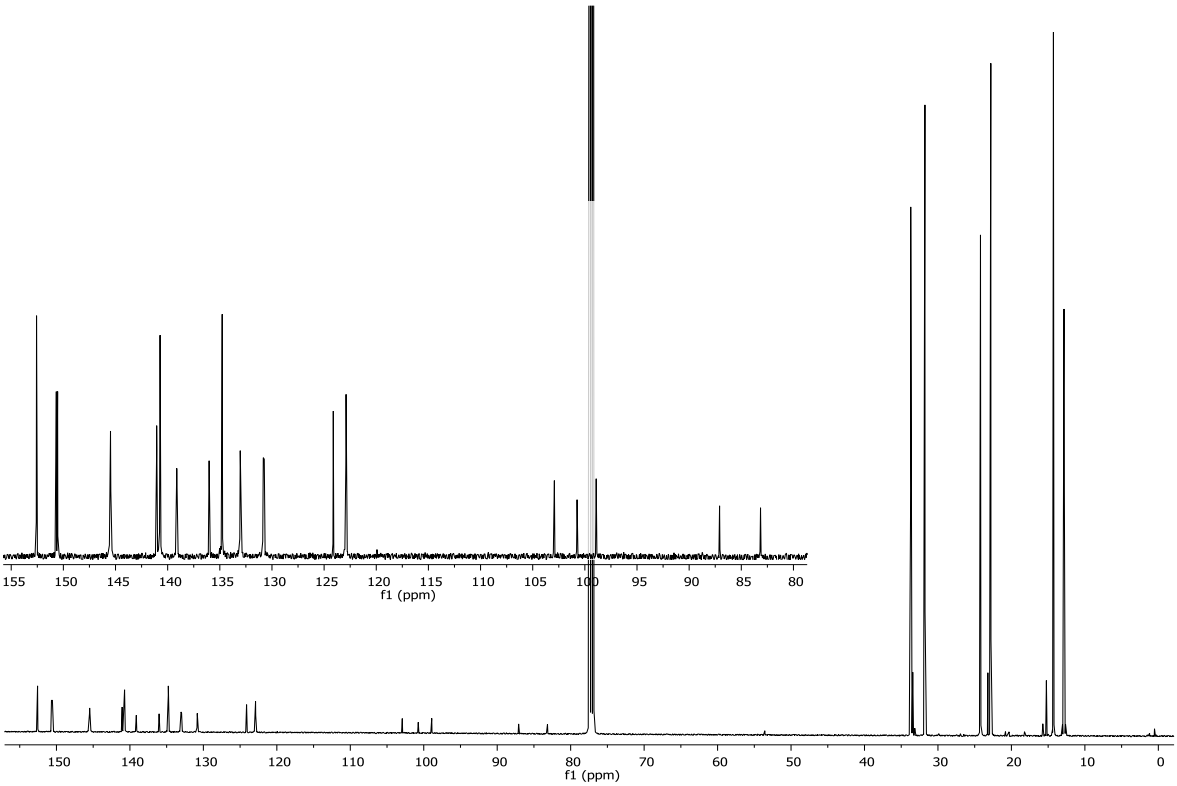

Figure S42: ^{13}C NMR spectrum of compound **HC_2-*l*-P2[e]-C_2H** (125 MHz, $CDCl_3$, 298 K).

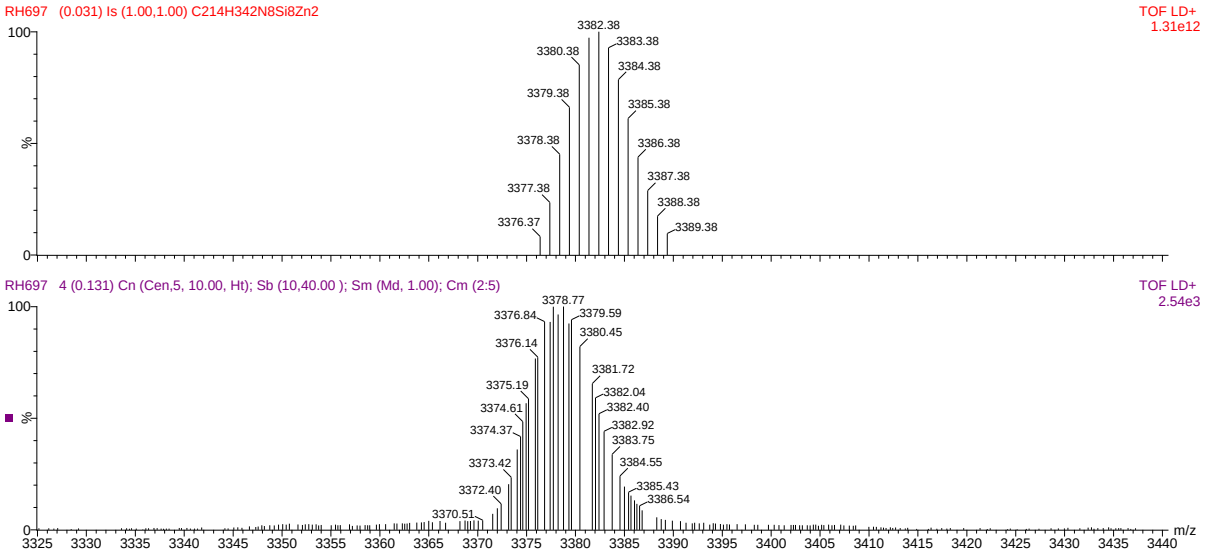

Figure S43: (top) Simulated MALDI-ToF spectrum of compound **HC_2-*l*-P2[e]-C_2H** ($[C_{214}H_{342}N_8Si_8Zn_2]^+$). (bottom) Measured MALDI-ToF spectrum of compound **HC_2-*l*-P2[e]-C_2H** (matrix: DCTB)**.**

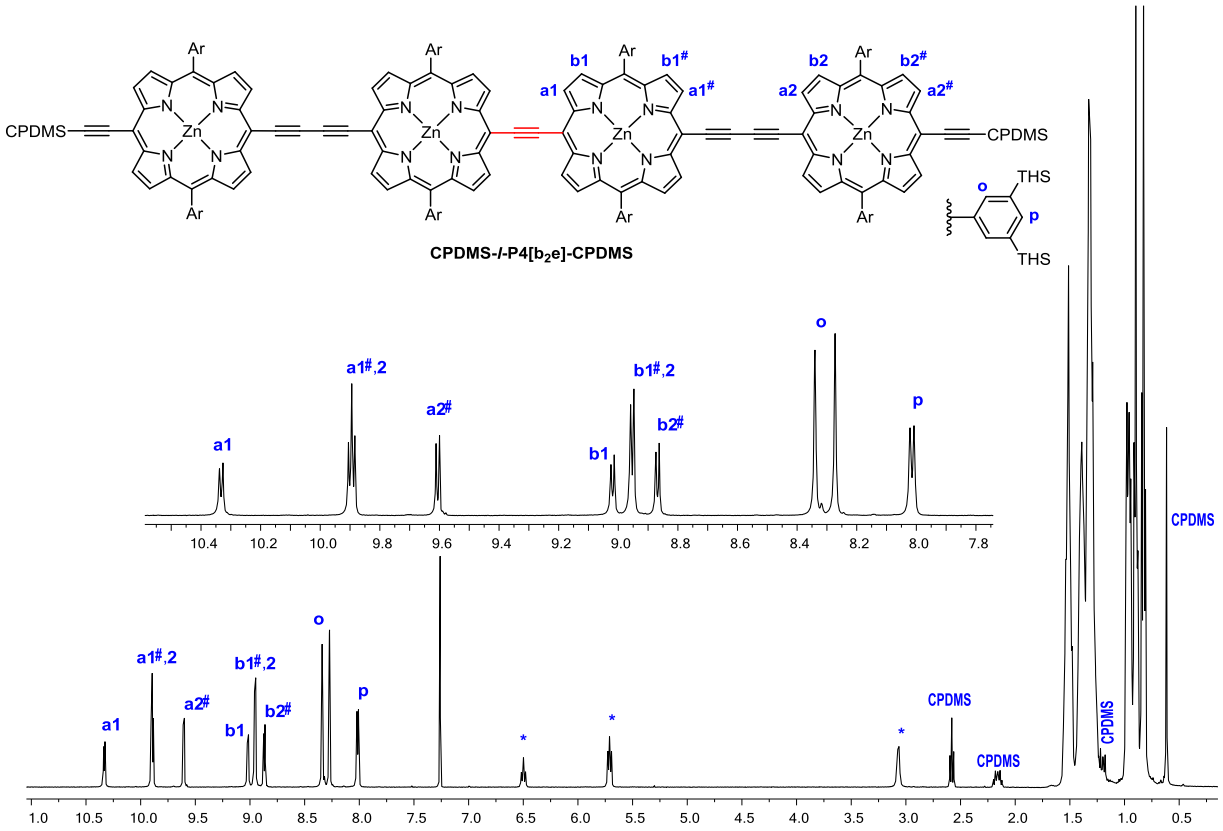

Figure S44: ^{1}H NMR spectrum of compound **CPDMS-*l*-P4[b_2e]-CPDMS** (400 MHz, $CDCl_3$, 298 K, * denotes coordinated pyridine).

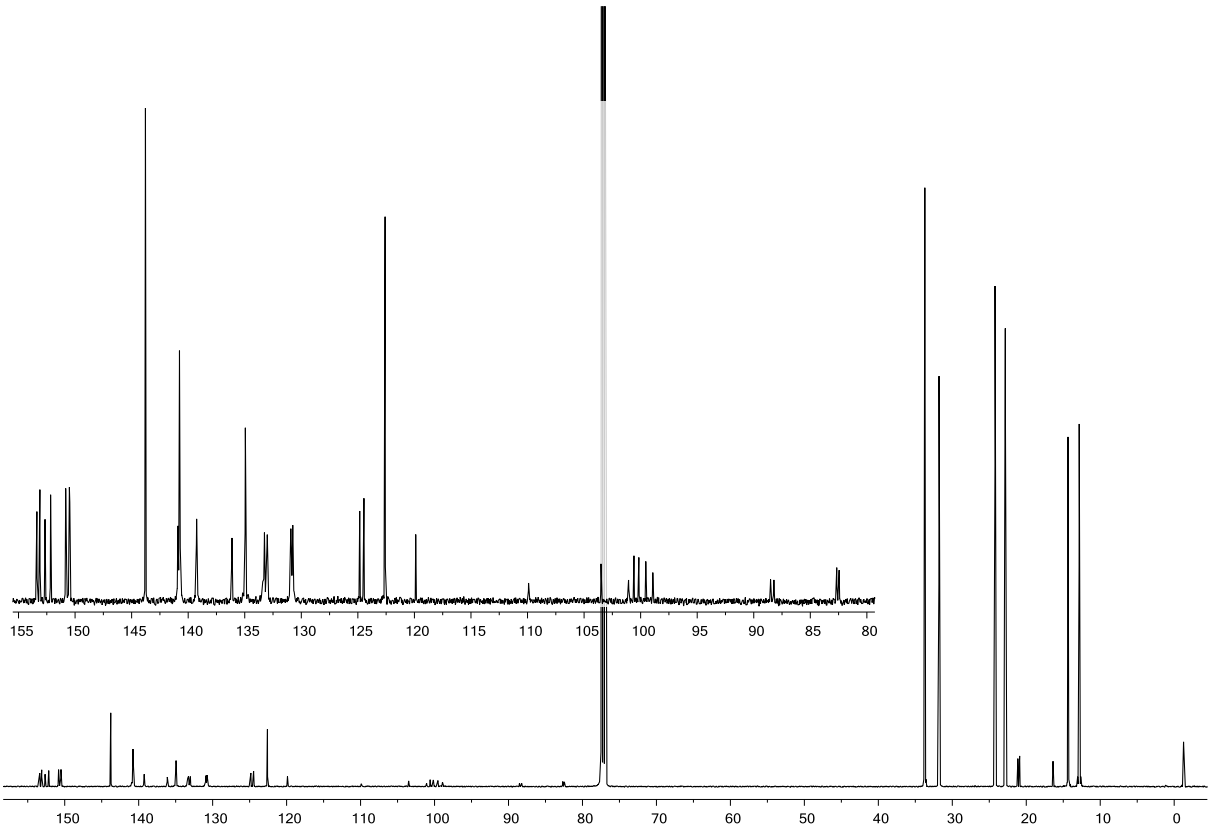

Figure S45: ^{13}C NMR spectrum of compound **CPDMS-*l*-P4[b$_2$e]-CPDMS** (125 MHz, $CDCl_3$, 298 K).

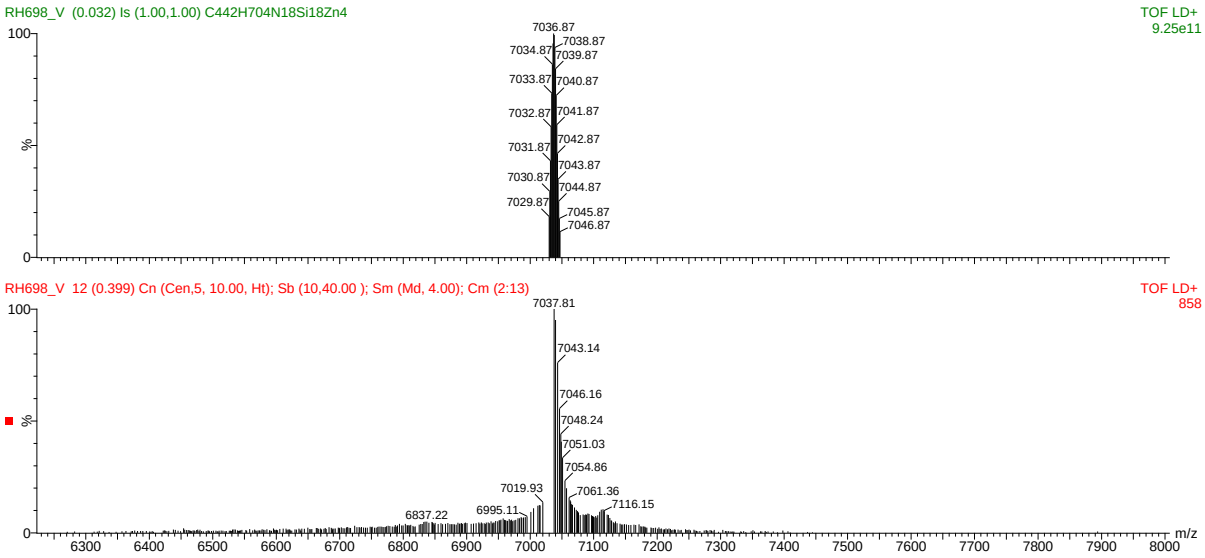

Figure S46: (top) Simulated MALDI-ToF spectrum of compound **CPDMS-*l*-P4[b$_2$e]-CPDMS** ($[C_{442}H_{704}N_{18}Si_{18}Zn_4]^+$). (bottom) Measured MALDI-ToF spectrum of compound **CPDMS-*l*-P4[b$_2$e]-CPDMS** (matrix: DCTB)**.**

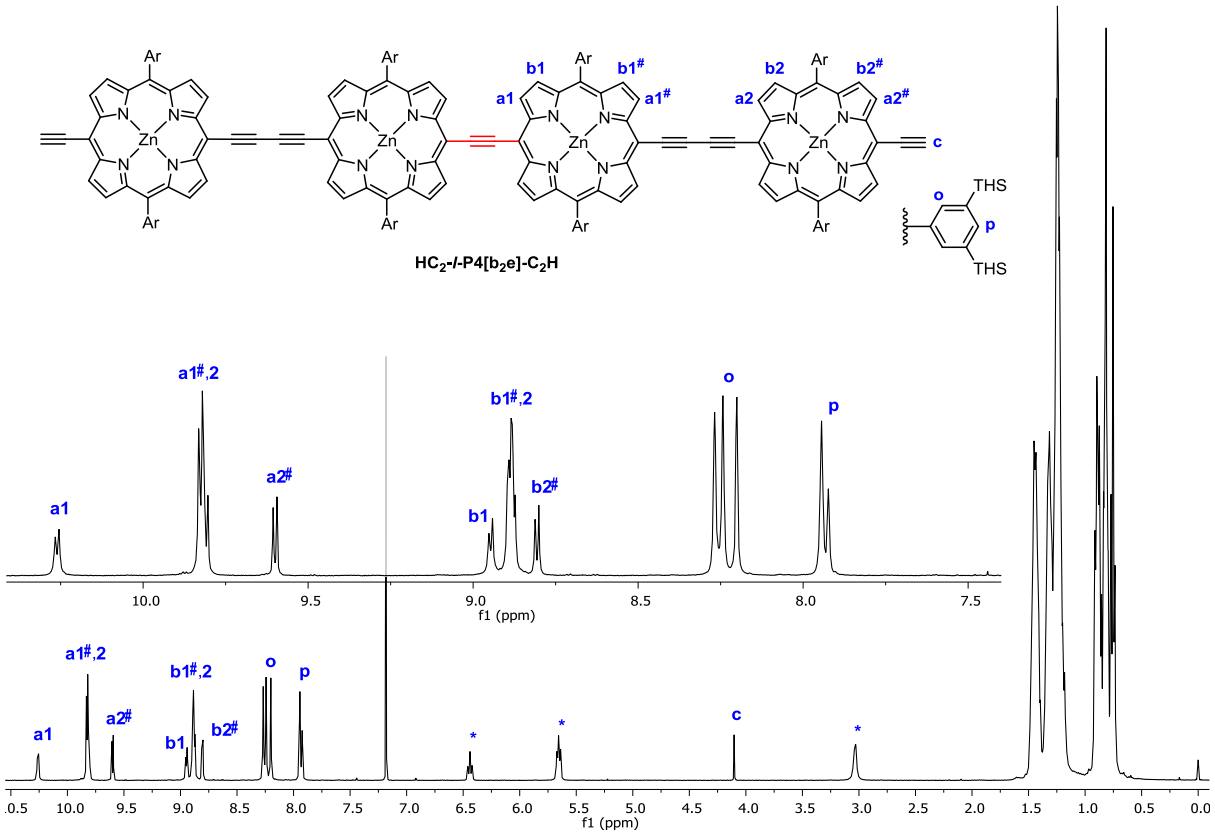

Figure S47: ^{1}H NMR spectrum of compound **HC_2-*l*-P4[b_2e]-C_2H** (400 MHz, $CDCl_3$, 298 K, * denotes coordinated pyridine).

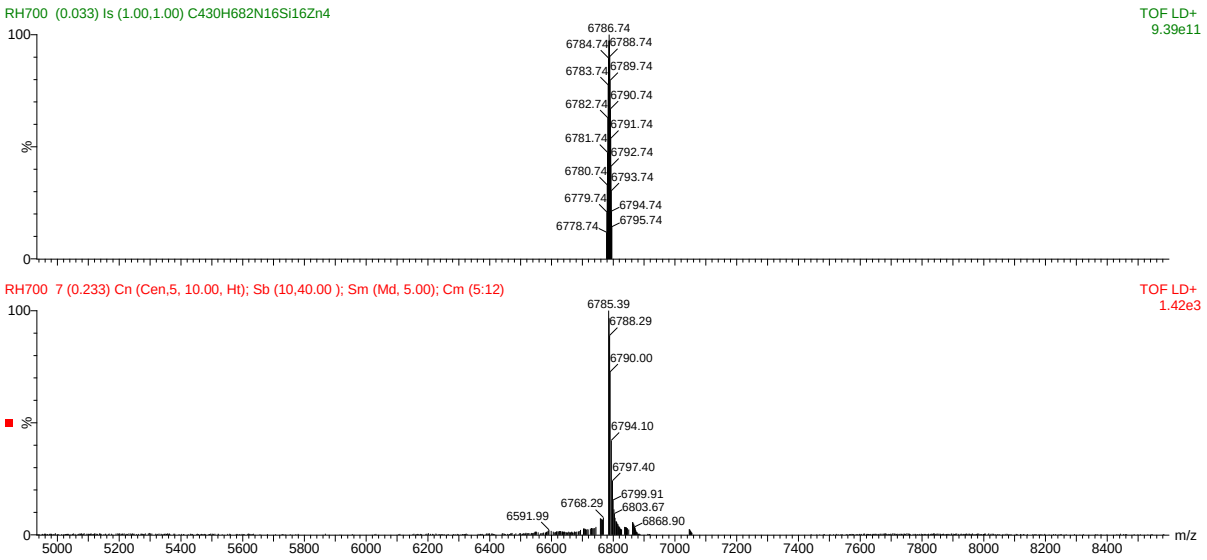

Figure S48: (top) Simulated MALDI-ToF spectrum of compound **HC_2-*l*-P4[b_2e]-C_2H** ($[C_{430}H_{682}N_{16}Si_{16}Zn_4]^+$). (bottom) Measured MALDI-ToF spectrum of compound **HC_2-*l*-P4[b_2e]-C_2H** (matrix: DCTB)**.**

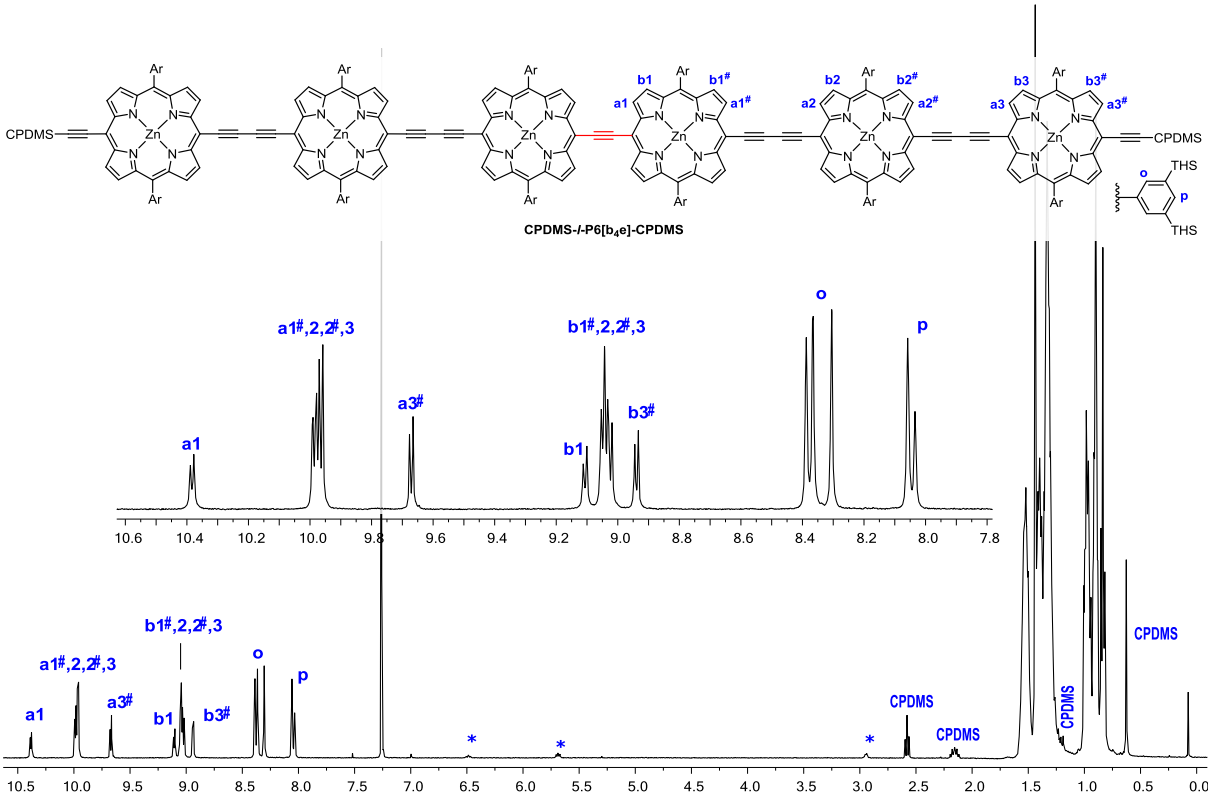

Figure S49: ^{1}H NMR spectrum of compound **CPDMS-*l*-P6[b$_4$e]-CPDMS** (400 MHz, $CDCl_3$, 298 K, * denotes coordinated pyridine).

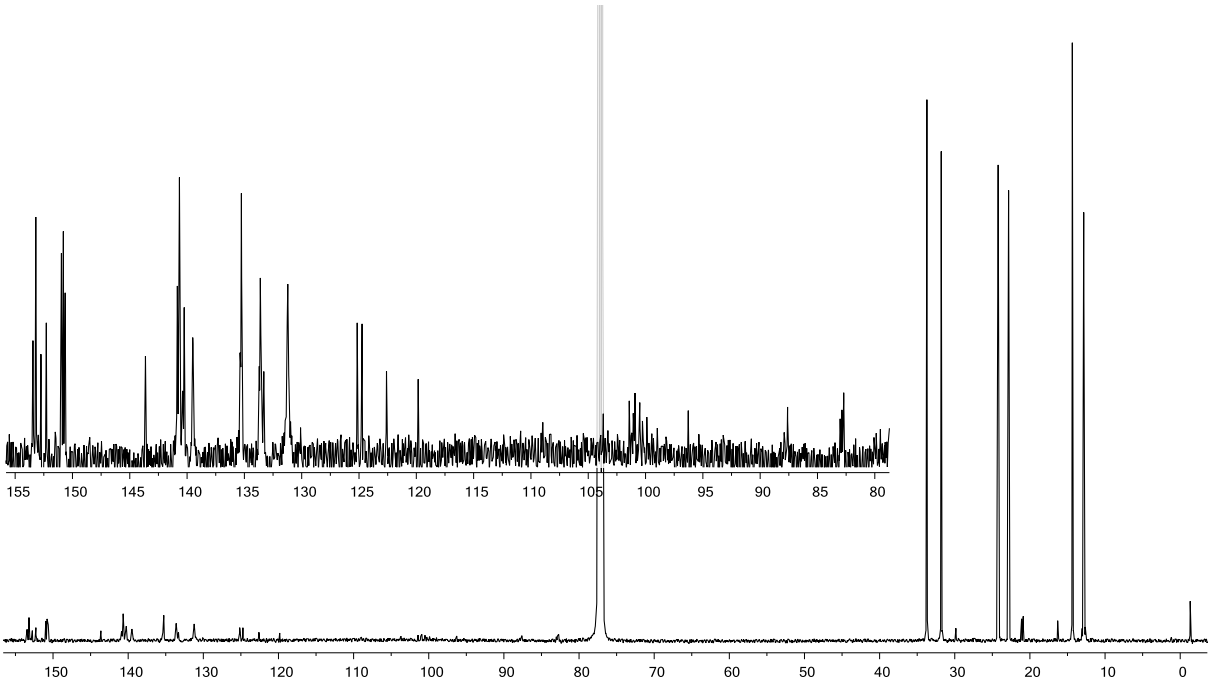

Figure S50: ^{13}C NMR spectrum of compound **CPDMS-*l*-P6[b$_4$e]-CPDMS** (125 MHz, $CDCl_3$, 298 K).

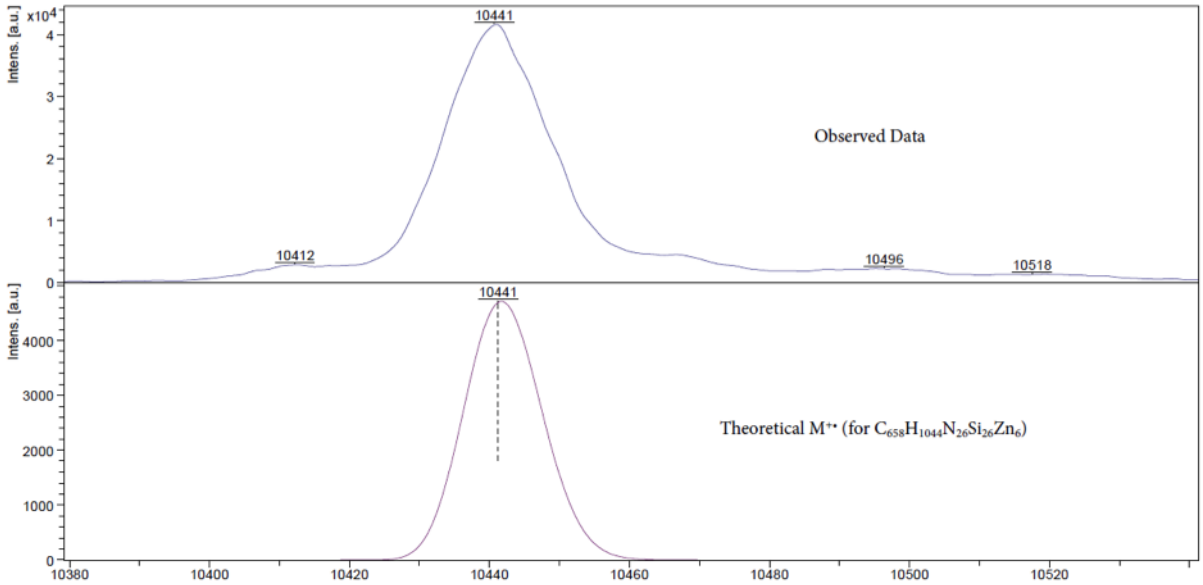

Figure S51: (top) Measured MALDI-ToF spectrum of compound **CPDMS-*l*-P6[b$_4$e]-CPDMS** (matrix: DCTB). (bottom) Simulated MALDI-ToF spectrum of compound **CPDMS-*l*-P6[b$_4$e]-CPDMS** ($[C_{658}H_{1044}N_{26}Si_{26}Zn_6]^+$).

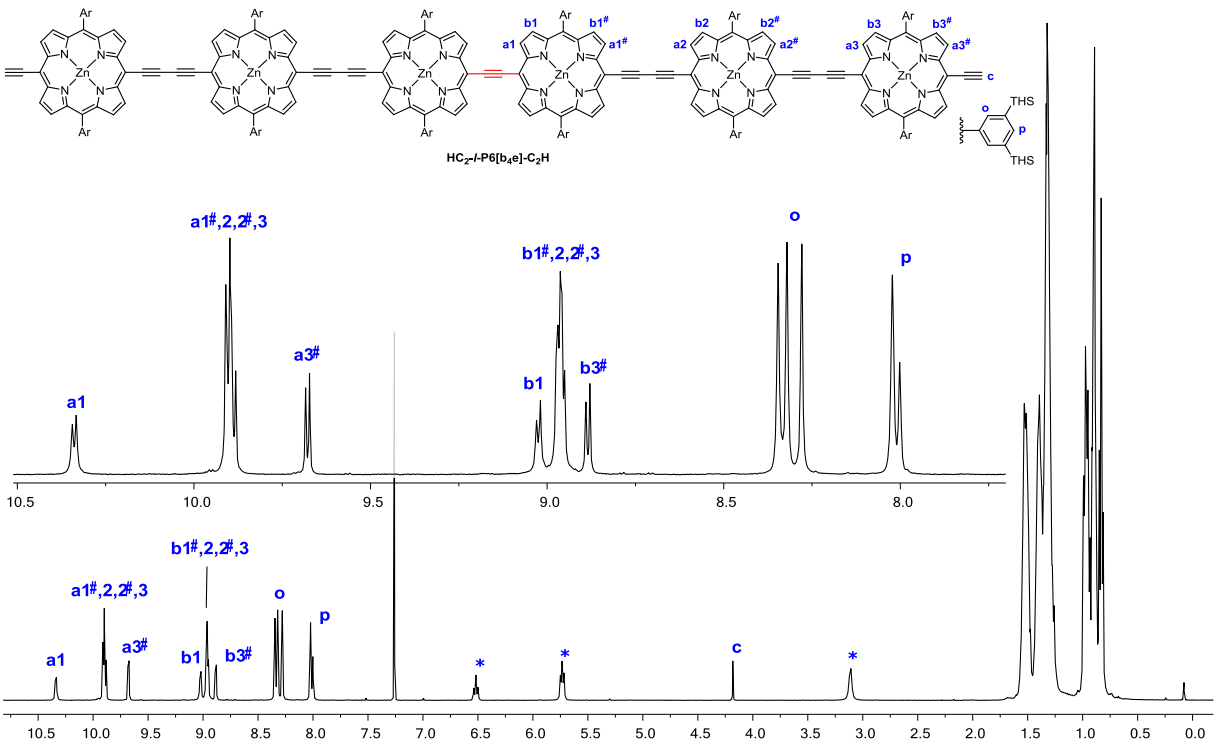

Figure S52: ^{1}H NMR spectrum of compound **HC$_2$-*l*-P6[b$_4$e]-C$_2$H** (400 MHz, $CDCl_3$, 298 K, * denotes coordinated pyridine).

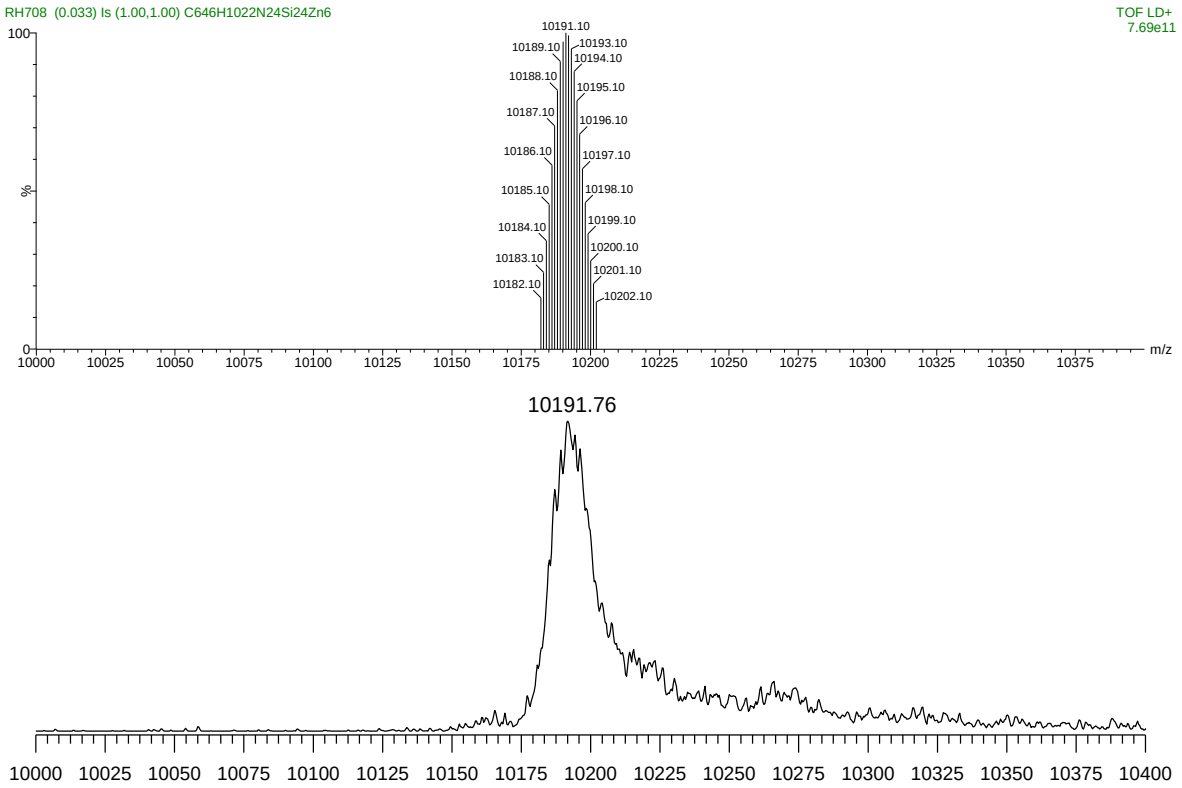

Figure S53: (top) Simulated MALDI-ToF spectrum of compound **HC_2-*l*-P6[b_4e]-C_2H** ($[C_{646}H_{1022}N_{24}Si_{24}Zn_6]^+$). (bottom) Measured MALDI-ToF spectrum of compound **HC_2-*l*-P6[b_4e]-C_2H** (matrix: DCTB)**.**

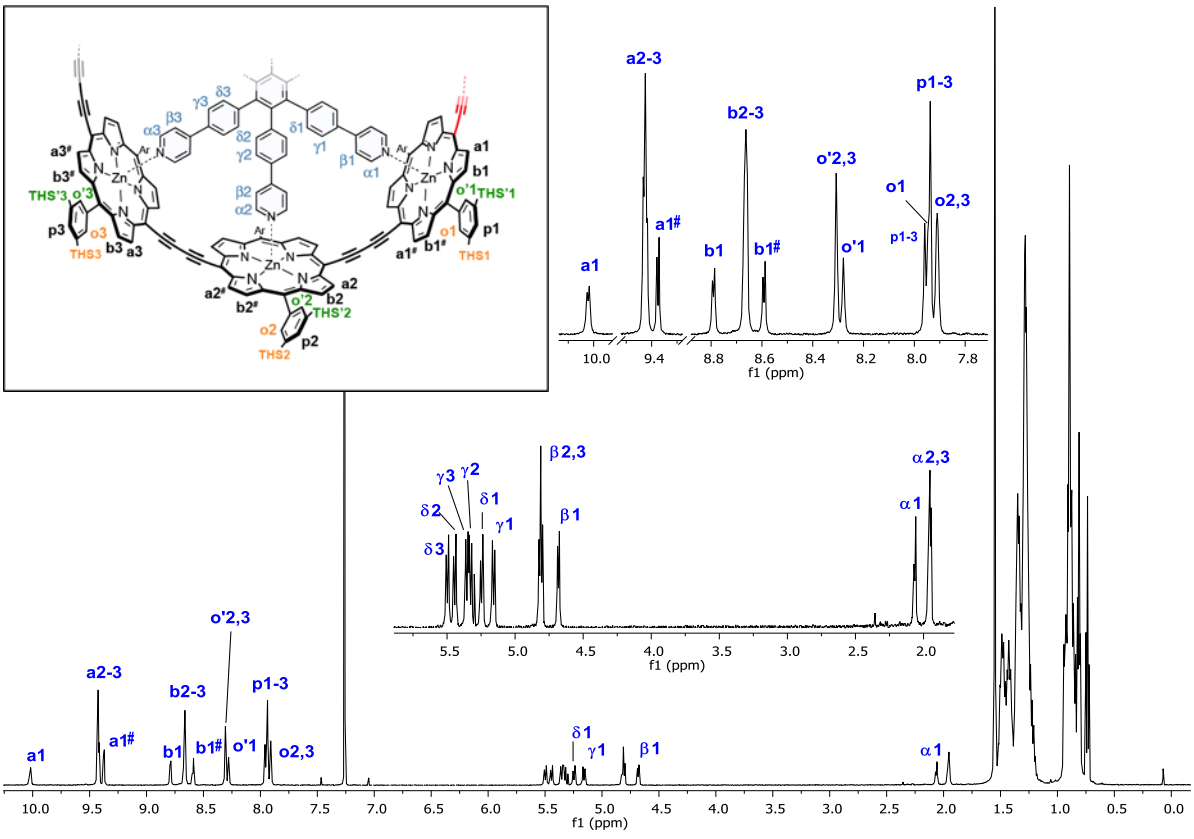

Figure S54: ^{1}H NMR spectrum of compound ***c*-P6[b_5e]·T6** (500 MHz, $CDCl_3$, 298 K).

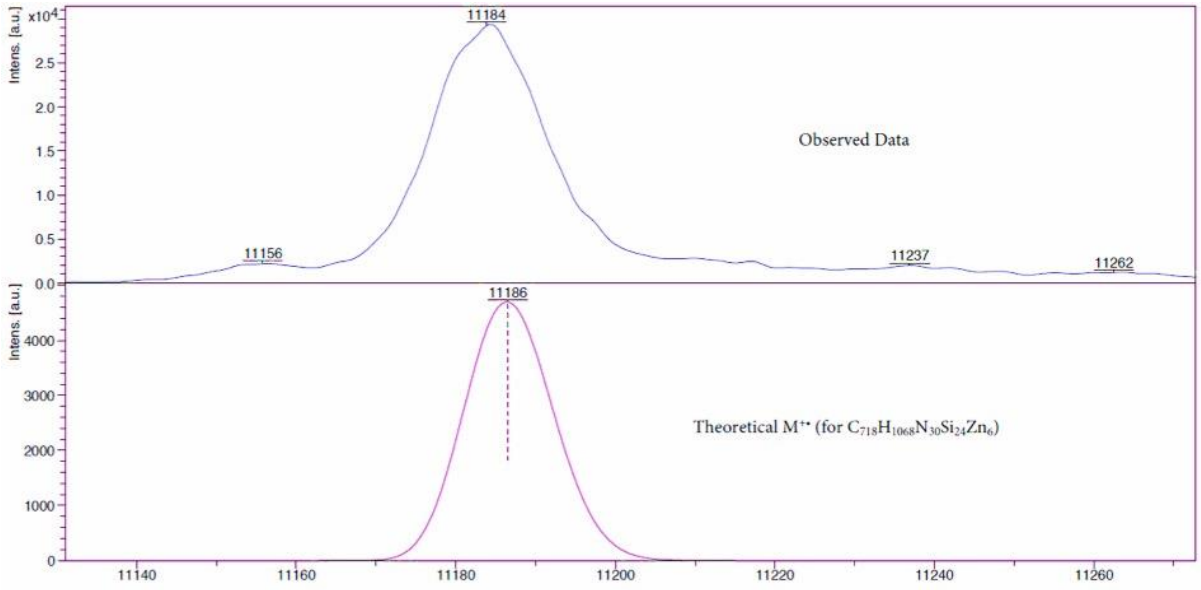

Figure S55: (top) Measured MALDI-ToF spectrum of compound ***c*-P6[b$_5$e]·T6** (matrix: DCTB). (bottom) Simulated MALDI-ToF spectrum of compound ***c*-P6[b$_5$e]·T6** ($[C_{718}H_{1068}N_{30}Si_{24}Zn_6]^+$).

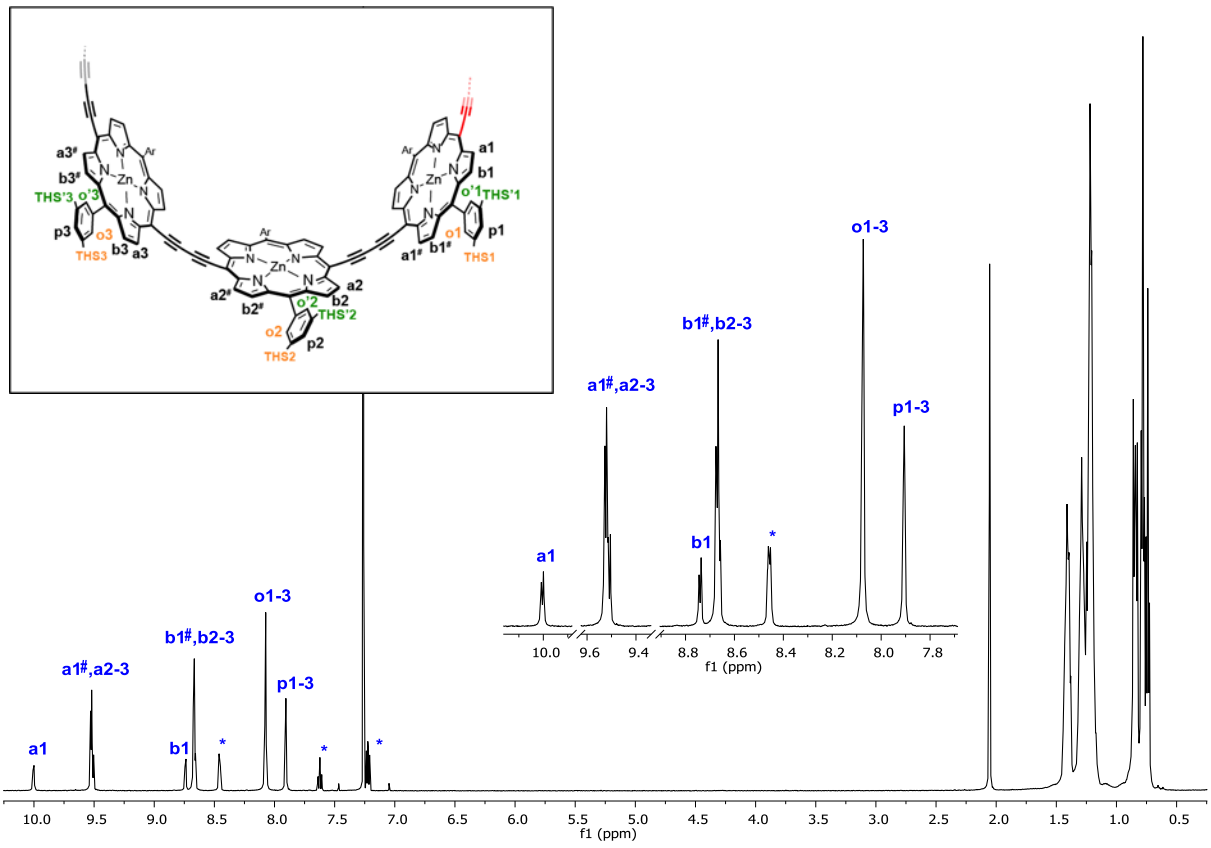

Figure S56: ^{1}H NMR spectrum of compound ***c*-P6[b$_5$e]** (500 MHz, $CDCl_3$ + 1% pyridine-d_5, 298 K, * denotes residual pyridine signals).

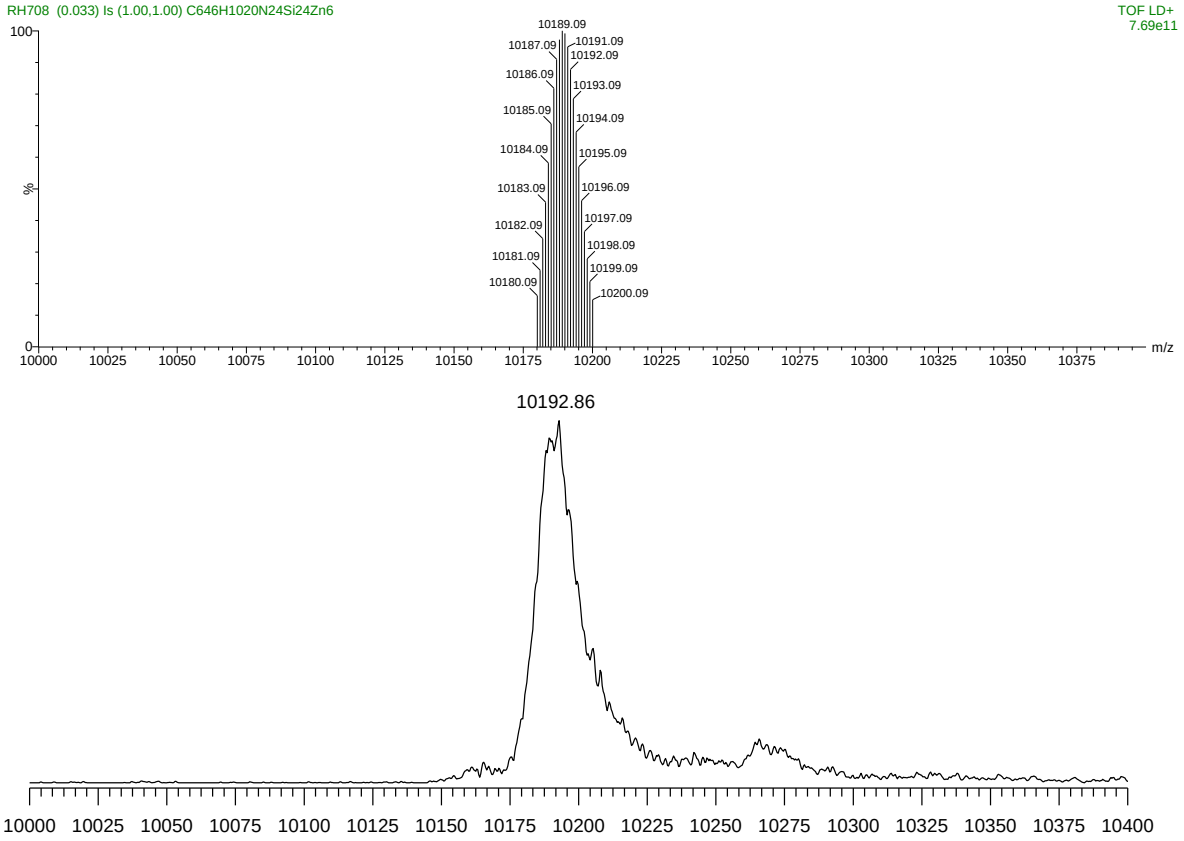

Figure S57: (top) Simulated MALDI-ToF spectrum of compound ***c*-P6[b_5e]** ($[C_{646}H_{1020}N_{24}Si_{24}Zn_6]^+$). (bottom) Measured MALDI-ToF spectrum of compound ***c*-P6[b_5e]** (matrix: DCTB)**.**

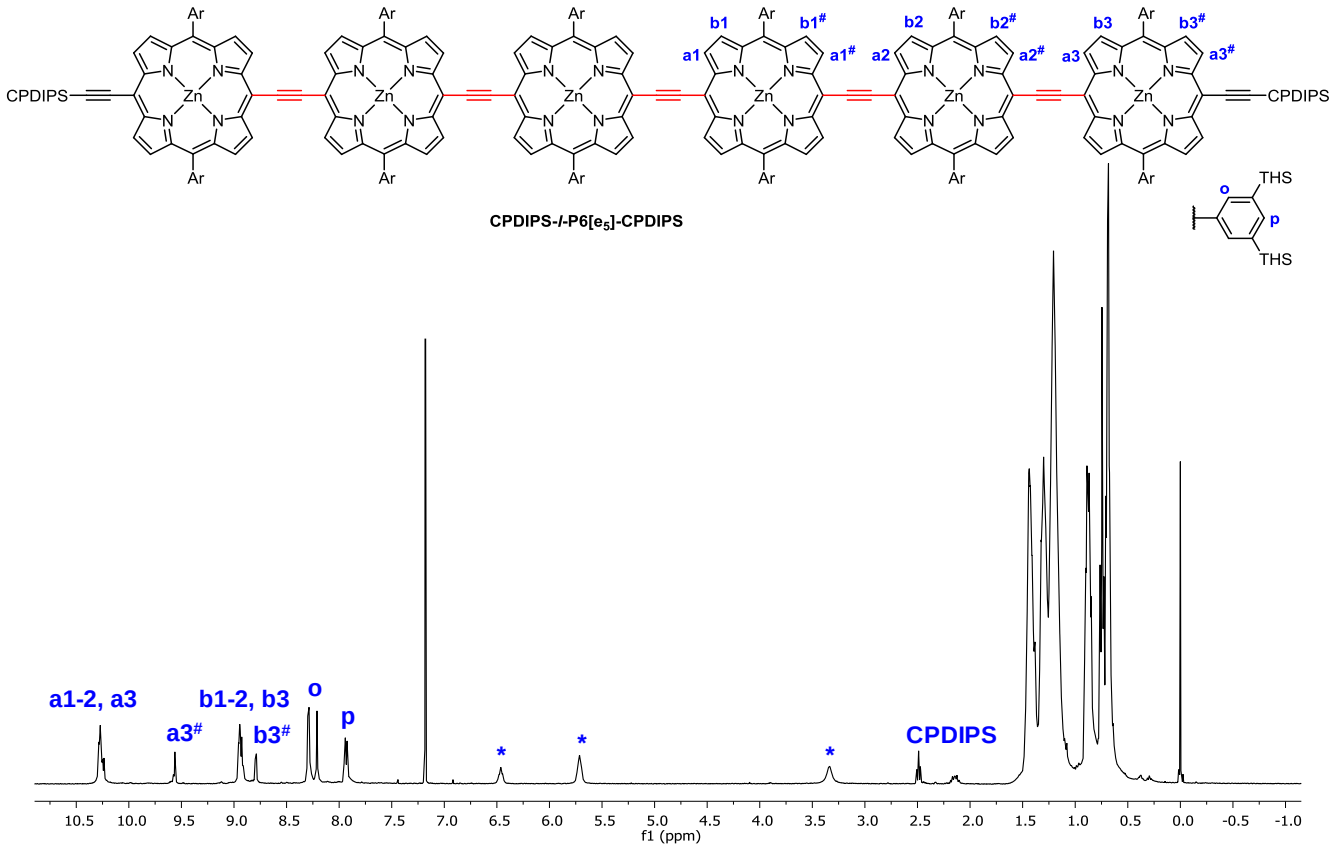

Figure S58: ^{1}H NMR spectrum of compound **CPDIPS-*l*-P6[e$_5$]-CPDIPS** (400 MHz, $CDCl_3$, 298 K, * denotes residual pyridine).

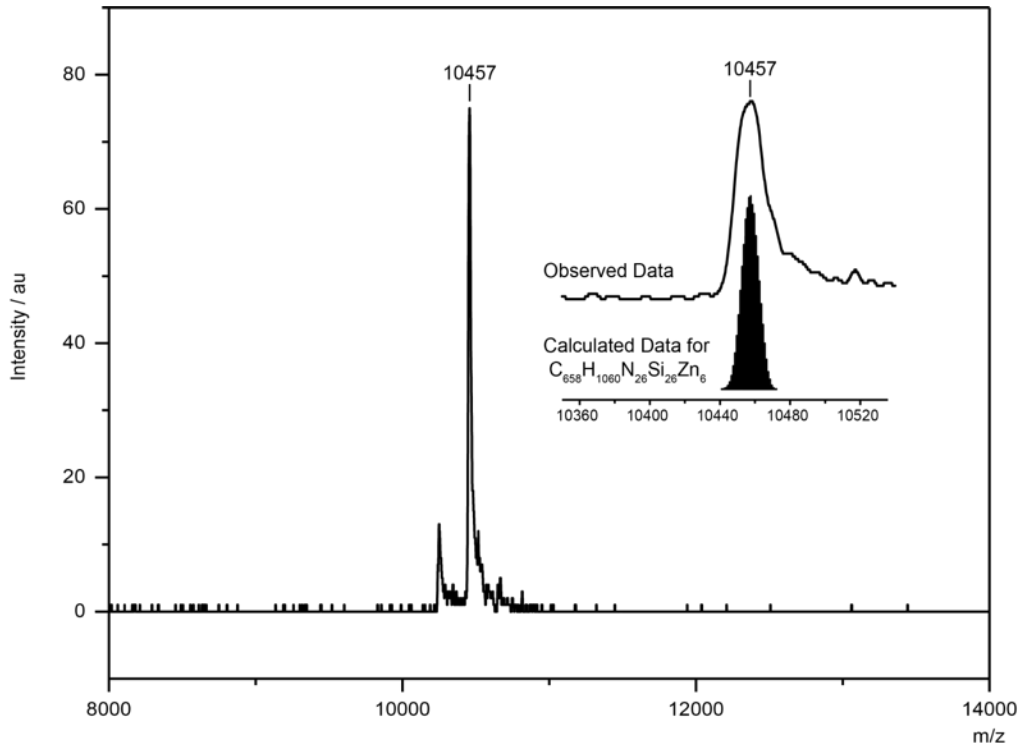

Figure S59: High-resolution MALDI-ToF spectrum of compound **CPDIPS-*l*-P6[e$_5$]-CPDIPS** (matrix: DCTB). Insert shows the predicted isotope distribution for **CPDIPS-*l*-P6[e$_5$]-CPDIPS** ($[C_{658}H_{1060}N_{26}Si_{26}Zn_6]^+$).

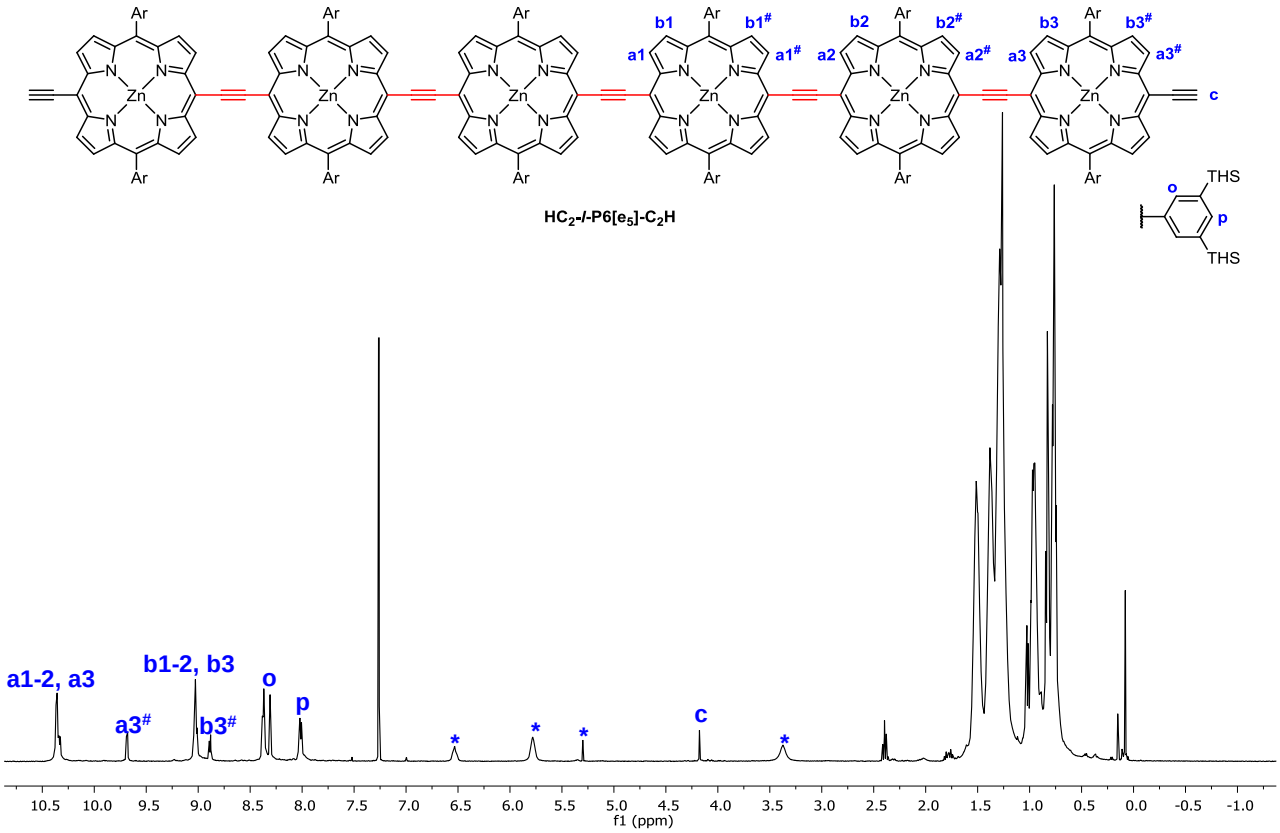

Figure S60: ^{1}H NMR spectrum of compound **HC_2-*l*-P6[e_5]-C_2H** (400 MHz, $CDCl_3$, 298 K, * denotes residual pyridine).

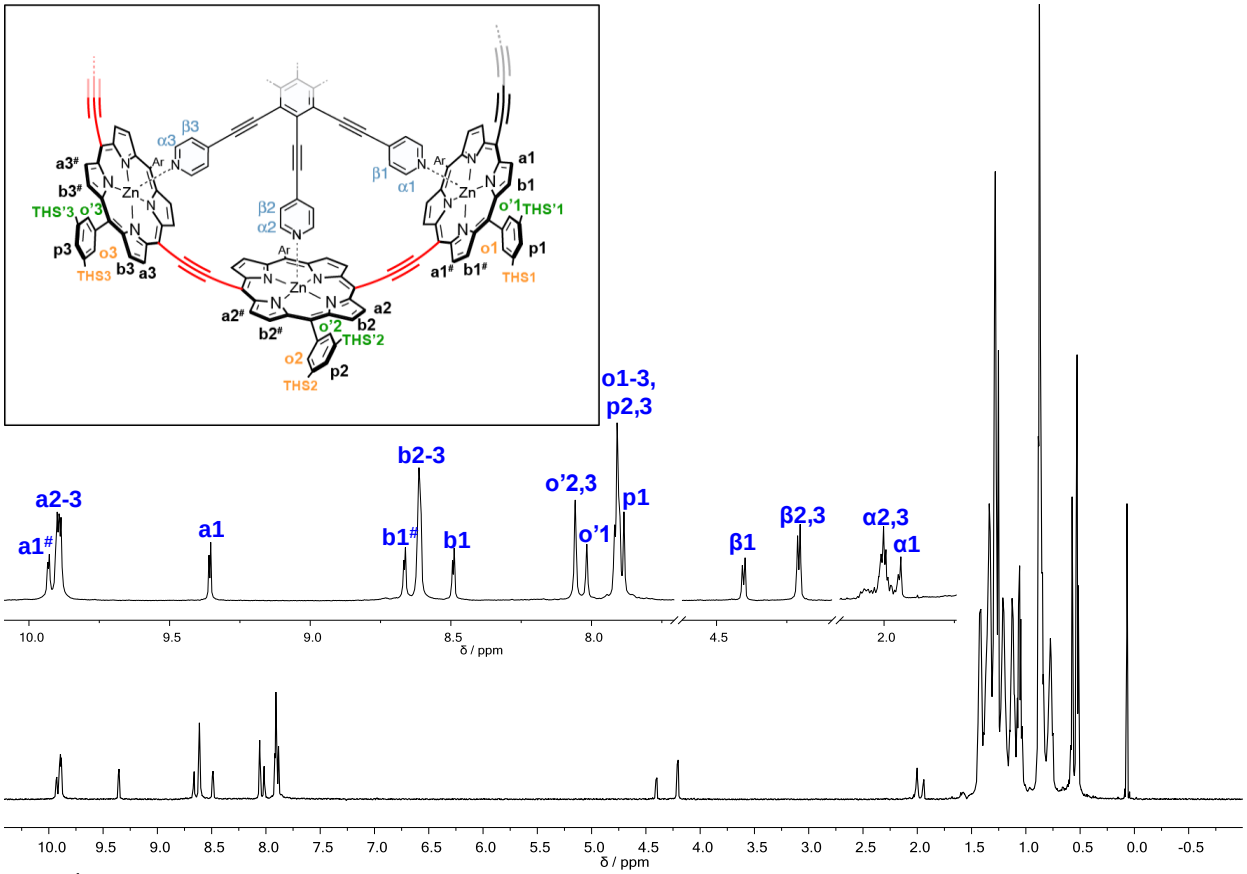

Figure S61: ^{1}H NMR spectrum of compound ***c*-P6[be_5]·T6*** (700 MHz, $CDCl_3$, 298 K).

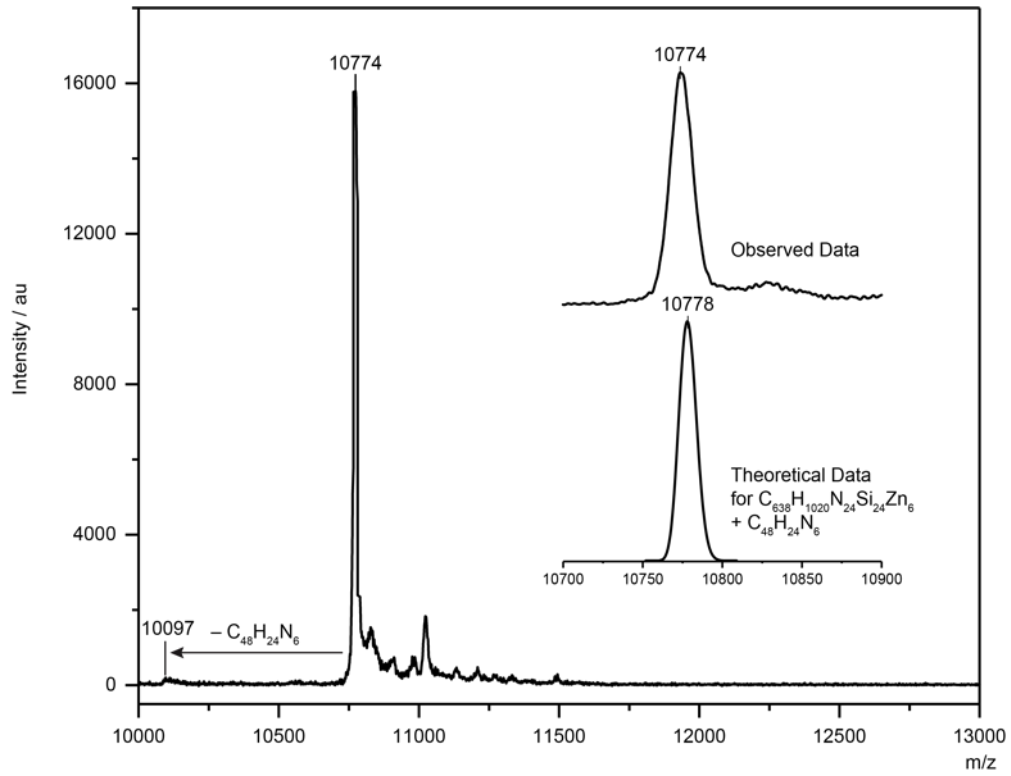

Figure S62: High-resolution MALDI-ToF spectrum of compound ***c*-P6[be$_5$]·T6*** (matrix: DCTB). Insert shows the predicted isotope distribution for ***c*-P6[be$_5$]·T6*** ($[C_{686}H_{1044}N_{30}Si_{24}Zn_6]^+$).

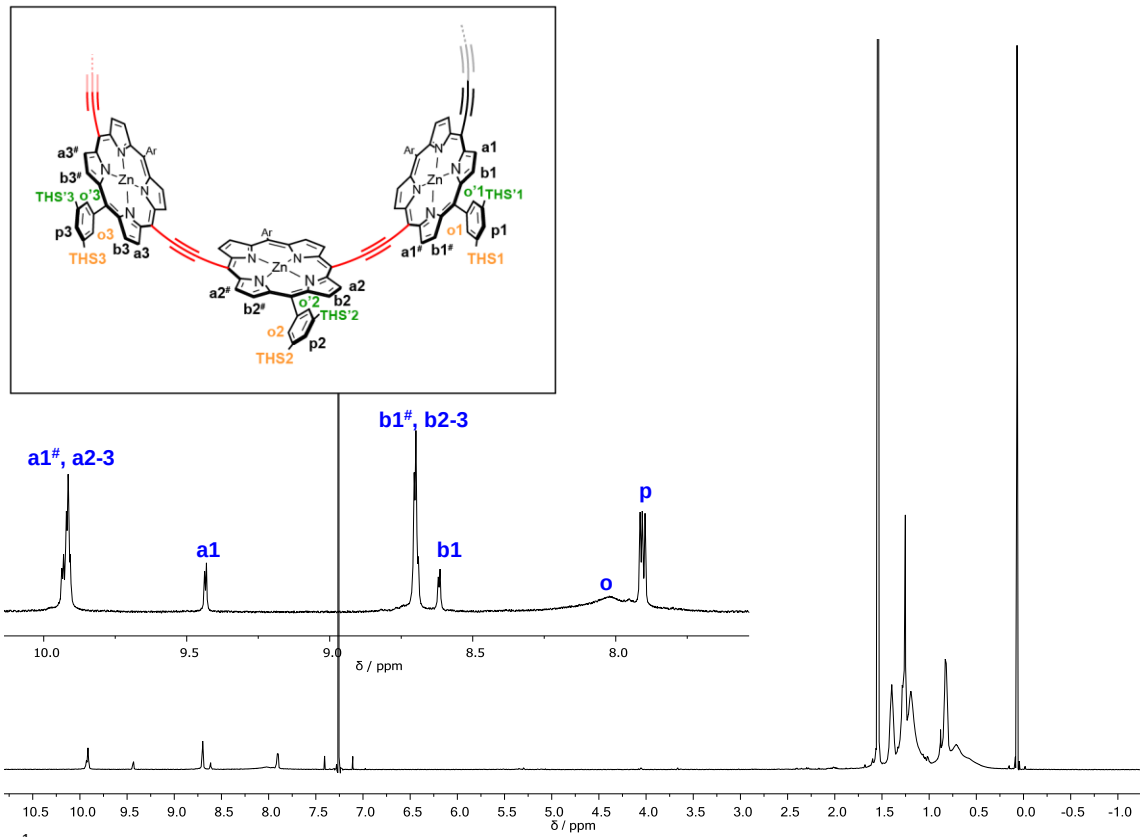

Figure S63: ^{1}H NMR spectrum of compound ***c*-P6[be$_5$]** (700 MHz, $CDCl_3$, 298 K). The ortho resonances are in slow exchange on the NMR timescale and appear broadened.

6 UV-vis-NIR Titrations

6.1 Estimation of Formation Constants

The binding constants of the templates **T6** and **T6*** with ***c*-P6[b$_5$e]**, ***c*-P6[b$_6$]**, ***c*-P6[be$_5$]** and ***c*-P6[e$_6$]** were determined by denaturation titrations (break-up titration) with the competing ligands *N*-methylimidazole or pyridine. In order to determine the strain energy of ***c*-P6[b$_5$e]**, the binding constant for **HC$_2$-*l*-P6[b$_4$e]-C$_2$H** was determined using pyridine as a competing ligand.

Using the data from these denaturation titrations (K_{dn} = denaturation constant) and the formation constant of the single site binding event of the competing ligand with a zinc-porphyrin monomer (K_{ref} = association constant for *N*-methyl imidazole or pyridine to THS-monomer), allows us to derive the formation binding constant (K_f) between the porphyrin nanorings and the templates using the following equation:

$$K_{\mathrm{f}} = \frac{K_{\mathrm{ref}}^{6}}{K_{\mathrm{dn}}}$$

via the thermodynamic cycle shown in Figure S64.

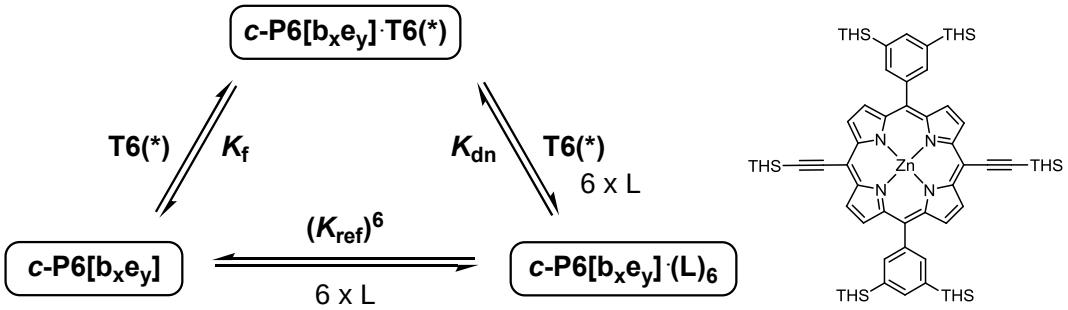

Figure S64: (left) Generalized thermodynamic cycle of ***c*-P6[b$_x$e$_y$]·T6(*)** relating the formation constant of the template complex (K_f) to the denaturation constant (K_{dn}) and the binding constant of each porphyrin unit for the competing ligand L (K_{qu} and K_{Me}, respectively). (right). Structure of the THS-monomer, used to determine K_{ref}; THS = trihexylsilyl.

Table S5: Summary of UV-vis-NIR reference titrations with THS-monomer.

complex	K_{ref} (M^{-1})	K_σ	$K_{chem\ ref}$
***l*-P1·pyridine**	$(1.3 \pm 0.1) \times 10^4$	2	$(6.5 \pm 0.6) \times 10^3$
***l*-P1·methylimidazole**	$(4.2 \pm 0.4) \times 10^5$	2	$(2.0 \pm 0.2) \times 10^5$
***l*-P1·4-phenylpyridine**	$(3.4 \pm 0.3) \times 10^4$	2	$(1.7 \pm 0.2) \times 10^4$
***l*-P1·(4-phenylethynyl)pyridine**	$(6.3 \pm 0.6) \times 10^3$	2	$(3.2 \pm 0.3) \times 10^3$

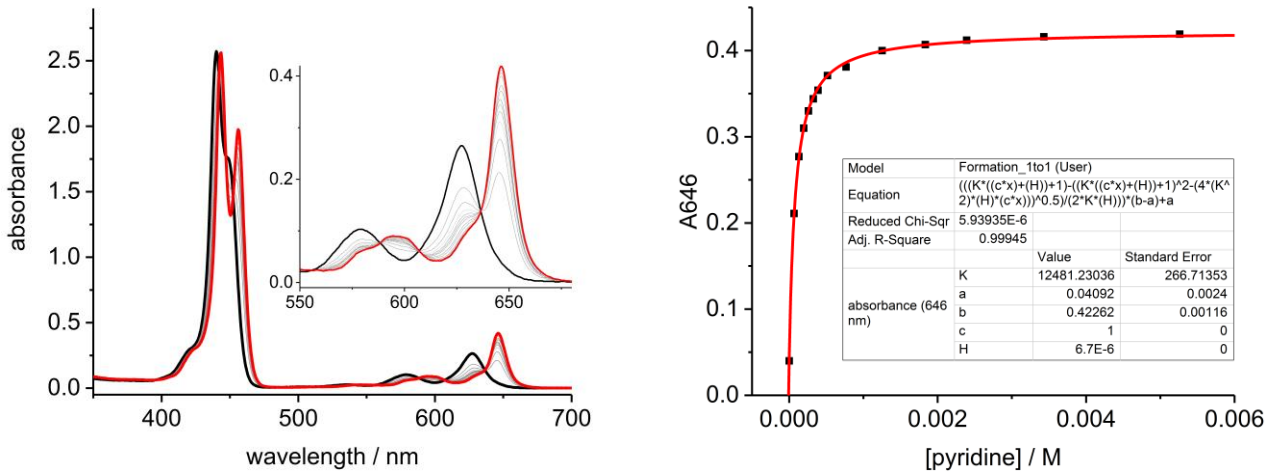

Figure S65: UV-vis titration of pyridine and THS-monomer (run 1, toluene, 298 K, [THS-monomer] = 6.7 µM, K_{ref} = 1.2 × 10^4 M^{-1}).

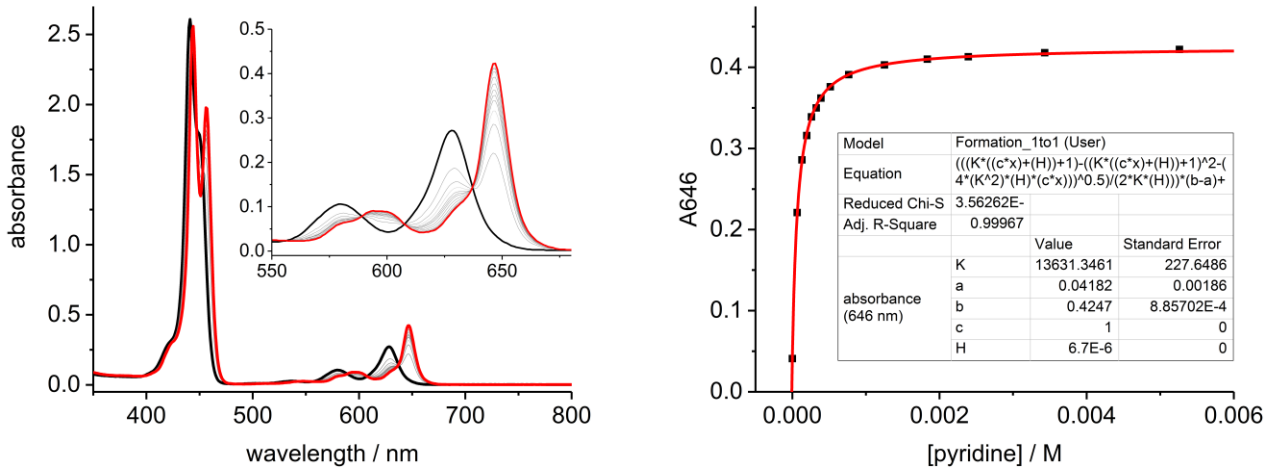

Figure S66: UV-vis titration of pyridine and THS-monomer (run 2, toluene, 298 K, [THS-monomer] = 6.7 µM, K_{ref} = 1.4 × 10^4 M^{-1}).

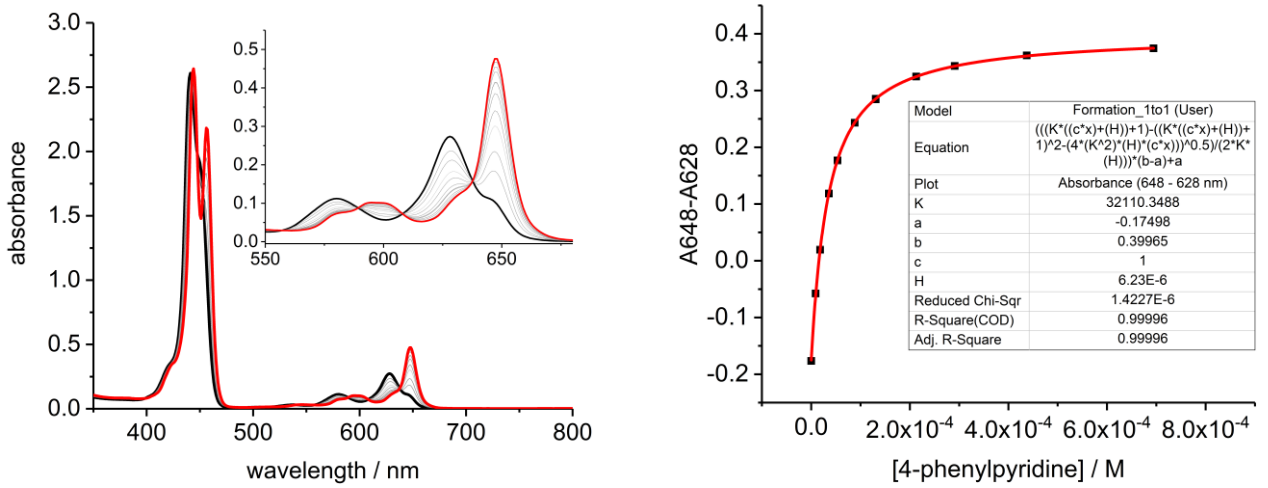

Figure S67: UV-vis titration of 4-phenylpyridine and THS-monomer (run 1, toluene, 298 K, [THS-monomer] = 6.2 µM, K_{ref} = 3.2 × 10^4 M^{-1}).

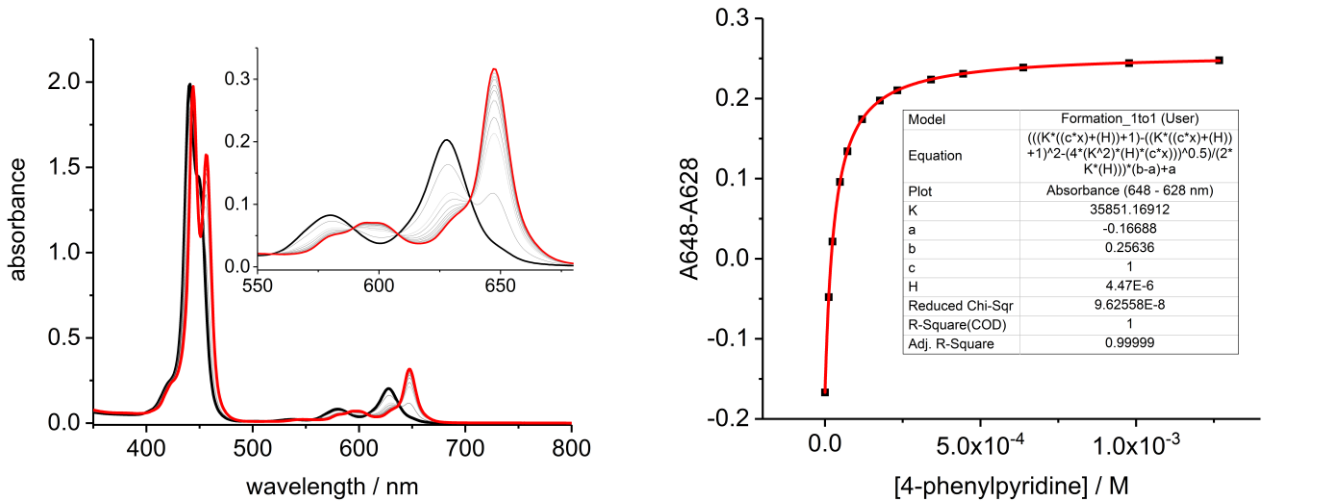

Figure S68: UV-vis titration of 4-phenylpyridine and THS-monomer (run 2, toluene, 298 K, [THS-monomer] = 4.5 µM, K_{ref} = 3.6 × 10^4 M^{-1}).

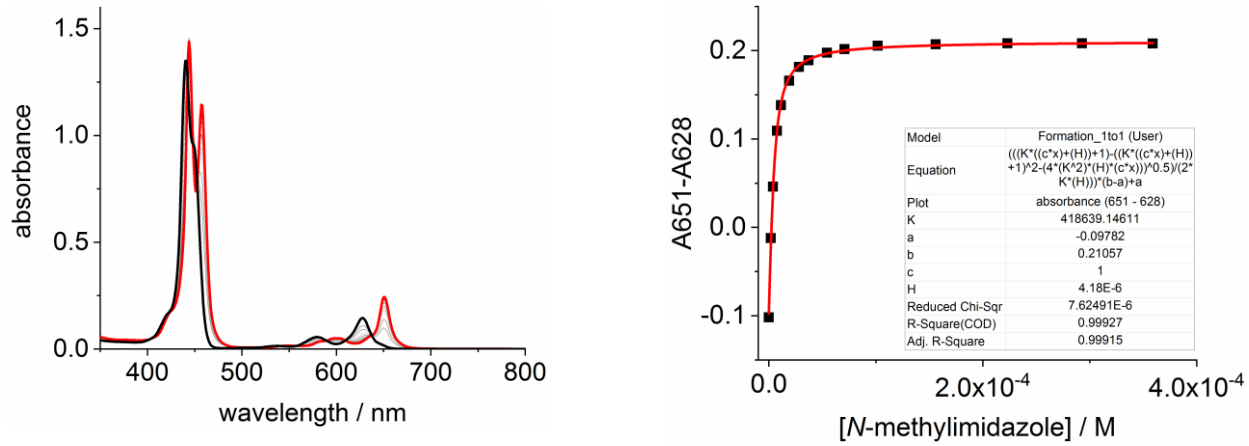

Figure S69: UV-vis titration of *N*-methylimidazole and THS-monomer (run 1, toluene, 298 K, [THS-monomer] = 4.2 µM, K_{ref} = 4.2 × 10^5 M^{-1}).

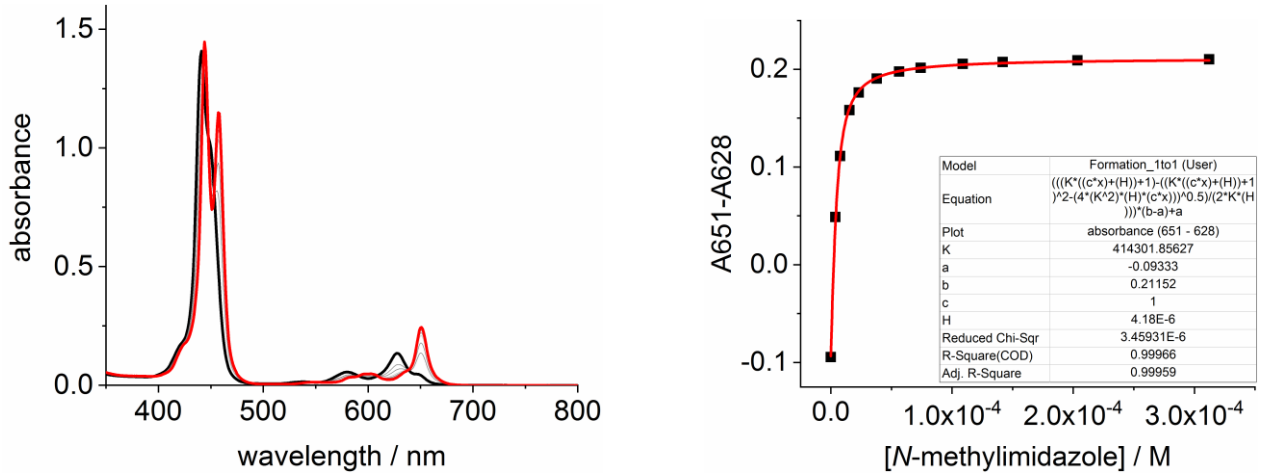

Figure S70: UV-vis titration of *N*-methylimidazole and THS-monomer (run 2, toluene, 298 K, [THS-monomer] = 4.2 µM, K_{ref} = 4.1 × 10^5 M^{-1}).

Table S6: Summary of denaturation constants and formation constants (measured in toluene at 298 K).

complex	denaturant	K_{dn} (M^{-5})	K_f (M^{-1})	log K_f (M^{-1})
HC_2-*l*-P6[e_5]-C_2H·T6*	pyridine	$(7.4 \pm 0.7) \times 10^{8}$	$(6.5 \pm 3.9) \times 10^{15}$	15.8 ± 0.3
HC_2-*l*-P6[b_4e]-C_2H·T6	pyridine	$(5.9 \pm 0.7) \times 10^{4}$	$(8.2 \pm 5.0) \times 10^{19}$	19.9 ± 0.3
HC_2-*l*-P6[b_5]-C_2H·T6	pyridine	$(7.0 \pm 3.0) \times 10^{3}$	$(6.9 \pm 5.1) \times 10^{20}$	20.8 ± 0.3
c*-P6[e_6]·T6	pyridine	$(5.1 \pm 0.4) \times 10^{-5}$	$(9.5 \pm 5.7) \times 10^{28}$	29.0 ± 0.3
c*-P6[be_5]·T6	*N*-methylimidazole	$(1.9 \pm 0.3) \times 10^{-5}$	$(2.9 \pm 1.8) \times 10^{38}$	38.5 ± 0.3
***c*-P6[b_5e]·T6**	*N*-methylimidazole	$(1.4 \pm 0.1) \times 10^{-2}$	$(3.9 \pm 2.3) \times 10^{35}$	35.6 ± 0.3
***c*-P6[b_6]·T6**	*N*-methylimidazole	$(5.4 \pm 0.6) \times 10^{-4}$	$(1.0 \pm 0.6) \times 10^{37}$	37.0 ± 0.3

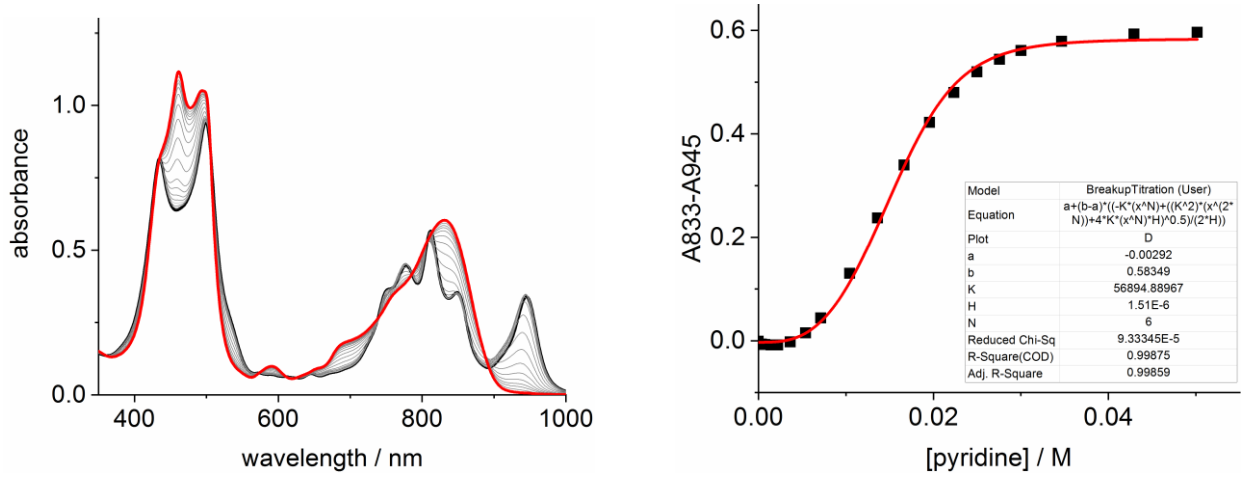

Figure S71: UV-vis-NIR titration of pyridine and **HC_2-*l*-P6[b_4e]-C_2H·T6** illustrating the removal of the **T6** template (run 1, toluene, 298 K, [**HC_2-*l*-P6[b_4e]-C_2H·T6**] = 1.5 µM, $K_{dn} = 5.7 \times 10^4$ M^{-5}).

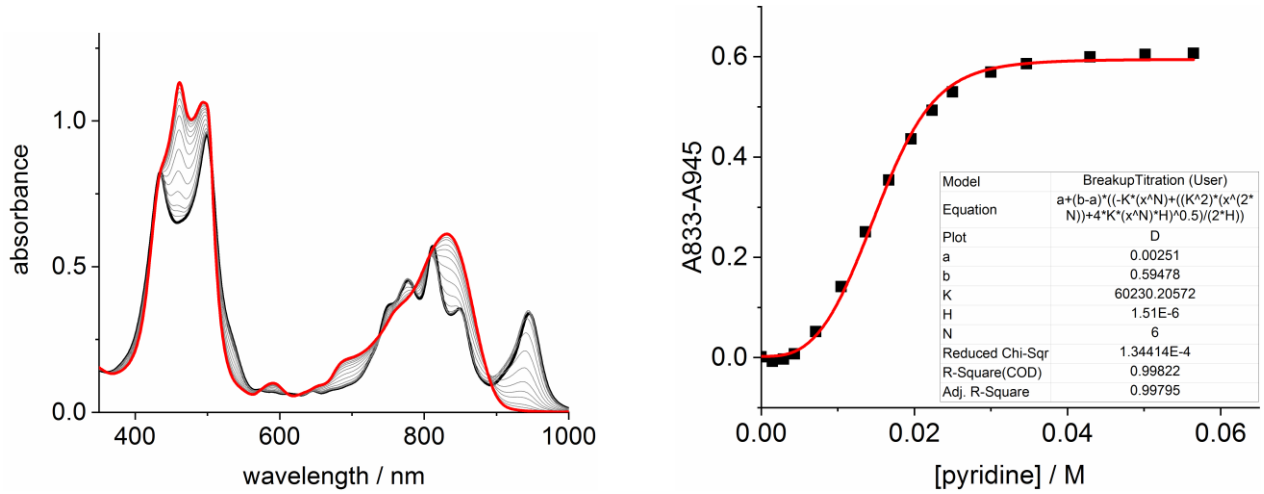

Figure S72: UV-vis-NIR titration of pyridine and **HC_2-*l*-P6[b_4e]-C_2H·T6** illustrating the removal of the **T6** template (run 2, toluene, 298 K, [**HC_2-*l*-P6[b_4e]-C_2H·T6**] = 1.5 µM, $K_{dn} = 6.0 \times 10^4$ M^{-5}).

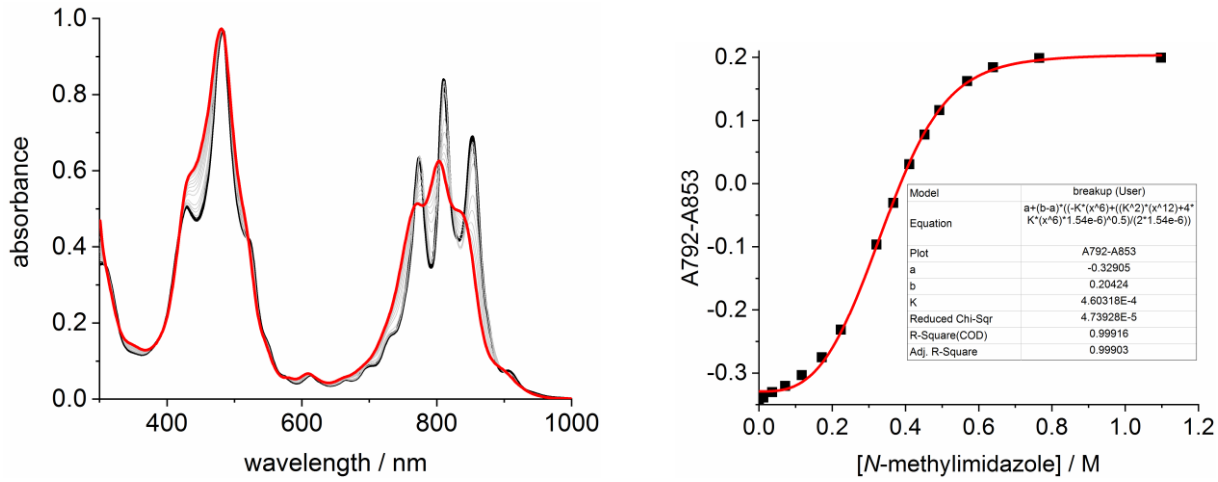

Figure S73: UV-vis-NIR titration of *N*-methylimidazole and ***c*-P6[b$_6$]·T6** illustrating the removal of the **T6** template (run 1, toluene, 298 K, [***c*-P6[b$_6$]·T6**] = 1.5 μM, $K_{dn} = 4.6 \times 10^{-4}$ M^{-5}).

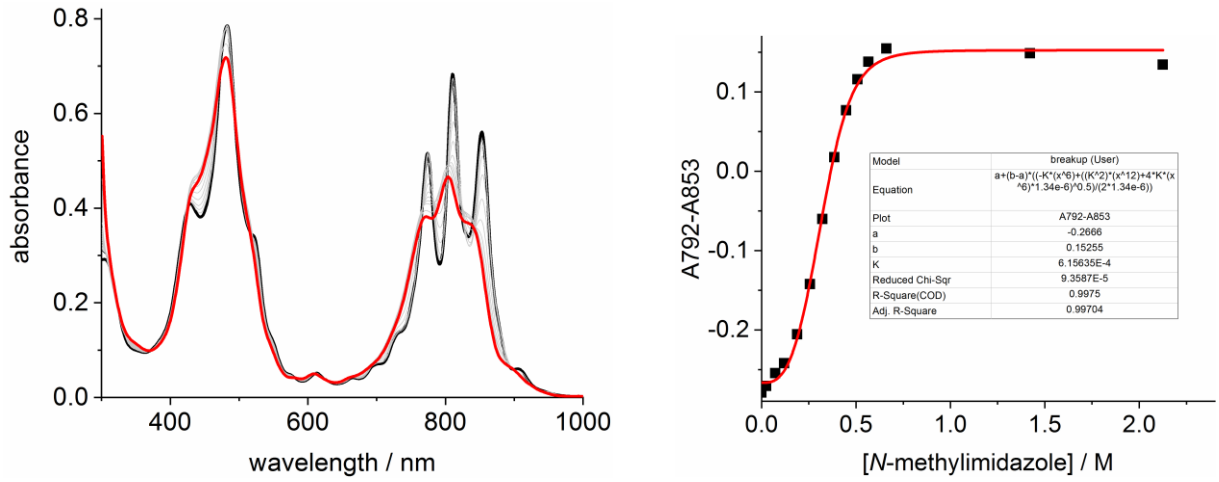

Figure S74: UV-vis-NIR titration of *N*-methylimidazole and ***c*-P6[b$_6$]·T6** illustrating the removal of the **T6** template (run 2, toluene, 298 K, [***c*-P6[b$_6$]·T6**] = 1.3 μM, $K_{dn} = 6.1 \times 10^{-4}$ M^{-5}).

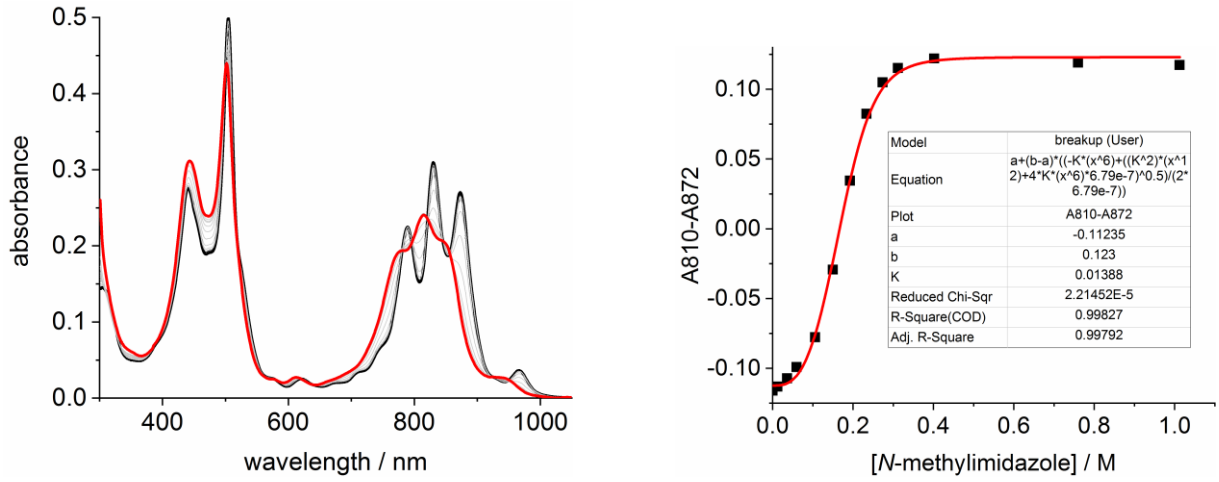

Figure S75: UV-vis-NIR titration of *N*-methylimidazole and ***c*-P6[b$_5$e]·T6** illustrating the removal of the **T6** template (run 1, toluene, 298 K, [***c*-P6[b$_5$e]·T6**] = 0.68 μM, $K_{dn} = 1.4 \times 10^{-2}$ M^{-5}).

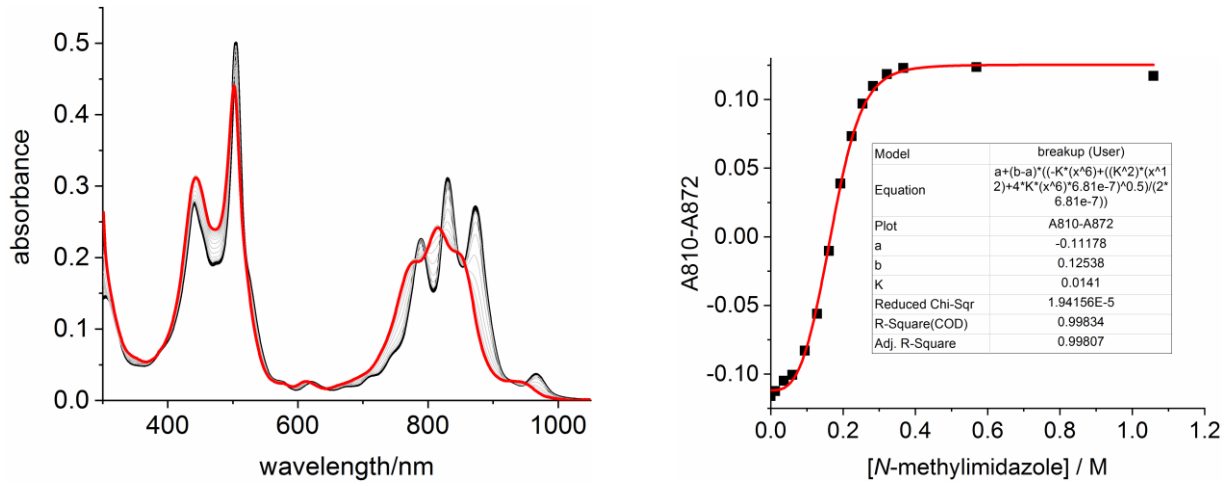

Figure S76: UV-vis-NIR titration of *N*-methylimidazole and ***c*-P6[b$_5$e]·T6** illustrating the removal of the **T6** template (run 2, toluene, 298 K, [***c*-P6[b$_5$e]·T6**] = 0.68 µM, $K_{dn} = 1.4 \times 10^{-2}$ M^{-5}).

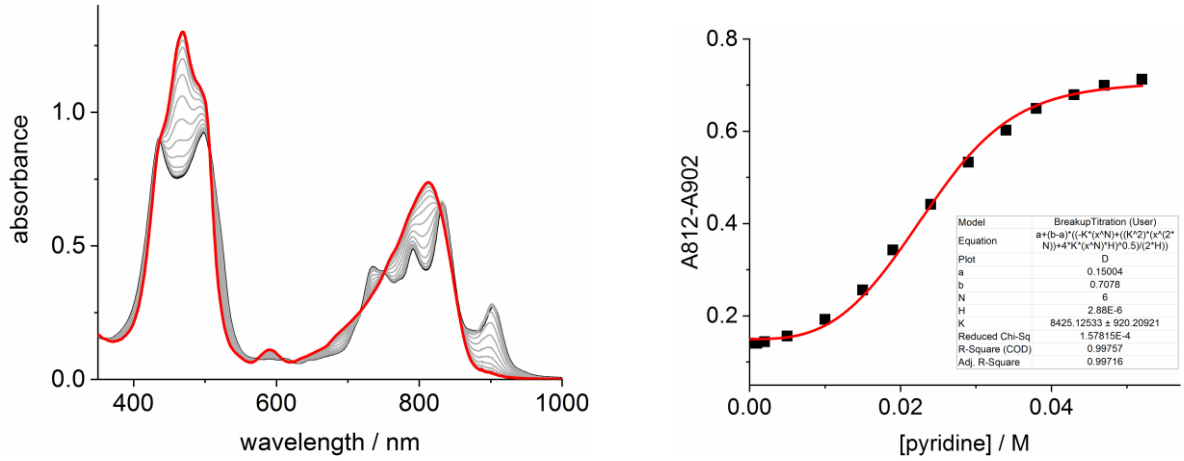

Figure S77: UV-vis-NIR titration of pyridine and **HC$_2$-*l*-P6[b$_5$]-C$_2$H·T6** illustrating the removal of the **T6** template (run 1, toluene, 298 K, [**HC$_2$-*l*-P6[b$_5$]-C$_2$H·T6**] = 2.9 µM, $K_{dn} = 8.4 \times 10^3$ M^{-5}).

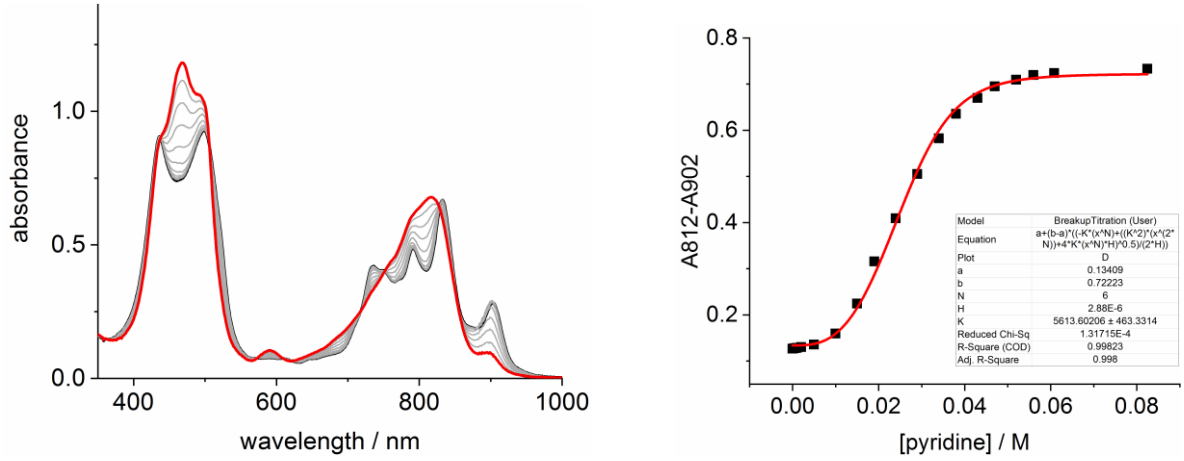

Figure S78: UV-vis-NIR titration of pyridine and **HC$_2$-*l*-P6[b$_5$]-C$_2$H·T6** illustrating the removal of the **T6** template (run 2, toluene, 298 K, [**HC$_2$-*l*-P6[b$_5$]-C$_2$H·T6**] = 2.9 µM, $K_{dn} = 5.6 \times 10^3$ M^{-5}).

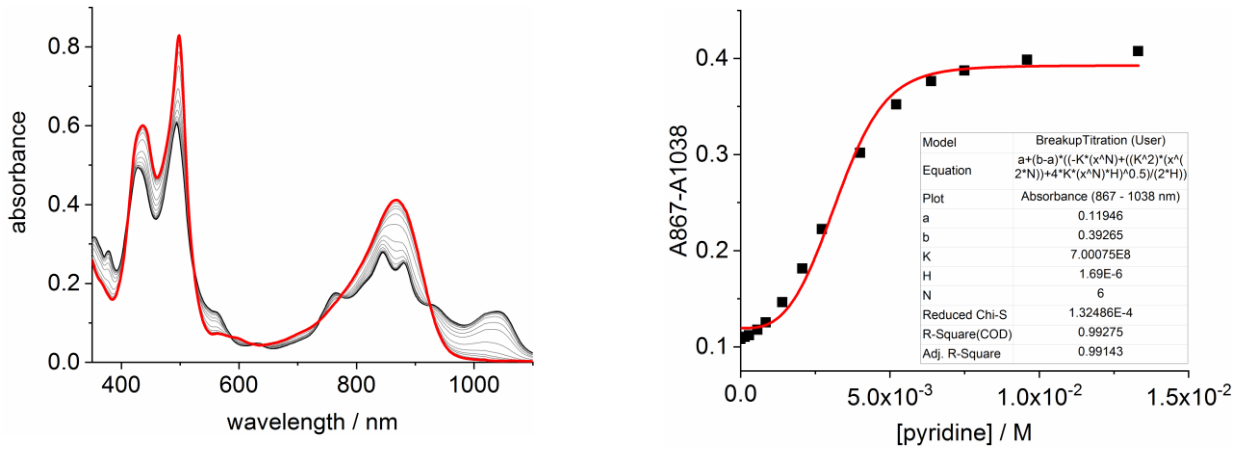

Figure S79: UV-vis-NIR titration of pyridine and **HC_2-*l*-P6[e_5]-C_2H·T6*** illustrating the removal of the **T6*** template (run 1, toluene, 298 K, [**HC_2-*l*-P6[e_5]-C_2H·T6***] = 1.7 μM, $K_{dn} = 7.0 \times 10^8$ M^{-5}).

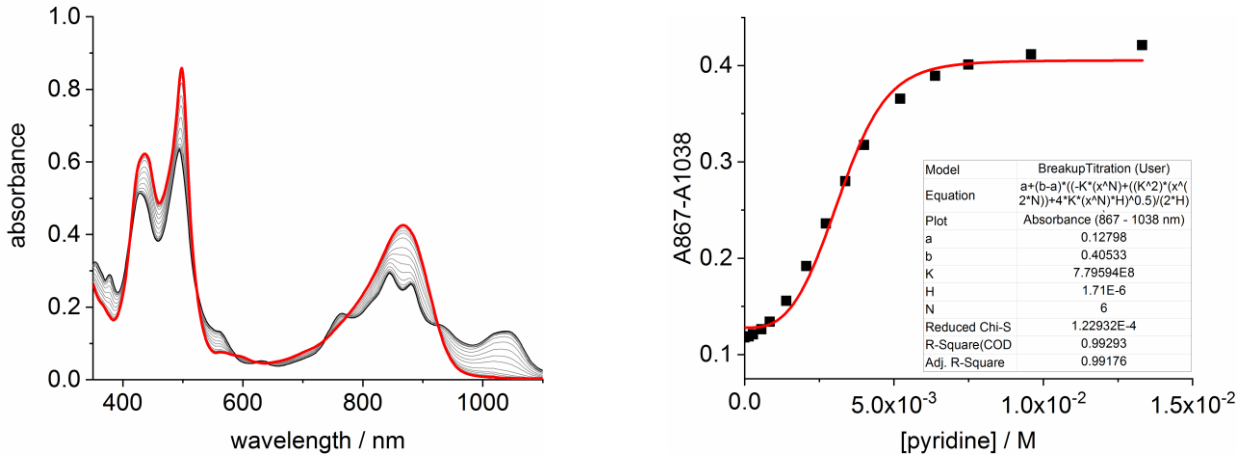

Figure S80: UV-vis-NIR titration of pyridine and **HC_2-*l*-P6[e_5]-C_2H·T6*** illustrating the removal of the **T6*** template (run 2, toluene, 298 K, [**HC_2-*l*-P6[e_5]-C_2H·T6***] = 1.7 μM, $K_{dn} = 7.8 \times 10^8$ M^{-5}).

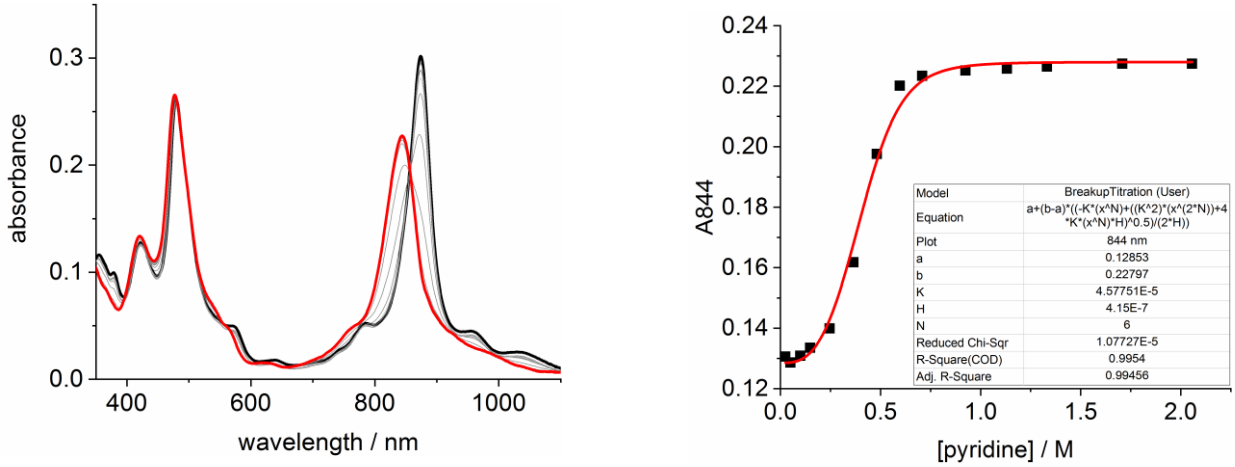

Figure S81: UV-vis-NIR titration of pyridine and ***c*-P6[e_6]·T6*** illustrating the removal of the **T6*** template (Run 1, toluene, 298 K, [***c*-P6[e_6]·T6***] = 0.42 μM, $K_{dn} = 4.6 \times 10^{-5}$ M^{-5}).

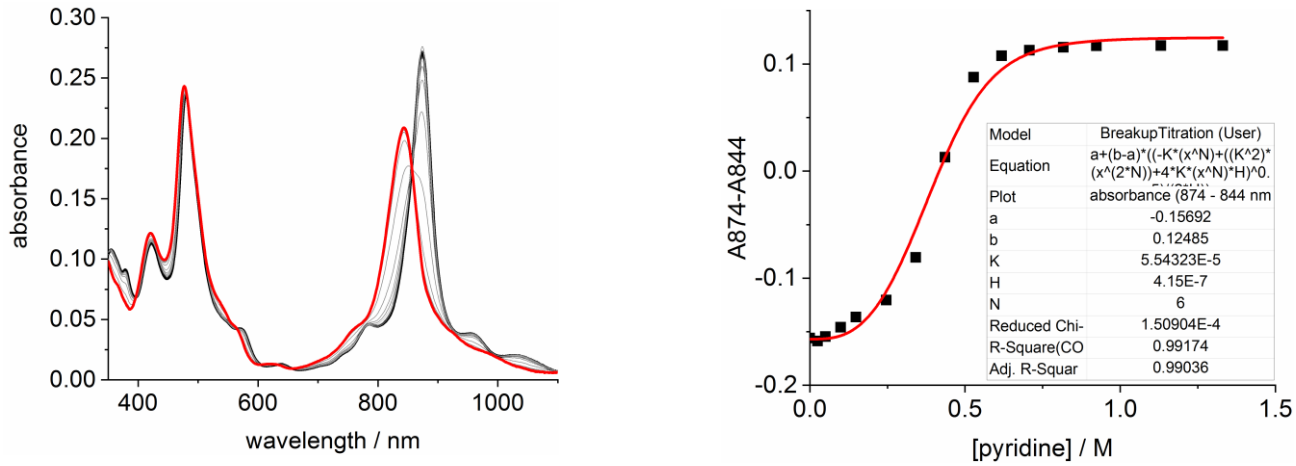

Figure S82: UV-vis-NIR titration of pyridine and ***c*-P6[e$_6$]·T6*** illustrating the removal of the **T6*** template (run 2, toluene, 298 K, [***c*-P6[e$_6$]·T6***] = 0.42 µM, $K_{dn} = 5.5 \times 10^{-5}$ M^{-5}).

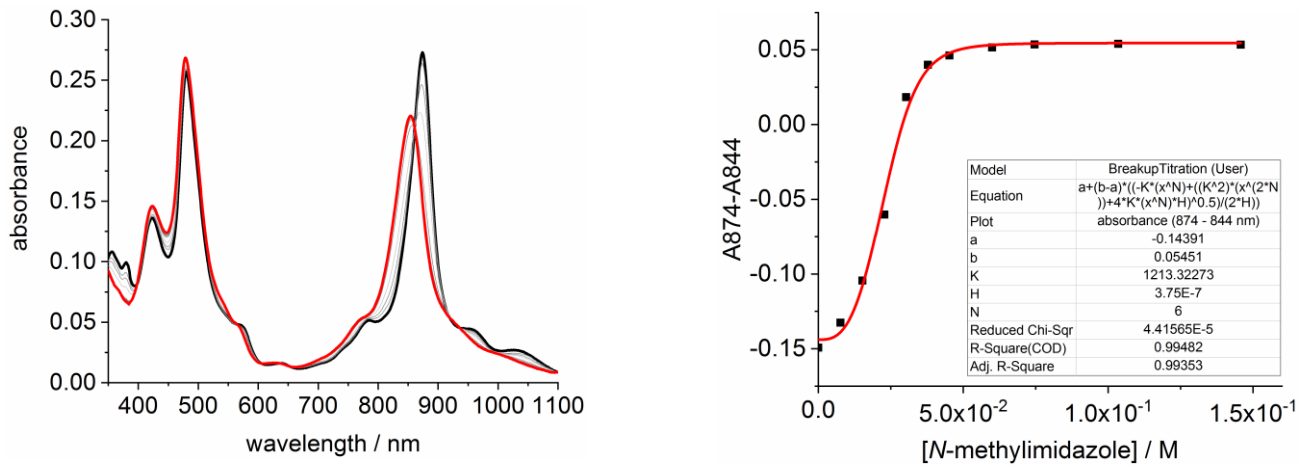

Figure S83: UV-vis-NIR titration of *N*-methylimidazole and ***c*-P6[e$_6$]·T6*** illustrating the removal of the **T6*** template (run 1, toluene, 298 K, [***c*-P6[e$_6$]·T6***] = 0.38 µM, $K_{dn} = 1.2 \times 10^{4}$ M^{-5}).

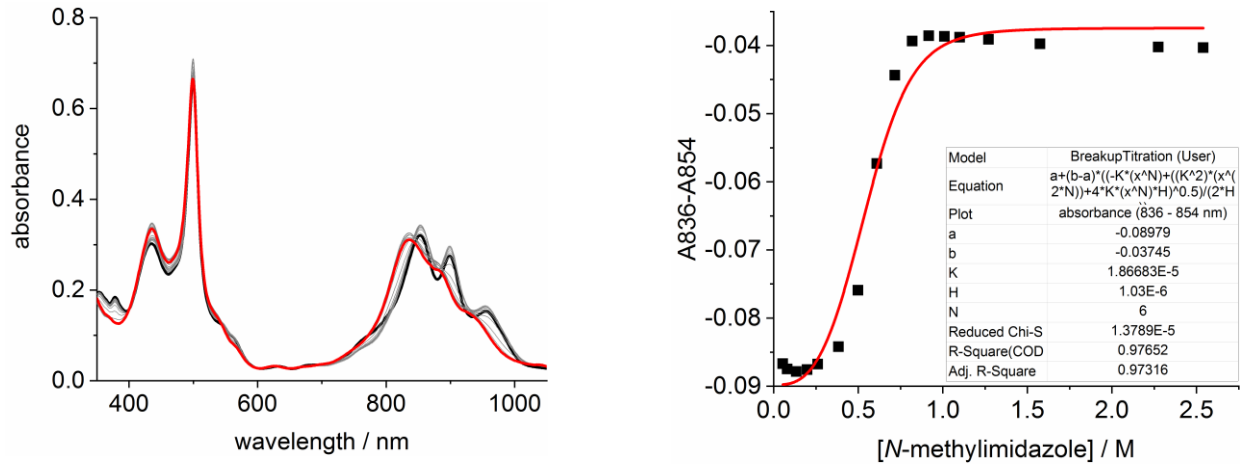

Figure S84: UV-vis-NIR titration of *N*-methylimidazole and ***c*-P6[be$_5$]·T6*** illustrating the removal of the **T6*** template (run 1, toluene, 298 K, [***c*-P6[be$_5$]·T6***] = 1.0 µM, $K_{dn} = 1.9 \times 10^{-5}$ M^{-5}).

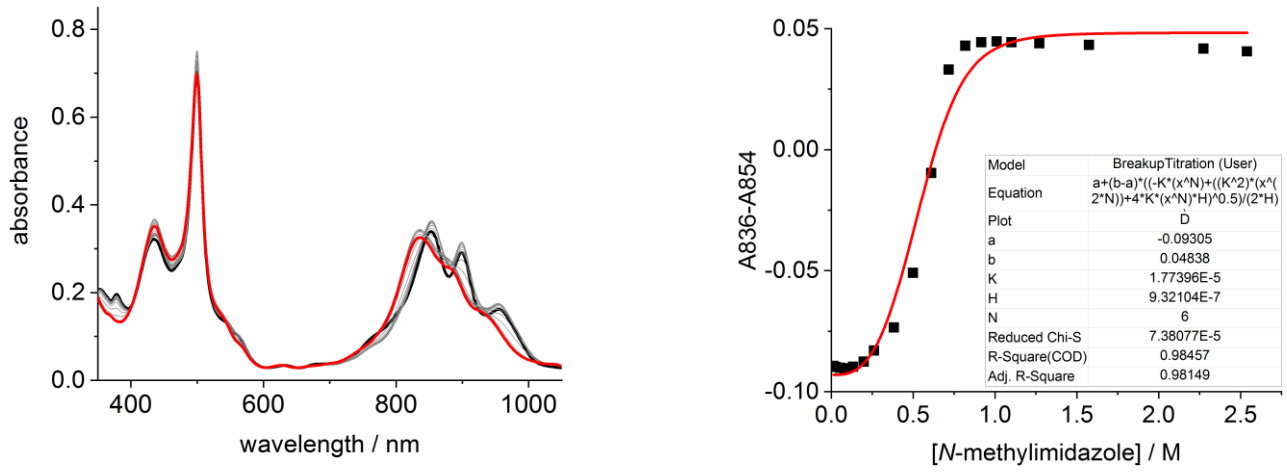

Figure S85: UV-vis-NIR titration of *N*-methylimidazole and ***c*-P6[be$_5$]·T6*** illustrating the removal of the **T6*** template (run 2, toluene, 298 K, [***c*-P6[be$_5$]·T6***] = 0.97 µM, K_{dn} = 1.8 × 10^{-5} M^{-5}).

6.2 Estimation of Statistically-Corrected Effective Molarities

Average effective molarities were calculated using the equation:

$$\overline{EM} = \sqrt[5]{\frac{K_{\text{chem}}}{K_1^6}}$$

where K_{chem} is the statistically corrected formation constant of the nanoring-template complex ($K_{\text{chem}} = K_f/K_\sigma$) and K_1 is the statistically corrected binding constant for a reference ligand (4-phenylpyridine for **T6**; 4-phenylethynyl pyridine for **T6***) from Table S5. Statistical factors (K_σ) were calculated using Benson's symmetry number method (and it works out that in every case the value is 768).[7–9]

Table S7: Summary of formation constants and effective molarities.

complex	log K_f (M^{-1})	log K_{chem} (M^{-1})	$\overline{\text{EM}}$ (M)	log$\overline{\text{EM}}$
HC$_2$-*l*-P6[e$_5$]-C$_2$H·T6*	15.8 ± 0.3	12.9 ± 0.3	0.024 ± 0.006	–1.6 ± 0.1
HC$_2$-*l*-P6[b$_4$e]-C$_2$H·T6	19.9 ± 0.3	17.0 ± 0.3	0.020 ± 0.005	–1.7 ± 0.1
HC$_2$-*l*-P6[b$_5$]-C$_2$H·T6	20.9 ± 0.3	18.0 ± 0.3	0.032 ± 0.007	–1.5 ± 0.1
c*-P6[e$_6$]·T6	29.0 ± 0.3	26.1 ± 0.3	10 ± 2	1.0 ± 0.1
c*-P6[be$_5$]·T6	38.5 ± 0.3	35.6 ± 0.3	830 ± 190	2.9 ± 0.1
***c*-P6[b$_5$e]·T6**	35.6 ± 0.4	32.7 ± 0.4	28 ± 6	1.4 ± 0.1
***c*-P6[b$_6$]·T6**	37.0 ± 0.4	34.1 ± 0.4	52 ± 6	1.7 ± 0.1

6.3 Calculations of experimental strain energies

ΔG_f for each nanoring-template complex is calculated from the formation constant K_f using:

$$\Delta G_f = -RTln(K_f)$$

where K_f is the formation constant of the complex from Table S7, R is the gas constant (8.314 J K^{-1} mol^{-1}) and T is temperature (298 K).

The strain energy of the cyclic complexes can be expressed as the difference in binding energy between corresponding cyclic and linear oligomers, assuming that the major difference in binding strength is related to the strain energy.

$$\Delta G_{strain} = \Delta G_{f,cyclic} - \Delta G_{f,linear}$$

Table S8: Summary of formation constants, binding energies and estimated strain energies

complex	log K_f (M^{-1})	ΔG_f (kJ mol^{-1})	related linear system	ΔG_{strain} (kJ mol^{-1})
HC_2-*l*-P6[e_5]-C_2H·T6*	15.8 ± 0.3	90 ± 2	–	–
HC_2-*l*-P6[b_4e]-C_2H·T6	19.9 ± 0.3	113 ± 2	–	–
HC_2-*l*-P6[b_5]-C_2H·T6	20.8 ± 0.3	119 ± 2	–	–
c*-P6[e_6]·T6	29.0 ± 0.3	166 ± 2	**HC_2-*l*-P6[e_5]-C_2H·T6***	76 ± 3[a]
c*-P6[be_5]·T6	38.5 ± 0.3	220 ± 2	**HC_2-*l*-P6[e_5]-C_2H·T6***	130 ± 3
***c*-P6[b_5e]·T6**	35.6 ± 0.3	203 ± 2	**HC_2-*l*-P6[b_4e]-C_2H·T6**	90 ± 3
***c*-P6[b_6]·T6**	37.0 ± 0.3	211 ± 2	**HC_2-*l*-P6[b_5]-C_2H·T6**	92 ± 3

[a]substantial distortion of the template

7 NMR Binding Competition Experiments

A competition NMR experiment was designed to compare the affinities of ***c*-P6[b_6]** and ***c*-P6[b_5e]** for the template **T6** (Figure S86). Although the ^{1}H-NMR spectra of ***c*-P6[b_6]·T6**, ***c*-P6[b_6]**, ***c*-P6[b_5e]·T6** and ***c*-P6[b_5e]** overlap, several peaks are unique for ***c*-P6[b_6]·T6** and ***c*-P6[b_5e]·T6** (Figure S87), particularly the β resonances from bound **T6**. Solutions of equal quantities of ***c*-P6[b_6]** and ***c*-P6[b_5e]·T6** (1:1 mole ratio; approximately 1 mg of each; 0.1 µmol) in $CDCl_3$ (0.5 mL) were mixed in an NMR tube (Figure S87**, top**). The exchange of the template **T6** proceeds very slowly without presence of a competing ligand to catalyze the de-coordination of **T6**, therefore, *N*-methylimidazole (40 µL, 500 µmol) as a stronger competing ligand was added. After 1 hour, equilibrium was achieved; the solution was evaporated, and *N*-methyl imidazole was removed under vacuum. The solid residue was dissolved in $CDCl_3$ (0.5 mL). ^{1}H NMR integration showed that the mole ratio of ***c*-P6[b_6]·T6** and ***c*-P6[b_5e]·T6** was 1.25, indicating a marginally higher affinity of ***c*-P6[b_6]** towards **T6** (Figure S88, bottom). This experiment was also conducted in the complementary order, starting with an equimolar mixture of ***c*-P6[b_5e]** and ***c*-P6[b_6]·T6**, yielding a similar result (mole ratio = 1.21, Figure S89). This confirms that the mixture is at equilibrium under these experimental conditions.

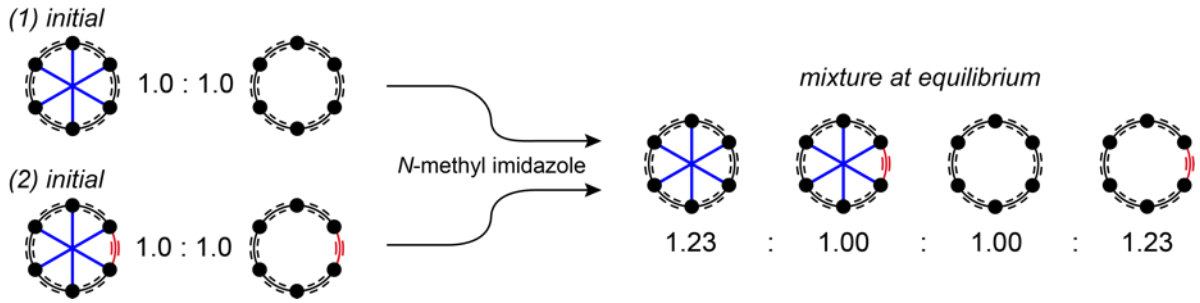

Figure S86: Competitive binding experiment investigating the relative affinity of ***c*-P6[b_6]** and ***c*-P6[b_5e]** towards **T6**.

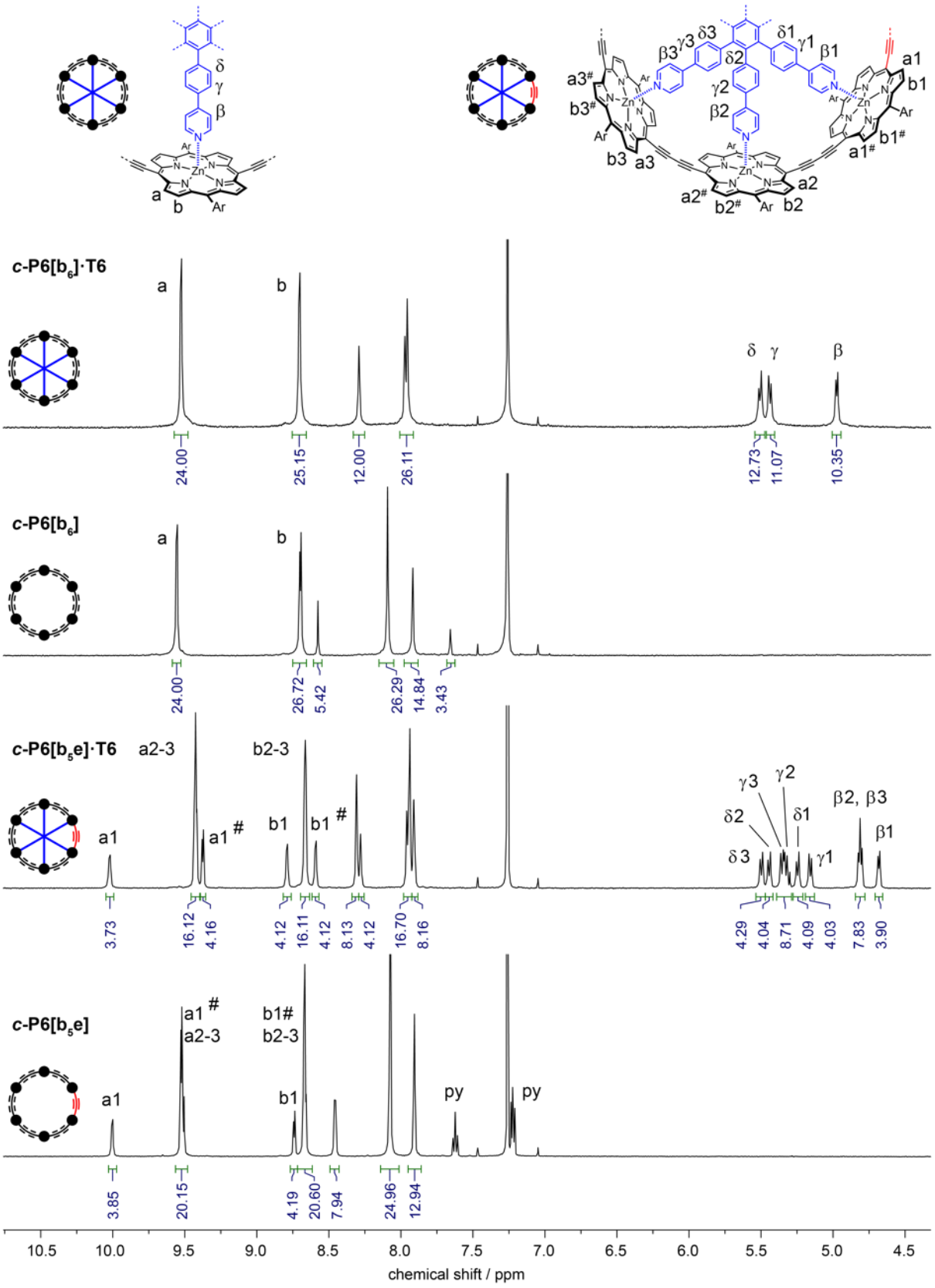

Figure S87: ^{1}H-NMR spectra (500 MHz, $CDCl_3$, 298 K) of pure compounds (from top to bottom): ***c*-P6[b$_6$]·T6**, ***c*-P6[b$_6$]**, ***c*-P6[b$_5$e]·T6** and ***c*-P6[b$_5$e]**. Resonances a1 and b1 stand out the porphyrin regions providing a measure for the ***c*-P6[b$_5$e]**·system. **T6** β resonances in ***c*-P6[b$_5$e]·T6** and ***c*-P6[b$_6$]·T6** are split and provide the cleanest measure for the ***c*-P6[b$_5$e]·T6** / ***c*-P6[b$_6$]·T6** ratio.

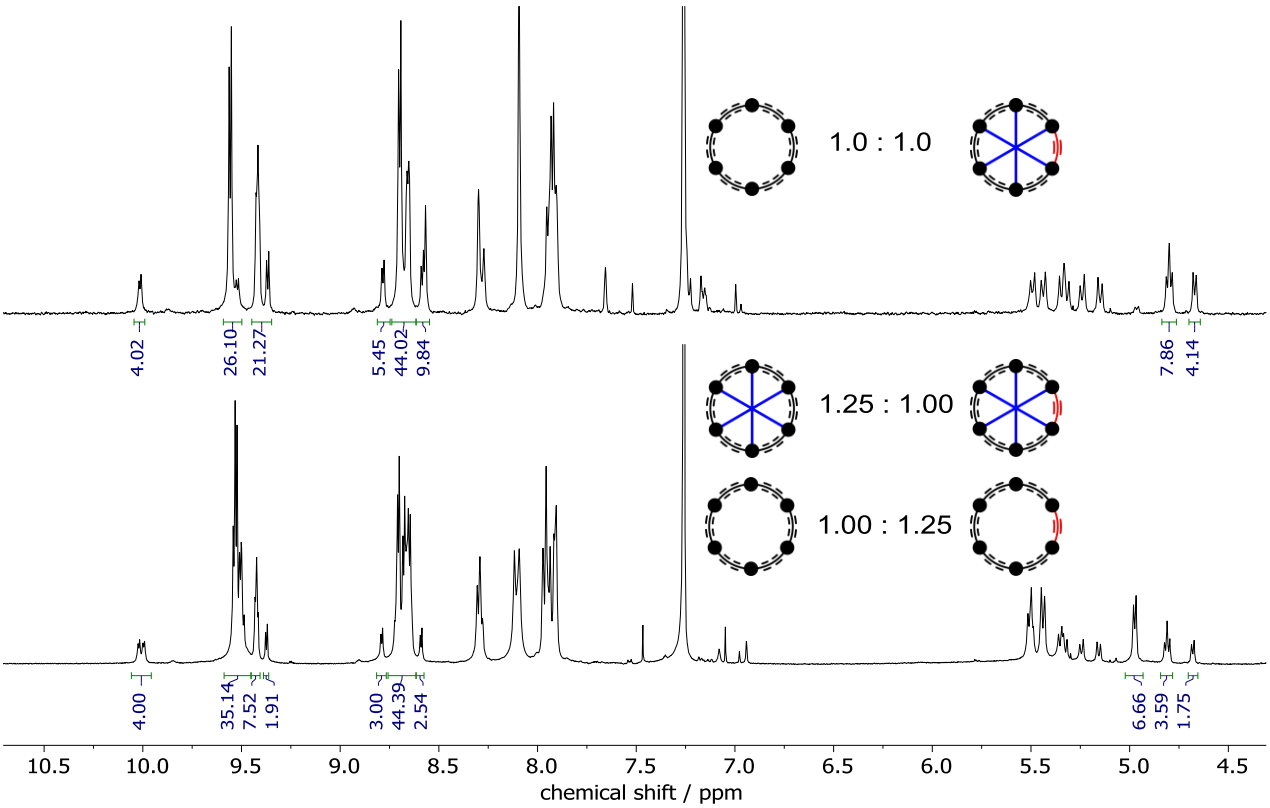

Figure S88: ^{1}H-NMR spectra (500 MHz, $CDCl_3$, 298 K) of an initially equimolar mixture ***c*-P6[b$_6$]** and ***c*-P6[b$_5$e]·T6** (top) and after template redistribution catalyzed by *N*-methylimidazole (bottom).

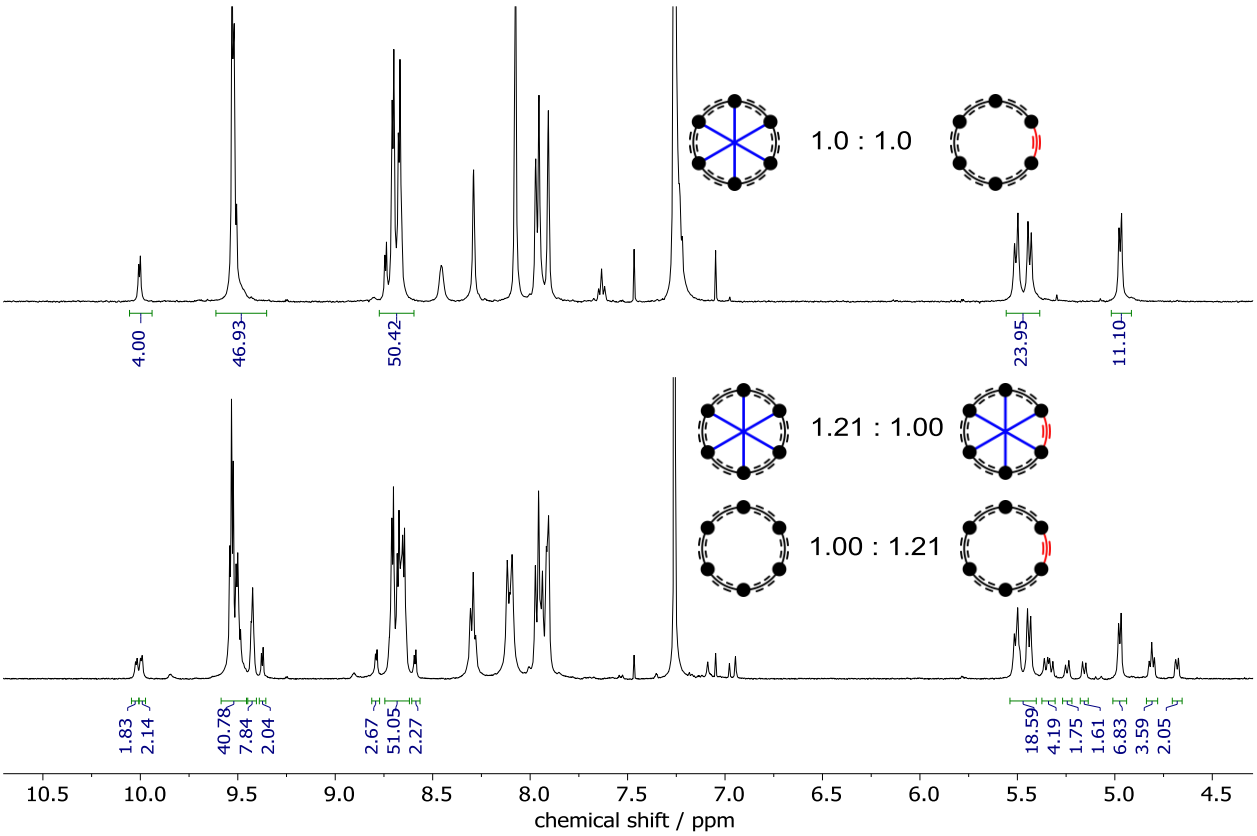

Figure S89: ^{1}H-NMR spectra (500 MHz, $CDCl_3$, 298 K) of initially equimolar mixture ***c*-P6[b$_6$]·T6** and ***c*-P6[b$_5$e]** (top) and after template redistribution catalyzed by *N*-methylimidazole (bottom).

8 Photophysical Measurements

Fluorescence quantum yields Φ_f were measured using linear butadiyne-linked porphyrin hexamer as a reference.[10] Its reported Φ_f of 28% (toluene, 1% pyridine) was further verified using an integrating sphere. The following formula was used for the calculation of the relative Φ_f:

$$\Phi_f(\mathrm{S}) = \Phi_r(\mathrm{R}) \cdot \frac{1-10^{-A_R}}{1-10^{-A_S}} \cdot \frac{n_S^2}{n_R^2} \cdot \frac{\int I_S(\upsilon)d\upsilon}{\int I_R(\upsilon)d\upsilon}$$

where A is the optical density at the excitation wavelength, n the refractive index of the solvent, $\int I_S(\upsilon)d\upsilon$ the integrated spectral fluorescence photon flux which was approximated by the integrated blank and dark-count corrected signals of the emission (in wave-numbers).

The low quantum yield and red-shifted emission of most of the reported compounds prevented us from measuring absolute quantum yields using an integrating sphere. Several accumulated spectra were necessary to obtain emission profiles with acceptable signal-to-noise. All fluorescence samples were prepared with optical densities < 0.1 under ambient conditions. The potential degradation of the samples was assessed by their UV-vis-NIR absorption spectra showing in all cases no observable decomposition even after >300 cycles (5 hours), indicating remarkable stability. Excitation spectra of all compounds were acquired at several different emission wavelengths.

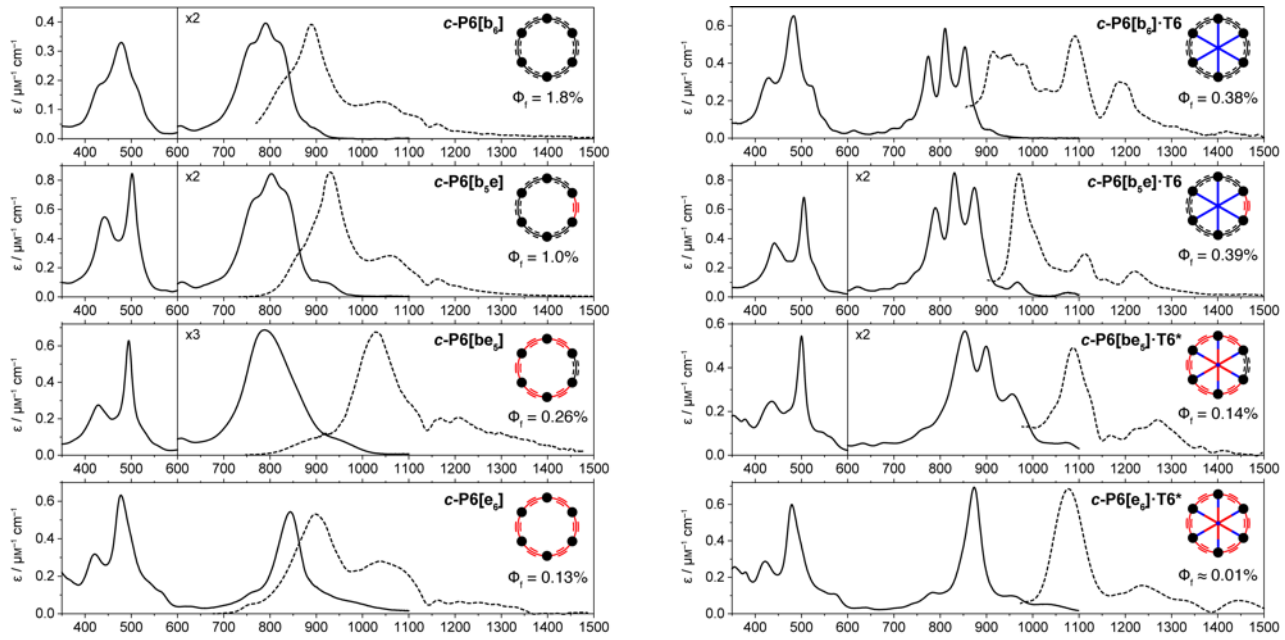

Figure S90: Steady-state absorption (black lines) and fluorescence (dashed lines) spectra at 295 K of (left) ***c*-P6[b$_6$]**, ***c*-P6[b$_5$e]**, ***c*-P6[be$_5$]**, ***c*-P6[e$_6$]** in toluene/1% pyridine and (right) ***c*-P6[b$_6$]·T6**, ***c*-P6[b$_5$e]·T6**, ***c*-P6[be$_5$]·T6***, ***c*-P6[e$_6$]·T6*** in toluene. Fluorescence quantum yields are given in %. The indentation at 1140 nm of the emission spectra is associated with solvent.

Fluorescence Lifetimes

All samples were excited at 810 nm with a power of 20 mW. Fluorescence emission was detected at 1050 nm. The fluorescence lifetimes τ were extracted by fitting a mono-exponential decay model to the experimentally observed fluorescence intensity: $I_F(t) = A\, e^{-t/\tau}$. The experimental fluorescence data with fits for each sample are shown in Figure S91 and the resulting lifetimes are given in Table S9. From the fluorescence lifetimes τ and the fluorescence quantum yields ϕ_f, the total, radiative and non-radiative decay rates (k_{tot}, k_{rad} and k_{nonrad}) are calculated for each sample using: $k_{tot} = 1/\tau$ and $k_{tot} = k_{rad} + k_{nonrad}$, with $k_{rad} = \phi_f * k_{tot}$. The rates are given in Table S9. The fluorescence of sample ***c*-P6[e$_6$]·T6*** was too weak ($\phi_f \approx 0.01\%$) to allow the recording of a reliable fluorescence decay.

Table S9. Fluorescence lifetimes τ (detected at 1050 nm, sample excited at 810 nm), total decay rate k_{tot}, radiative decay rate k_{rad}, non-radiative decay rate k_{nonrad}, and fluorescence quantum yields.

sample	τ (ns)	k_{tot} (1/ns)	k_{rad} (1/ns)	k_{nonrad} (1/ns)	ϕ_f (%)
***c*-P6[b$_6$]**	0.51	1.96	0.035	1.93	1.8
***c*-P6[b$_6$]·T6**	0.34	2.91	0.011	2.89	0.38
***c*-P6[b$_5$e]**	0.44	2.27	0.023	2.24	1.00
***c*-P6[b$_5$e]·T6**	0.32	3.17	0.012	3.16	0.39
***c*-P6[be$_5$]**	0.28	3.61	0.0094	3.60	0.26
c*-P6[be$_5$]·T6	0.22	4.51	0.0063	4.50	0.14
***c*-P6[e$_6$]**	0.49	2.02	0.0026	2.02	0.13

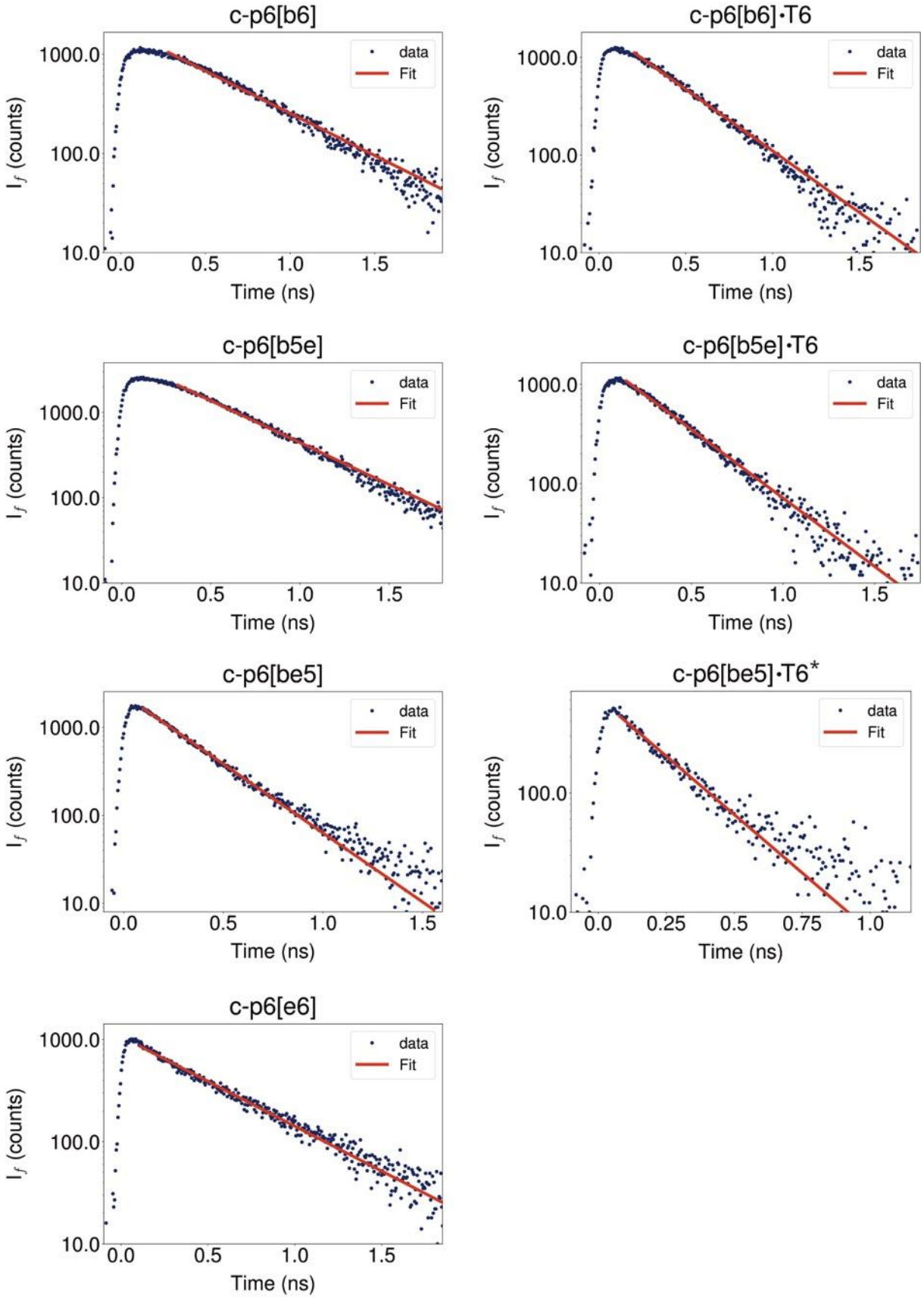

Fig. S91: Experimentally determined fluorescence lifetime decay (blue) and fits of a mono-exponential decay model to the data (red) for ***c*-P6[b_6]**, ***c*-P6[b_5e]**, ***c*-P6[be_5]**, ***c*-P6[e_6]** (left) and ***c*-P6[b_6]·T6**, ***c*-P6[b_5e]·T6**, ***c*-P6[be_5]·T6*** (right). The fluorescence decay was measured at 1050 nm.

9 Computational Chemistry

9.1 Geometry Optimization

All DFT calculations were carried out using Gaussian 16/A.03.[11] In all computational models, the aryl side-groups are truncated to –H. All geometries were optimized at the B3LYP[12] level of theory using the 6-31G* basis set.[12–15] Frequency calculations were performed for all structures confirming that geometries represent minima. The calculated Cartesian coordinates can be found in the provided .xyz files.

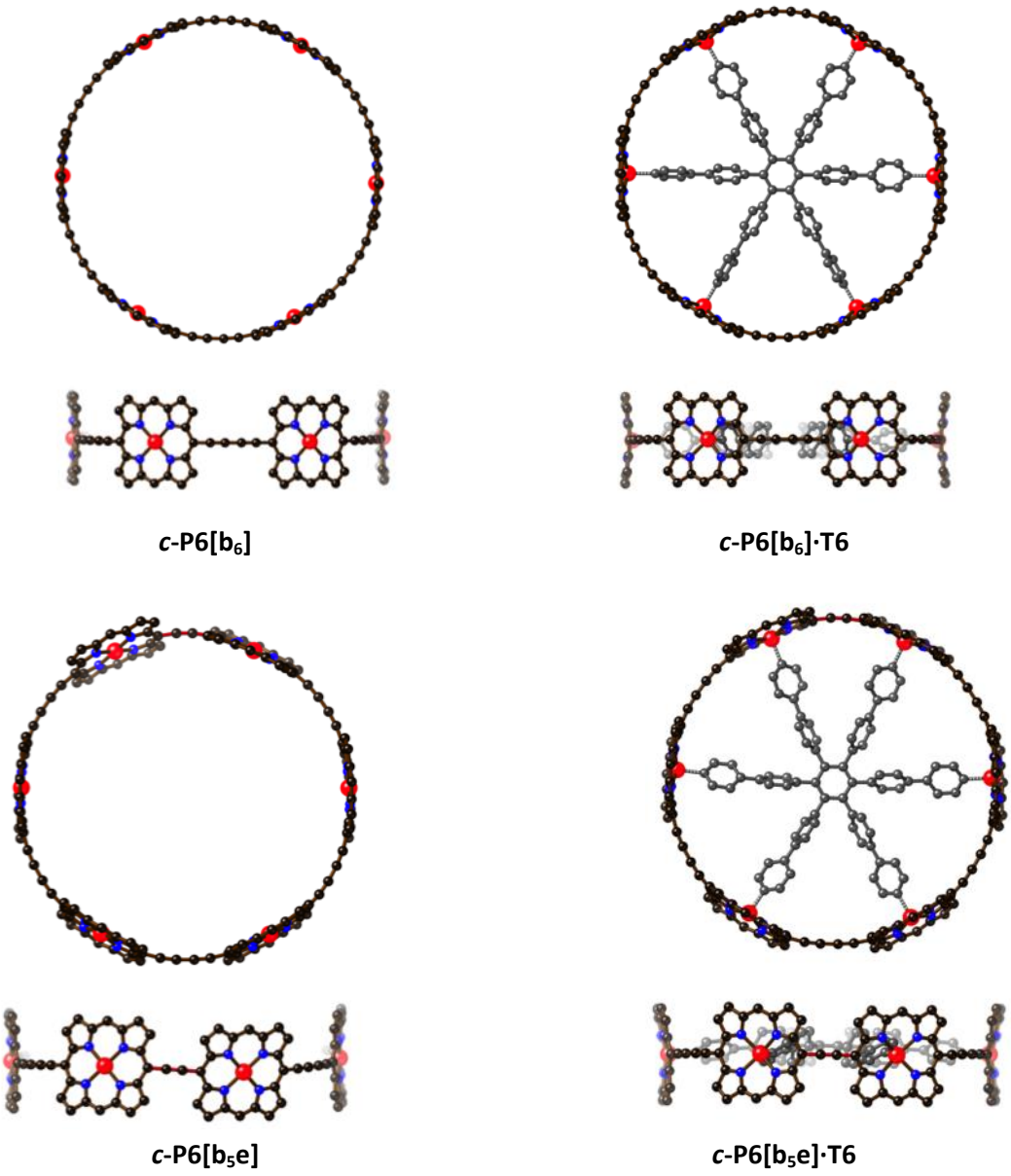

Fig. S92: Geometries from DFT calculations.

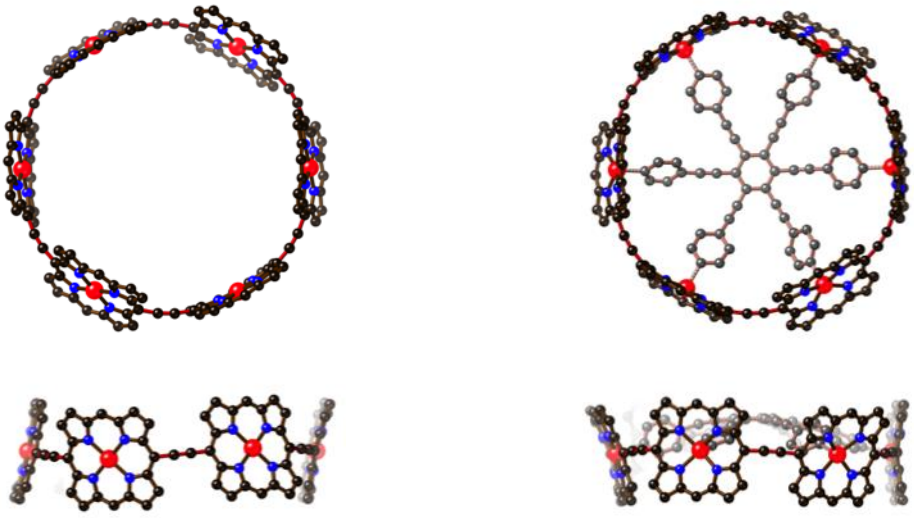

c*-P6[e$_6$]** ***c*-P6[e$_6$]·T6

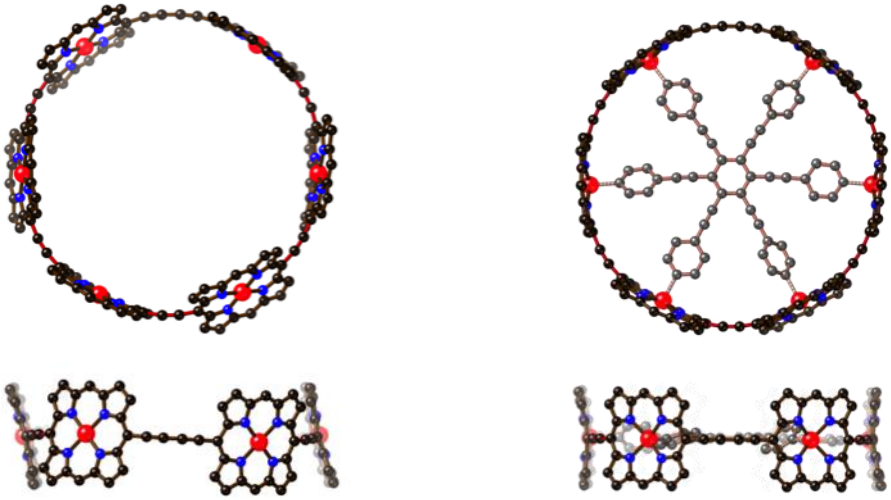

c*-P6[be$_5$]** ***c*-P6[be$_5$]·T6

Fig. S92 (continued): Geometries from DFT calculations.

9.2 Calculation of Strain Energy

The theoretical predicted strain of the DFT calculations (**ΔH_{strain}**) was estimated by homodesmotic reactions at the B3LYP/6-31G* level of theory. Subtraction of the relative energies gave the corresponding strain energy according to:

$$E_{\boldsymbol{c}-\mathbf{P6}[\mathbf{e6}]} + E_{\boldsymbol{l}-\mathbf{P2}[\mathbf{e1}]} - E_{\boldsymbol{l}-\mathbf{P8}[\mathbf{e7}]} = E_{\boldsymbol{strain}(\boldsymbol{c}-\mathbf{P6}[\mathbf{e6}])} \quad (1)$$

$$E_{\boldsymbol{c}-\mathbf{P6}[\mathbf{b6}]} + E_{\boldsymbol{l}-\mathbf{P2}[\mathbf{b1}]} - E_{\boldsymbol{l}-\mathbf{P8}[\mathbf{b7}]} = E_{\boldsymbol{strain}(\boldsymbol{c}-\mathbf{P6}[\mathbf{b6}])} \quad (2)$$

$$E_{\boldsymbol{c}-\mathbf{P6}[\mathbf{b5e}]} + E_{\boldsymbol{l}-\mathbf{P2}[\mathbf{e1}]} - E_{\boldsymbol{l}-\mathbf{P8}[\mathbf{e2b5}]} = E_{\boldsymbol{strain}(\boldsymbol{c}-\mathbf{P6}[\mathbf{b5e}])} \quad (3)$$

$$E_{\boldsymbol{c}-\mathbf{P6}[\mathbf{be5}]} + E_{\boldsymbol{l}-\mathbf{P2}[\mathbf{b1}]} - E_{\boldsymbol{l}-\mathbf{P8}[\mathbf{e5b2}]} = E_{\boldsymbol{strain}(\boldsymbol{c}-\mathbf{P6}[\mathbf{be5}])} \quad (4)$$

Table S10. Electronic and strain energies for the cyclic and linear oligo porphyrin compounds (B3LYP/6-31G*).

	Energy / Hartrees	Strain energy / kJ mol^{-1}
***c*-P6[e_6]**	–17055.23727	131.2
***c*-P6[b_6]**	–17512.21118	99.8
***c*-P6[b_5e]**	–17436.04888	105.2
***c*-P6[be_5]**	–17131.39974	114.7
***l*-P2[e_1]**	–5762.42020	-
***l*-P2[b_1]**	–5838.58050	-
***l*-P8[e_7]**	–22817.70792	-
***l*-P8[e_5b_2]**	–22970.02436	-
***l*-P8[b_7]**	–23350.83010	-
***l*-P8[e_2b_5]**	–23198.50955	-

Table S11. Electronic and binding energies for the cyclic oligo porphyrin compounds (B3LYP/6-31G*).

	Energy / Hartrees	Binding energy / kJ mol^{-1}
T6	–3101.117883	-
T6*	–2171.730162	-
c*-P6[e_6]·T6	–19227.07341	–144.4
***c*-P6[b_6]·T6**	–20613.47323	–275.0
***c*-P6[b_5e] ·T6**	–20537.30451	–252.9
c*-P6[be_5]·T6	–19303.25692	–215.5

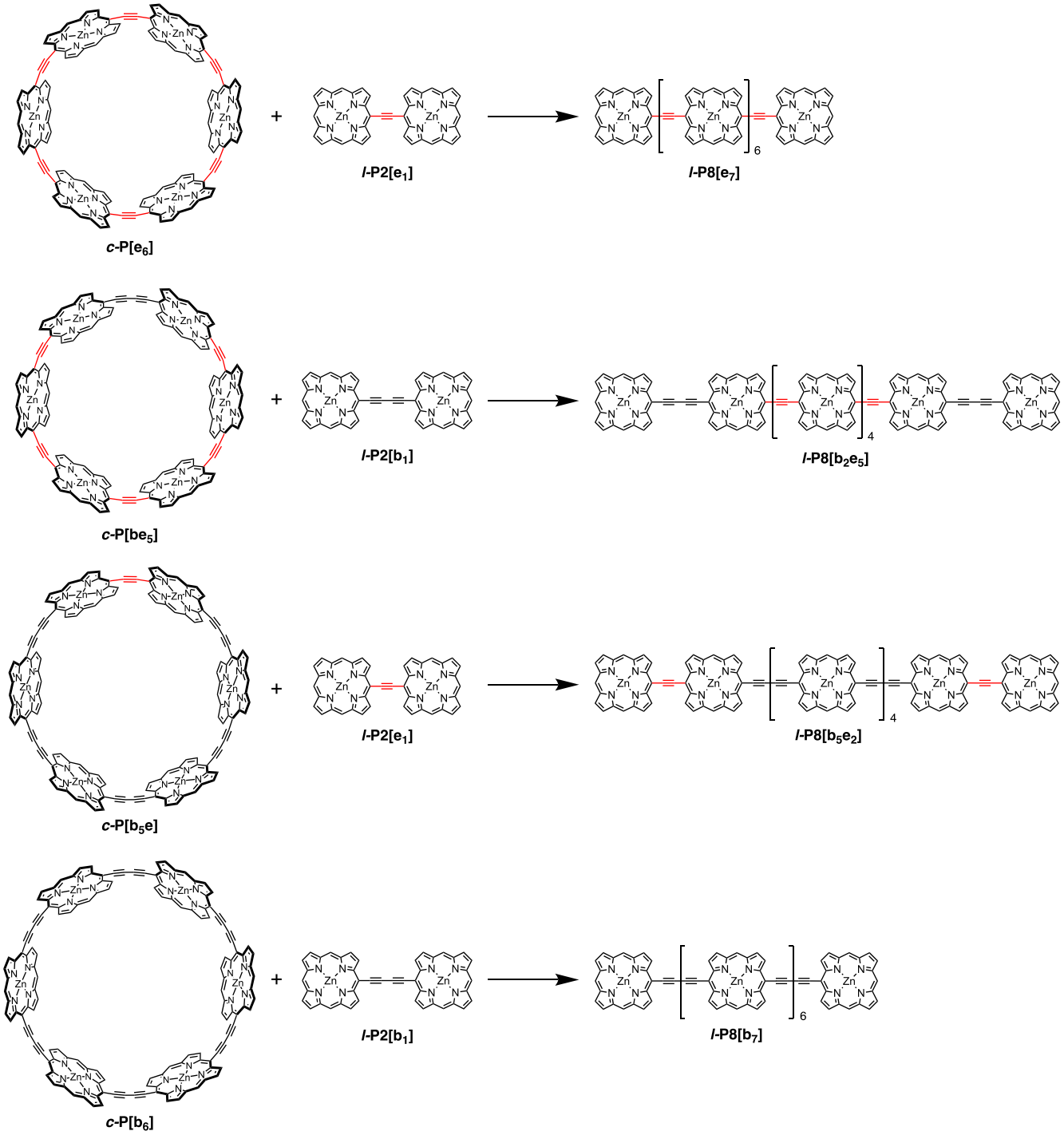

Fig. S93: Homodesmotic reactions used for strain calculations.

10 References

[1] Gong, J. Q.; Parkinson, P.; Kondratuk, D. V.; Gil-Ramírez, G.; Anderson, H. L.; Herz, L. M. Structure-Directed Exciton Dynamics in Templated Molecular Nanorings. *J. Phys. Chem. C* **2015**, *119*, 6414–6420.

[2] Grozema, F. C.; Houarner-Rassin, C.; Prins, P.; Siebbeles, L. D. A.; Anderson, H. L. Supramolecular Control of Charge Transport in Molecular Wires. *J. Am. Chem. Soc.* **2007**, *129*, 13370–13371.

[3] Rickhaus, M.; Vargas Jentzsch, A.; Tejerina, L.; Grübner, I.; Jirasek, M.; Claridge, T. D. W.; Anderson, H. L. Single-Acetylene Linked Porphyrin Nanorings. *J. Am. Chem. Soc.* **2017**, *139*, 16502–16505.

[4] Parkinson, P.; Knappke, C. E. I.; Kamonsutthipaijit, N.; Sirithip, K.; Matichak, J. D.; Anderson, H. L.; Herz, L. M. Ultrafast Energy Transfer in Biomimetic Multistrand Nanorings. *J. Am. Chem. Soc.* **2014**, *136*, 8217–8220.

[5] Hoffmann, M.; Kärnbratt, J.; Chang, M. H.; Herz, L. M.; Albinsson, B.; Anderson, H. L. Enhanced π-Conjugation around a Porphyrin[6] Nanoring. *Angew. Chem. Int. Ed.* **2008**, *47*, 4993–4996.

[6] Tait, C. E.; Neuhaus, P.; Peeks, M. D.; Anderson, H. L.; Timmel, C. R. Transient EPR Reveals Triplet State Delocalization in a Series of Cyclic and Linear π-Conjugated Porphyrin Oligomers. *J. Am. Chem. Soc.* **2015**, *137*, 8284–8293.

[7] Benson, S. W. Statistical Factors in the Correlation of Rate Constants and Equilibrium Constants. *J. Am. Chem. Soc.* **1958**, *80*, 5151–5154.

[8] Bailey, W. F., Monahan, A. S. Statistical Effects and the Evaluation of Entropy Differences In Equilibrium Processes. Symmetry Corrections and Entropy of Mixing. *J. Chem. Educ.* **1978**, *55*, 489–493

[9] Ercolani, G.; Piguet, C.; Borkovec, M.; Hamacek, J. Symmetry Numbers and Statistical Factors in Self-Assembly and Multivalency. *J. Phys. Chem. B* **2007**, *111*, 12195–12203.

[10] Yong, C.-K.; Parkinson, P.; Kondratuk, D. V.; Chen, W.-H.; Stannard, A.; Summerfield, A.; Sprafke, J. K.; O'Sullivan, M. C.; Beton, P. H.; Anderson, H. L.; Herz, L. M. Ultrafast Delocalization of Excitation in Synthetic Light-Harvesting Nanorings. *Chem. Sci.* **2015**, *6*, 181–189.

[11] Frisch, M. J.; Trucks, G. W.; Schlegel H. B.; Scuseria, G. E.; Robb M. A.; Cheeseman J. R.; Scalmani, G.; Barone, V.; Petersson, G. A.; Nakatsuji, H.; Li, X.; Caricato, M.; Marenich, A. V.; Bloino, J.; Janesko, B. G.; Gomperts, R.; Mennucci B.; Hratchian, H. P.; Ortiz, J. V.; Izmaylov, A. F.; Sonnenberg, J. L.; Williams-Young, D.; Ding, F.; Lipparini, F.; Egidi, F.; Rega, N.; Zheng, G.; Liang, W.; Hada, M.; Ehara, M.; Toyota, K.; Fukuda, R.; Hasegawa, J.; Ishida, M.; Nakajima, T.; Honda, Y.; Kitao, O.; Nakai, H.; Vreven, T.; Throssell, K.; Montgomery Jr., J. A.; Peralta, J. E.; Ogliaro, F.; Bearpark, M. J.; Heyd, J. J.; Brothers, E. N.; Kudin, K. N.; Staroverov, V. N.; Keith, T. A.; Kobayashi, R.; Normand, J.; Raghavachari, K.; Rendell, A. P.; Burant, J. C.; Iyengar, S. S.; Tomasi, J.; Cossi, M.; Millam, J. M.; Klene, M.; Adamo, C.; Cammi, R.; Ochterski, J. W.; Martin, R. L.; Morokuma, K.; Farkas, O.; Foresman, J. B.; Fox, D. J. Gaussian 16, Revision A.03, Gaussian Inc.: Wallingford CT 2016.

[12] Ditchfield, R.; Hehre, W. J.; Pople, J. A. Self-Consistent Molecular-Orbital Methods. IX. An Extended Gaussian-Type Basis for Molecular-Orbital Studies of Organic Molecules. *J. Chem. Phys.* **1971**, *54*, 724–728.

[13] Hehre, W. J.; Ditchfield, R.; Pople, J. A. Self-Consistent Molecular Orbital Methods. XII. Further Extensions of Gaussian-Type Basis Sets for Use in Molecular Orbital Studies of Organic Molecules. *J. Chem. Phys.* **1972**, *56*, 2257–2261.

[14] Hariharan, P. C.; Pople, J. A. The Influence of Polarization Functions on Molecular Orbital Hydrogenation Energies. *Theor. Chim. Acta* **1973**, *28*, 213–222.

[15] Rassolov, V. A.; Pople, J. A.; Ratner, M. A.; Windus, T. L. 6-31G* Basis Set for Atoms K through Zn. *J. Chem. Phys.* **1998**, *109*, 1223–1229.